MODELING PRODUCTION OF AROMATIC FROM N-PARAFFINS WITH CHEMICAL
EQUILIBRIA

Miss Thidarat Detsut

จุฬาลงกรณ์มหาวิทยาลัย
CHULALONGKORN UNIVERSITY

A Thesis Submitted in Partial Fulfillment of the Requirements
for the Degree of Master of Engineering in Chemical Engineering
Department of Chemical Engineering
FACULTY OF ENGINEERING
Chulalongkorn University
Academic Year 2019
Copyright of Chulalongkorn University

การจำลองการผลิตอะโรเมติกส์จากนอร์มอลพาราฟินด้วยสมดุลเคมี

น.ส.ฐิดารัตน์ เดชสุทธิ์

วิทยานิพนธ์นี้เป็นส่วนหนึ่งของการศึกษาตามหลักสูตรปริญญาวิศวกรรมศาสตรมหาบัณฑิต
สาขาวิชาวิศวกรรมเคมี ภาควิชาวิศวกรรมเคมี
คณะวิศวกรรมศาสตร์ จุฬาลงกรณ์มหาวิทยาลัย
ปีการศึกษา 2562
ลิขสิทธิ์ของจุฬาลงกรณ์มหาวิทยาลัย

Thesis Title	MODELING PRODUCTION OF AROMATIC FROM N-PARAFFINS WITH CHEMICAL EQUILIBRIA
By	Miss Thidarat Detsut
Field of Study	Chemical Engineering
Thesis Advisor	Associate Professor DEACHA CHATSIRIWECH, Ph.D.

Accepted by the FACULTY OF ENGINEERING, Chulalongkorn University in Partial Fulfillment of the Requirement for the Master of Engineering

.... Dean of the FACULTY OF
ENGINEERING
(Professor SUPOT TEACHAVORASINSKUN, Ph.D.)

THESIS COMMITTEE

.... Chairman
(Associate Professor TAWATCHAI CHARINPANITKUL, Ph.D.)

.... Thesis Advisor
(Associate Professor DEACHA CHATSIRIWECH, Ph.D.)

.... Examiner
(Pongtorn Charoensuppanimit, Ph.D.)

.... External Examiner
(Associate Professor Nurak Grisdanurak, Ph.D.)

ฐิดารัตน์ เดชสุทธิ์ : การจำลองการผลิตอะโรเมติกส์จากนอร์มอลพาราฟินด้วยสมดุลเคมี. (MODELING PRODUCTION OF AROMATIC FROM N-PARAFFINS WITH CHEMICAL EQUILIBRIA) อ.ที่ปรึกษาหลัก : รองศาสตราจารย์เดชา ฉัตรศิริเวช

ในงานวิจัยนี้ได้สร้างแบบจำลองทางคณิตศาสตร์เพื่อจำลองและพัฒนาแบบจำลองการผลิตอะโรเมติกส์จากนอร์มอลพาราฟินที่สภาวะสมดุลของปฏิกิริยา โดยใช้ตัวเร่งปฏิกิริยา ได้แก่ ZSM-5(80) และ Mo_2C โดยทำการตรวจสอบความแม่นยำด้วยการเปรียบเทียบข้อมูลที่คำนวณได้จากแบบจำลองกับค่าที่ได้จากผลการทดลอง ณ สภาวะที่ปฏิกิริยาเข้าสมดุลแล้ว ซึ่งช่วงอุณหภูมิที่ทำการศึกษาจะอยู่ในช่วง 450-500 องศาเซลเซียสภายใต้ความดันบรรยากาศที่ 1 atm ผลการศึกษา พบว่าแบบจำลองทางคณิตศาสตร์ที่เหมาะสมจะขึ้นกับชนิดของตัวเร่งปฏิกิริยาที่ใช้ในระบบ โดยแบบจำลองทางสมดุลปฏิกิริยานี้จะสามารถ เพิ่มความแม่นยำได้มากขึ้นหากทำการกำหนดผลได้ของอะโรเมติกส์เข้าไปในระบบ ซึ่งหากทำการเปรียบเทียบตัวแปรที่ใช้บอกความสามารถของเครื่องปฏิกรณ์ เช่น การเปลี่ยนแปลงสารตั้งต้น(Conversion) และผลได้จากปฏิกิริยา (yield) จะพบว่า แบบจำลองทางสมดุลจะสามารถใช้ได้ในช่วงอุณหภูมิและอัตราการป้อนที่ได้กำหนดไว้ นอกจากนี้แบบจำลองทางสมดุลยังสามารถใช้ในการทำนายผลของตัวเร่งปฏิกิริยาชนิดอื่นได้ แบบจำลองที่สร้างขึ้นจะสามารถคาดการณ์ปฏิกิริยาการผลิตเบนซีน โทลูอีนและไซลีนจากนอร์มอลพาราฟินจากตัวเร่งปฏิกิริยา อุณหภูมิและความดันที่หลากหลายได้ เพื่อเป็นประโยชน์ในเชิงอุตสาหกรรมและลดต้นทุนในห้องปฏิบัติการ

สาขาวิชา	วิศวกรรมเคมี	ลายมือชื่อนิสิต ....
ปีการศึกษา	2562	ลายมือชื่อ อ.ที่ปรึกษาหลัก ....

6070442921 : MAJOR CHEMICAL ENGINEERING

KEYWORD: CHEMICAL EQUILIBRIUM, AROMATIZATION, REACTION RATE,
                        MODELING

Thidarat Detsut : MODELING PRODUCTION OF AROMATIC FROM N-PARAFFINS WITH CHEMICAL EQUILIBRIA. Advisor: Associate Professor DEACHA CHATSIRIWECH, Ph.D.

Chemical Equilibrium models were constructed for modeling and developing the aromatic production model from the normal paraffin at the equilibrium of the reaction with catalysts, i.e. ZSM-5(80) and Mo_2C. The models were verified under operating temperatures of 450-500 ° C under atmospheric pressure at 1 atm. By examining the accuracy by comparing the data calculated from each model with the value obtained from the corresponding experiments at the condition that the reaction is balanced. The suitable equilibrium model depends on the type of catalyst used in the system. The accuracy of all equilibrium models could be improved by specifying the desired aromatic yield. In addition, based on the reactor performance, i.e. conversion, and yields, the limitation of the manipulated equilibrium models was evaluated within the operating temperatures and the ratio. Finally, the equilibrium models, could be employed to predict the reactor performance containing other types of catalysts with a variety of temperature and pressure for industrial benefits and reduce operating costs.

Field of Study:	Chemical Engineering	Student's Signature ....
Academic Year:	2019	Advisor's Signature ....

ACKNOWLEDGEMENTS

TABLE OF CONTENTS

LIST OF TABLES

LIST OF FIGURES

CHAPTER 1

INTRODUCTION

In this chapter, Researcher will discuss the research source and importance of problems, objectives, general information of benzene, toluene, xylene separation process and scope of research to find ways to improve modeling aromatics production process.

1.1 Motivation of this research work

The direct conversion of normal paraffin into aromatics is an important industrial process that has been the subject of extensive research. The results obtained on various catalysts and the possible mechanisms of this complex process are well documented in several excellent reviews [1–6].

Normal Paraffin include n-Hexane, n-Heptane and n-Octane are one of the components of natural gas liquids (NGL), and its reforming to olefins and aromatics is of practical importance which is use for a raw material in the petrochemical industry [15–19]. Natural gas is an energy source often used for heating, transportation, and electricity generation. The reservoir of natural gas increases rapidly higher than that of crude oil and expected to ahead of by the 21stcentury [4]. Moreover, The aromatization of n-alkanes is an important reaction with many industrial applications which could be carried out on both bifunctional (acid–metal) and monofunctional (only-metal) catalysts [2] such as an ingredient and refined into gasoline, solvent industry is distilled and separated at various temperatures. Resulting in various types of solutions as follows white Spirit in the coating industry, dry cleaning, polishing process and the pesticide industry while mixtures of benzene, toluene and xylene are aromatic hydrocarbons and are also upstream petrochemicals which are used for further production processes.

Normal Paraffin is a clear liquid that are made up of saturated hydrocarbons with a straight-chain structure. Normal Paraffin is the major raw material for the

manufacture of the LAB [9]. Normal Paraffin is extracted from kerosene which contains an average of 20/25% paraffin and therefore is generally produced close to a refinery as the kerosene, free of the paraffin removed has to be returned to the refinery. Over 80% of Normal Paraffin is used for the production of the LAB the remaining N-Paraffin may be further processed to obtain special solvents used for various industrial applications including synthetic resins, paints and varnishes, degreasing agents and printing inks [7]. Normal paraffin operates as a dissolver in industrial for producing polymers and resins, colors, artistic coverings and grease polisher, plasticizers and chloroparaffins; production of oils for aluminum cold rolling, catalyst carrier for olefin polymerization, raw materials for a wide range of applications.

More efficient economic conversion of paraffins to aromatics such as benzene, toluene, and xylenes and to do so without an outside source of hydrogen. It also would be desirable to upgrade in value the products of the process by increasing the xylene. Furthermore, it is desirable to increase the available ethane, which as a feedstock for the production of ethylene has a higher value than methane [11].

Mixtures of benzene, toluene and xylene are aromatic hydrocarbons and are also upstream petrochemicals which are used for further production processes. Around 80% of benzene produce three main chemicals, including ethylbenzene, cumene, and cyclohexane. Furthermore, ethylbenzene is essential for manufacturing polystyrene while cumene is produced for use in packaging, construction and household goods. Next, toluene advantages in commercial have assorted fields, e.g. gasoline, paints, cleaning agents and rubber. Besides, benzene, trinitrotoluene (TNT), nylon, plastics and polyurethanes are also manufactured from toluene. Overall, aromatics are feedstock of plastic pellets and synthetic fibers in various petrochemical industries, for example automotive parts, electronic appliances and textiles [12].

At the present time, there are many researches demonstrating the experiments converting C_6, C_7, C_8 to aromatics including benzene, toluene and xylene with different conditions, e.g., catalyst, temperature, pressure and reactant

components. It is obvious that aromatics production from n-hexane, n-heptane and n-octane are value enhancement because not only economic values of the aromatics but also C_6, C_7, and C_8 which can be more usage alternatives.

Therefore, the objective of this research is to develop the model of benzene, toluene and xylene productions from n-hexane, n-heptane and n-octane with chemical equilibria over the catalyst. All of these studies were exclusively restricted to the reactions of C_6, C_7, C_8 compounds [1–10].

This research is sincerely expected finding optimized models would explain and more clarify the several reactions. Furthermore, it would be beneficial to develop and actualize in commercial part and predict reaction results with other conditions to save laboratory cost and simplify the method predicting the process of aromatics production. Then In this study, it is curious to use chemical equilibrium concept for describing the fraction of components and the models would originate with the assistance of computer simulation, Aspen Plus simulation to fit with research results.
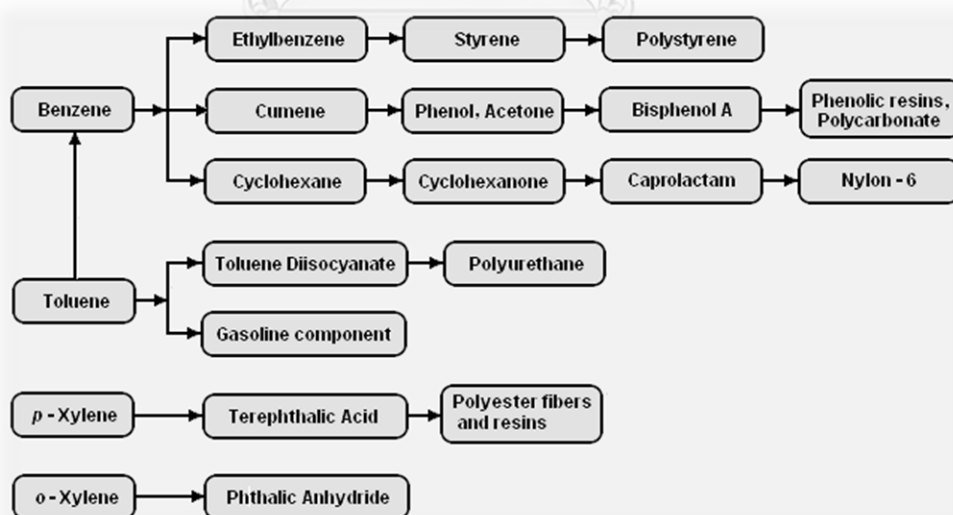
Figure 1: Diagram of the petrochemicals derived from Benzene, Toluene and Xylenes (as a group, referred to as BTX)

1.2 Research objective

To develop the model of benzene, toluene and xylene productions or aromatics production from Normal Paraffin with chemical equilibria over different catalysts.

1.3 Scope of this research work

1.3.1 To propose chemical reactions of Normal Paraffin to be aromatics (BTX) by using Aspen Plus V9 programs for calculation and other researches for comparison.

1.3.2 Interested variables which effected to the model were temperatures, pressures, and catalysts.

1.3.3 The reaction temperatures were varied between 550 °C and 600 °C to find the lowest temperature which the reaction can occur.

1.3.4 The reaction pressure was used to investigate the model were equal to the other researches and then vary between 1 atm and 10 atm to predict other conditions.

1.3.5 All existing compound in the main reactions (aromatization) and the sides reactions (thermal cracking) would be well-defined hydrocarbons, for example C_6, C_7, C_8.

1.3.6 The model would be an equilibrium model and kinetic energy is not considered.

1.4 Expected output

The appropriate simulation model for the reaction network of aromatics production.

1.5 Research methodology

For this work, the research methodology consists of several steps as below:
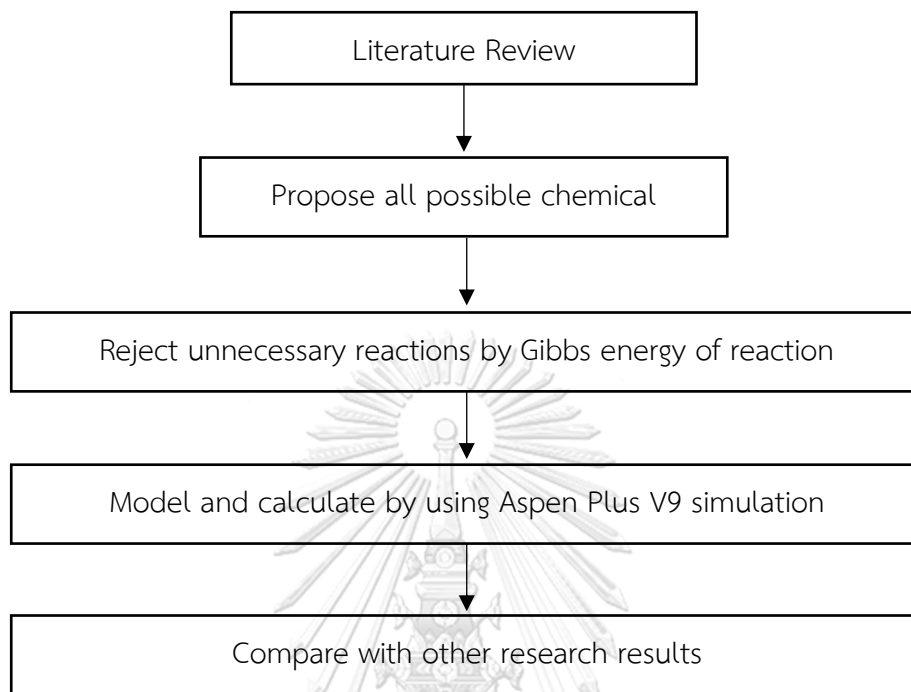
Figure 2: Research methodology

1.6 Implementation plan

There are 8 steps plan to conduct in this research work as shown in Table 1

1.6.1 Conduct a literature survey and review with a focus on the production of aromatic from normal paraffins.

1.6.2 Propose all possible chemical reactions, including main reactions and side reactions.

1.6.3 Calculate Gibbs energy of reaction to reject impossible reactions.

1.6.4 Calculate conversions, equilibrium constants, compositions and etc. from Aspen Plus V9.

1.6.5 Model the reactions over different catalysts by comparing with other researches

1.6.6 Make discussion of all experimental results and making conclusions.

1.6.7 Prepare manuscript to publish.

1.6.8 Write thesis book and prepare thesis defending examination.

Table 1: Implementation plan.

Activity	Monthly (2019)												Monthly (2020)						
	1	2	3	4	5	6	7	8	9	10	11	12	1	2	3	4	5	6	7
Conduct literature survey and reviews	X	X	X	X	X	X	X	X	X	X	X	X	X	X	X	X	X	X	X
Propose all possible chemical reactions		X	X	X	X	X	X	X	X	X	X	X	X	X	X	X			
Calculate Gibbs energy of reaction to reject impossible reactions.					X	X	X	X	X	X	X	X	X	X					
Calculate conversions, equilibrium constants, compositions and etc. from Aspen Plus V9.						X	X	X	X	X	X	X	X	X					
Model and calculate by using Aspen Plus V9 simulation						X	X	X	X	X	X	X	X	X					
Make discussion of experiment results and making conclusions						X	X	X	X	X	X	X	X	X	X	X	X	X	X
Prepare manuscript to publish															X	X	X		X
Write thesis book and prepare thesis defending examination															X	X	X	X	X

CHAPTER 2

FUNDAMENTAL KNOWLEDGE

In order to modeling and developing the aromatic production model from normal paraffin at the equilibrium of the reaction with catalysts, basic knowledge and understanding are important. Hence, basic knowledge of Chemical Equilibrium, heterogeneous catalyst, and aspen plus V9 are described in this chapter.

2.1 Chemical equilibrium

2.1.1 Principle

Chemical equilibrium is a state in which the rate of the forward reaction equals the rate of the backward reaction. In other words, there is no net change in concentrations of reactants and products. This kind of equilibrium is also called dynamic equilibrium [14].

In a chemical reaction, a reversible reaction enables a closed system to be an equilibrium state at one point when a forward reaction rate is equal to a backward reaction rate. Moreover, at the equilibrium state, the system is not static but it is thoroughly changing, called dynamic equilibrium. If the system is disturbed by external influence, such as temperature or pressure change, the equilibrium state would be destroyed. However, when disturbance is stopped, the system could re-balance itself after the chance [16]. According to Le Chatelier's principle, result of chemical equilibria of reactions that achieves a new equilibrium state will be predicable when concentration, pressure, or temperature changes.

Adding reactant concentrations will shift the equilibrium to the right, leading to more production while adding product concentrations will shift the equilibrium to the left, enabling the reactants to increase. Besides, pressure or volume alteration will affect to a reaction which reactants and products are gaseous while a system in

liquid and solid phases will not be disturbed much. A difference of total product moles and total reactant moles in a reaction is a determination where the reaction will be driven. To illustrate, increasing pressure or decreasing volume will drive a reaction to the side that includes fewer gaseous moles. Likewise, decreasing pressure or increasing volume will drive a reaction to the side of additional gaseous moles. Lastly, a change in temperature will also impact to the equilibrium, which depends on types of the reaction, including endothermic and exothermic reactions. The equilibrium will be restored similarly to the change in concentration. For instant, heat is absorbed in the endothermic reaction, so the heat would be represented as a reactant while for the exothermic reaction, heat would be represented as a product since heat will be released [22]. Therefore, raising the temperature on the endothermic reaction will drive the reaction to the right because heat is referred to the reactant. Conversely, raising the temperature on the exothermic reaction will drive the reaction to left.

2.1.2 Equilibrium constant

For a gas-phase reaction, aA(g) + bB(g) $\leftrightarrows$ cC(g) + dD(g), the expression for K_p is:[11]

$$K_P = \frac{(P_c)^c (P_D)^d}{(P_A)^a (P_B)^b}$$

In fact, there are many reactions occurring in the reactor, hence K_P would be represented as $K_{P(n)}$ where n is a number of any reaction. To illustrate, there are reactions as follows:

$$rR(g) \leftrightarrows sS(g) + tT(g) \qquad \text{-------- reaction (1)}$$
$$xX(g) \leftrightarrows yY(g) + zZ(g) \qquad \text{-------- reaction (2)}$$

Then, Kp of both reactions would be

$$K_{p1} = \frac{(P_S)^s (P_T)^t}{(P_R)^r}$$

and

$$K_{p2} = \frac{(P_Y)^y (P_Z)^z}{(P_X)^x}$$

2.2 Heterogeneous catalyst

Heterogeneous catalyst refers to the form of catalysis where the phase of the catalyst different from the reactant. The great majority of heterogeneous catalyst is solids and the great majority of reactant is liquids or gases. The advantage of this catalyst is easy to separate from the reaction mixtures. The catalyst also consists of two main parts, the first part is called the active phase, which site that reaction occurs (i.e. metal, metal oxide, metal sulfide and metal phosphide). The second part is called the support phase, which site that the active phase disperses on its surface. The support phase will promote the catalytic reaction, which is porous materials. There are various materials used as catalyst support including activated carbon, zeolites, silica gels, activated clay and activated alumina. The supporting materials have high surface characteristics, which will achieve a good distribution of the active metal catalyst.

In heterogeneous catalyst, the reactant is diffused and adsorbed to the catalyst surface, which the formation of the chemical bond. After the reaction, the product is desorbed and diffused away from the catalyst surface. For the solid catalyst, the surface area is also important, which will affect the active phase distribution as well as catalytic performance. However, the morphology of catalyst support will enhance the product yield and protect the catalyst deactivation via

coke formation. Hence, the development of the catalyst is an important key to increase the reaction rate [18].

Heterogeneous catalysis plays an important role in the modern energy and chemical technology since it is capable of improving the selectivity, activity and efficiency of the catalysts. Phases of a reaction will be gas or liquid phase, which is operated over a solid catalyst [10]. The catalyst compositions consist of active phase, support and promoter.

2.2.1 Active phase and support

The active phase or the active site is typically dispersed in pores of a support or a carrier in the form of nanocrystallites of 1 nanometer to a few nanometers, leading catalytic efficiency to be the best [13]. while adding promoter is to improve physical or chemical properties of the catalyst. The active phase is the site where surface reaction occurs and is ordinarily metal forms, for instance, metals, metal oxides, metal sulfides, metal carbides and so on. However, the support is also an integral part to emphasize capability of the supported metal, especially high surface area for higher quantity of dispersing metal particles [21]. Moreover, the pore diameters are necessary to be suitable for metal sizes, and the pore diameters depend on support materials. There are various the support materials for different purposes, physical and chemical properties. To illustrate, alumina is the most widely used support, following by silica. Others are still important for commercial carriers, consisting of magnesia, titania, aluminosilicates and calcium aluminate [25].

2.2.2 Pores

Physical properties of pore (e.g. pore volume, pore diameter and pore size distribution) obviously affect to enhance the surface area that locates the active site and restrict reactant and product sizes that influents to the selectivity. However, catalyst agglomeration or growth of metal particles which would be pore blockage is

an issue of activity decay because the pore volume decreases. Therefore, the selectivity will also decline [21, 22].

2.2.3 Zeolite

Generally, a catalyst of aromatics production is ZSM-5, which is a type of a zeolite and perhaps loads metal particles to enhance the catalytic efficiency. The zeolites contain acid sites, involving hydrogenolysis (cracking), isomerization and oligomerization (polymerization). The zeolites basically have wide range of silicon to aluminum ratio and are vastly applied in many applications such as oil refining industry, fine chemical industry, environment protection industry, electrochemical industry and chemical anticorrosion industry. Apart from acid catalyst property, they also can be molecular sieve property for accessible components [22].

2.2.4 Aluminum oxide (Al_2O_3)

Aluminum oxide is widely used as basic material of catalytic support because of its high chemical inertness, strength and hardness. Aluminum oxide is a white odorless crystalline powder. Water insoluble. Properties (both physical and chemical) vary according to the method of preparation; different methods give different crystalline modifications. The variety formed at very high temperature is quite inert chemically. Aluminum oxide possesses excellent surface area owing to the small particle size, which results in high activity of the surface for a catalyst support [19]. Mesoporous has excellent properties such as highly uniform channels, large surface area and narrow pore size distribution. It has been widely used as adsorbents, catalysts support, and other ceramic applications [22].

2.2.5 Silicon dioxide (SiO_2)

Silica based supports and catalysts are widely used in the manufacture of process intermediates & fine chemicals, elastomers & polymers, alternative energy,

water treatment & environmental controls. Silica has relatively stable chemical properties at normal temperatures and does not react with many chemicals, but can be transformed. The amorphous silica is more reactive than crystalline silica because amorphous silica has a greater surface. Therefore, amorphous silica (amorphous silica) is often used as a catalyst component.

2.2.6 Molybdenum carbide catalyst (Mo_2C)

Molybdenum Carbide is a chemical compound which consists of Molybdenum metal and Carbon. This compound has very high melting point which is 2690 ℃. The compound is in white powder form at room temperature [25]. Mo_2C is an attractive catalyst for fuel reforming reactions because it possesses both a high activity and a high coking resistance. Moreover, Mo_2C catalyst is a potential and low cost [21]. The Mo_2C shows a performance similar to that of a blank run (in the absence of catalyst), the catalyst exhibits excellent stability over the 24 h test [24]. Generally, the reaction pathways of aromatics production were investigated on Mo_2C deposited on ZSM-5. Its efficiency sensitively depended on the composition of zeolite. Deposition of Mo_2C markedly changed the catalytic performance of ZSM-5, and the dehydrogenation and the aromatization processes came into prominence [23]. Furthermore, Molybdenum Carbide have high hardness, good thermal and mechanical stability, and excellent corrosion resistance. By these properties of Molybdenum Carbide nanoparticles/nanopowder are good choice to be used as coating material and as additive. For the applications desired high chemical resistance Molybdenum Carbide nanoparticles/nanopowder are useful. Since Molybdenum Carbide nanoparticles/nanopowder are hard materials, they are used in tool bits for cutting tools. [24,25].

2.3 Aspen plus V9 program
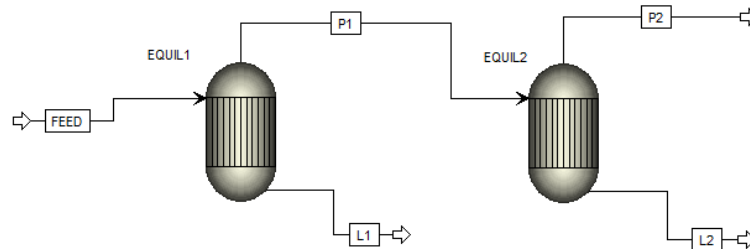
Figure 3: Simple Equilibrium Reactor in Aspen Plus program

Aspen plus program enables steady-state simulation of a wide range of process including production of chemicals, hydrocarbons, pharmaceuticals, solids, polymers, petroleum assays and blends, and other applications [31]. ASPEN is a process simulation software package widely used in industry today. Given a process design and an appropriate selection of thermodynamic models, ASPEN uses mathematical models to predict the performance of the process. This information can then be used in an iterative fashion to optimize the design [29]. This accurate modeling of thermodynamic properties is particularly important in the separation of non-ideal mixtures, and ASPEN has a large data bases of regressed parameters. ASPEN can handle very complex processes, including multiple-column separation systems, chemical reactors, distillation of chemically reactive compounds, and even electrolyte solutions like mineral acids and sodium hydroxide solutions. ASPEN does not design the process. It takes a design that the user supplies and simulates the performance of the process specified in that design. Therefore, a solid understanding of the underlying chemical engineering principles is required to supply reasonable values of input parameters and to evaluate the suitability of the results obtained [32]. Process Modeling Aspen Plus V9 is a program developed by Aspen Technology. The software installer includes 97 files and is usually about 765.42 KB (783,792

bytes). A majority of the PCs this is running on, most OS versions are Windows 10. The distribution of this has mostly been seen in the United States [33].

2.3.1 Base method

The components in the process are hydrocarbons, then Peng-Robinson method was preferred. However, the method would consider interaction between each component in the mixture, which it can be estimated from the Polymath with difficulty. Hence, ideal model was also performed for contrasting.

2.3.2 Equilibrium reactor

The model was regarded as equilibrium state which the forward reaction rate and the reverse reaction rate are equivalent, so equilibrium reactor was operated instead.

2.3.3 Effect of temperature on the reaction performance

From the formulas, temperature influents the reaction result, especially conversion. Although high temperature leads to higher conversion, coke formation probably occurs. Then, temperature varying was performed to estimate the lowest possible reaction temperature.

2.3.4 Effect of pressure on the reaction performance

Most experiments from the literature reviews are demonstrated at atmospheric pressure, then the model would be interested in higher operating pressure.

CHAPTER 3

LITERATURE REVIEWS

This chapter is a review of relevant literature about the reaction to produce aromatic products. The topics of this chapter are categorized the interesting literature into three major parts included the main reactions were reaction producing benzene toluene and xylene directly, the side reactions were unexpected reactions, particularly thermal cracking, dehydrogenation, hydrocracking and sample of related research.
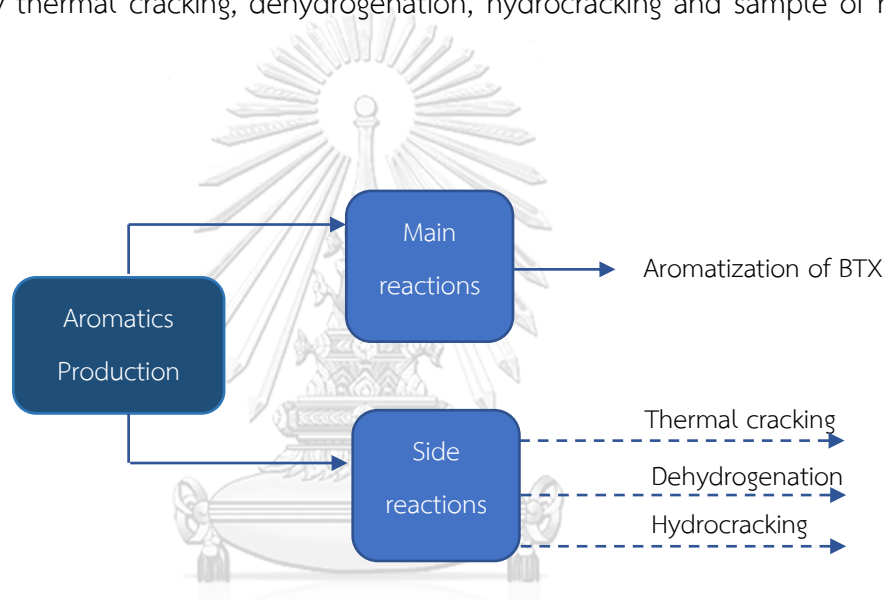
Figure 4: The main and side reaction to produce aromatics product

3.1 Aromatization

Aromatization is a chemical reaction in which an aromatic system is the conversion of a nonaromatic hydrocarbon to an aromatic hydrocarbon. Typically, aromatization is achieved by dehydrogenation of existing cyclic compounds, illustrated by the conversion of cyclohexane into benzene. Aromatization includes the formation of heterocyclic systems [21].
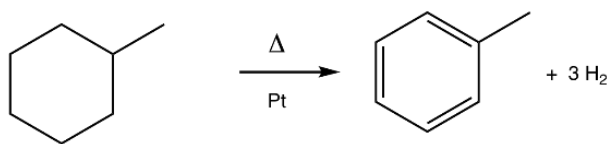
Figure 5: Example The conversion of methylcyclohexane to toluene

The conversion of methylcyclohexane to toluene is a classic aromatization reaction. This platinum (Pt)-catalyzed process is practiced on scale in the production of gasoline from petroleum [27]. There are four common methods of aromatization.

1. Dehydrogenation of naphthenes

Naphthenes are a class of cyclic aliphatic hydrocarbons obtained from petroleum. They have the general formula C_nH_{2n}. The simplest naphthene is cyclohexane, C_6H_{12}. Catalytic dehydrogenation converts it to benzene.

$$C_6H_{12} \longrightarrow C_6H_6 + 3H_2 \tag{1}$$

2. Dehydroisomerization of naphthenes

Methylcyclopentane, C_6H_{12} is catalytically isomerized and dehydrogenated to form benzene.

$$C_5H_9CH_3 \longrightarrow C_6H_6 + 3H_2 \tag{2}$$
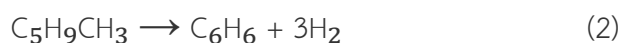
3. Dehydrocyclization of aliphatic hydrocarbons

Heptane is catalytically converted to toluene.

$$C_7H_{16} \longrightarrow C_6H_5CH_3 + 4H_2 \tag{3}$$
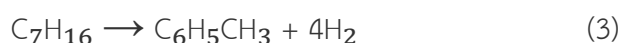
Small amounts of platinum on acidified alumina accomplish reactions (1), (2), and (3) readily.

4. Condensation of hydrocarbons

Heptane is catalytically converted to benzene during the cracking of petroleum at 500-800 °C.

$$C_7H_{16} \longrightarrow C_6H_6 + CH_4 + 3H_2$$

3.1.1 Industrial practice

Although not practiced under the name, aromatization is a cornerstone of oil refining. One of the major reforming reactions is the dehydrogenation of naphthenes into aromatics. The process, which is catalyzed by platinum, is exemplified in the conversion methylcyclohexane (a naphthene) into toluene (an aromatic) [32]. Dehydrocyclization converts paraffins (acyclic hydrocarbons) into aromatics [33]. A related aromatization process includes dehydroisomerization of methylcyclopentane to benzene:
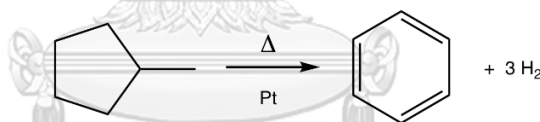
Figure 6: Example chemical equation for an aromatization reaction starting with methylcyclopentane.

3.1.2 Aromatization pathways

For cyclohexane, cyclohexene, and cyclohexadiene, dehydrogenation is the conceptually simplest pathway for aromatization. The activation barrier decreases with the degree of unsaturation. Thus, cyclohexadiene are especially prone to aromatization. Formally, dehydrogenation is a redox process. Dehydrogenative aromatization is the reverse of arene hydrogenation. As such, hydrogenation catalysts are effective for the reverse reaction [31].

3.2 Thermal cracking

Thermal cracking is a process in which hydrocarbons present in crude oil are subject to high heat and temperature to break the molecular bonds and breaking down long-chained, higher-boiling hydrocarbons into shorter-chained, lower-boiling hydrocarbons [35]. Thermal cracking is a refining process in which heat and pressure are used to break down, rearrange, or combine hydrocarbon molecules.

In 1913, the thermal cracking process was developed, which subjected heavy fuels to both pressure and intense heat, physically breaking the large molecules into smaller ones [31,35].

C_8H_{10} (p-xylene) $\longrightarrow$ $C_6H_6 + C_2H_4$

C_8H_{10} (o-xylene) $\longrightarrow$ $C_6H_6 + C_2H_4$

C_8H_{10} (m-xylene) $\longrightarrow$ $C_6H_6 + C_2H_4$

3.3 Dehydrogenation

Dehydrogenation is a chemical reaction that involves the removal of hydrogen from an organic molecule. It is the reverse of hydrogenation. Dehydrogenation is an important reaction because it converts alkanes, which are relatively inert and thus low-valued, to olefins, which are reactive and thus more valuable. Alkenes are precursors to aldehydes, alcohols, polymers, and aromatics [31]. Dehydrogenation processes are used extensively to produce aromatics and styrene in the petrochemical industry. Such processes are highly endothermic and require temperatures of 500 ℃ and above [31,32]. Dehydrogenation also converts saturated fats to unsaturated fats. Enzymes that catalyze dehydrogenation are called dehydrogenases.

$n-C_6H_{14}$ (hexane) $\longrightarrow$ $C_6H_{12} + H_2$
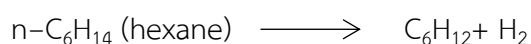
3.4 Hydrocracking

Hydrocracking is a catalytic cracking process assisted by the presence of added hydrogen gas. Unlike a hydrotreater, hydrocracking uses hydrogen to break C-C bonds (hydrotreatment is conducted prior to hydrocracking to protect the catalysts in a hydrocracking process). In the year 2010, 265×106 tons of petroleum was processed with this technology. The main feedstock is vacuum gas oil, a heavy fraction of petroleum [35].
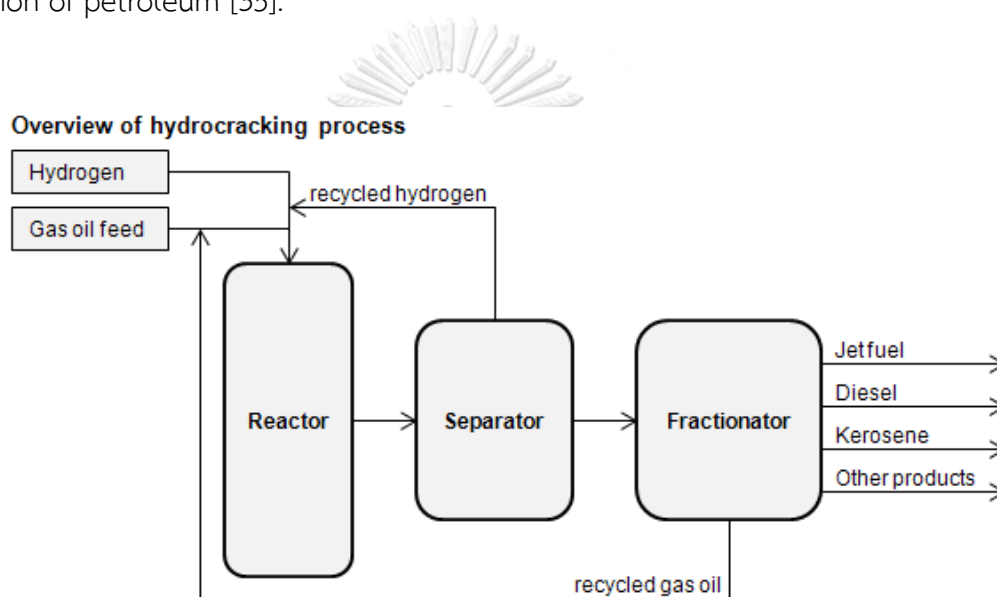
Figure 7: Example Hydrocracking Process.

The products of this process are saturated hydrocarbons; depending on the reaction conditions (temperature, pressure, catalyst activity) these products range from ethane, LPG to heavier hydrocarbons consisting mostly of isoparaffins. Hydrocracking is normally facilitated by a bifunctional catalyst that is capable of rearranging and breaking hydrocarbon chains as well as adding hydrogen to aromatics and olefins to produce naphthenes and alkanes [35,37].

$$C_8H_{10} \text{ (ethylbenzene (e)) + H}_2 \longrightarrow \quad C_7H_8 + CH_4$$
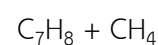
The major products from hydrocracking are jet fuel and diesel, but low Sulphur naphtha fractions and LPG are also produced [32]. All these products have a very low content of sulfur and other contaminants. It is very common in Europe and Asia because those regions have high demand for diesel and kerosene. In the US, fluid catalytic cracking is more common because the demand for gasoline is higher [39].

The hydrocracking process depends on the nature of the feedstock and the relative rates of the two competing reactions, hydrogenation and cracking. Heavy aromatic feedstock is converted into lighter products under a wide range of very high pressures (1,000-2,000 psi) and fairly high temperatures (750°-1,500 °F, 400-800 °C), in the presence of hydrogen and special catalysts [41].

The primary functions of hydrogen are, thus [40]:

1. preventing the formation of polycyclic aromatic compounds if feedstock has a high paraffinic content,
2. reducing tar formation,
3. reducing impurities,
4. preventing buildup of coke on the catalyst,
5. converting sulfur and nitrogen compounds present in the feedstock to hydrogen sulfide and ammonia, and
6. achieving high cetane number fuel.

3.5 Conversion of hydrocarbons to aromatics over different catalysts

3.5.1 HZSM-5 catalyst

n-Hexane (C_6H_{14}) reacted with HZSM-5 as a catalyst at 550℃, and W/F ratio is 20 g.h/mole. Then, products of the reactions would be hydrogen, methane, ethane, ethene, propane, propene, butane, butene 1-Pentene, cyclohexane, cyclohexene and

aromatics. The research shows mechanisms of hexane transformation, and the reactions are as follows [14]:

$$C_6H_{14} \longrightarrow C_6H_{12} + H_2$$
$$C_6H_{14} \longrightarrow C_6H_{10} + 2H_2$$
$$C_6H_{14} \longrightarrow C_5H_{10} + CH_4$$
$$C_6H_{14} \longrightarrow C_4H_8 + C_2H_6$$
$$C_6H_{14} \longrightarrow C_3H_8 + C_3H_6$$
$$C_6H_{14} \longrightarrow C_2H_4 + C_4H_{10}$$
$$nC_6H_{14} \longrightarrow aromatics$$
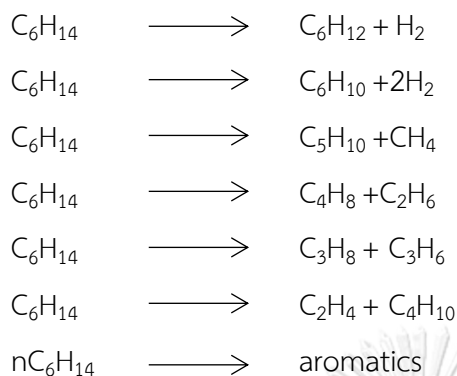
Moreover, there are another reaction step presented with the same conditions. Contrarily, products from the reactions occurred only propane, propylene and aromatics as shown below [14]:

$$C_6H_{14} \longrightarrow C_3H_8 + C_3H_6$$
$$C_6H_{14} \longrightarrow C_6H_6 + 4H_2$$
$$nC_6H_{14} \longrightarrow aromatics$$

Last but not least, the last reaction mechanism starts with hexane converting to hexene and by-product is hydrogen before aromatization from hexene. However, hexene oligomers can crack to be small hydrocarbon components [14,16].

$$C_6H_{14} \longrightarrow C_6H_{12} + H_2$$
$$nC_6H_{12} \longrightarrow C_6H_6 + 3H_2$$
$$nC_6H_{12} \longrightarrow aromatics$$
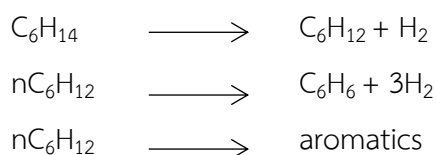
Above all, it is important for dehydrogenation of hexane at the first step by converting to hexene because of aromatic selectivity increase, which is illustrated in figure 8 and 9. They were operated at 550°C, 1 atm and W/F ratios equal to 1.4-11.4 g.h/mole [15,18].
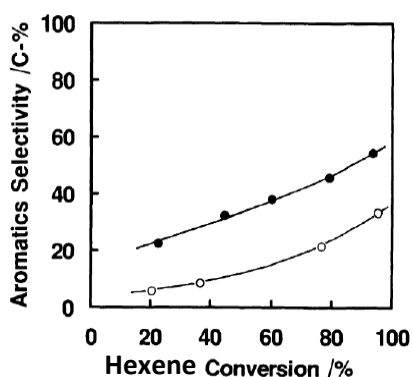
Figure 8: Relation between conversion of hexane and selectivity to aromatics on Ga loaded HZSM-5 (●) and HZSM-5 (○), Reaction conditions: 550 ℃, 1.4-11.4 g.h/mole, 1 atm.

Figure 9: Relation between conversion of hexene and selectivity to aromatics on Ga loaded HZSM-5 (●) and HZSM-5 (○), Reaction conditions: 550 ℃, 0.024-11.4 g.h/mole, 1 atm.

From the both figures 8 and 9, it can be seen that the selectivity of hexene from the main primary product of hexane aromatization over HZSM-5 rose significantly over hexene conversion to finish at just under 60% while the hexane selectivity is only almost 40%. The aromatics in the products chiefly included benzene, toluene, xylene and trimethylbenzene. In fact, methyl cyclohexadiene was found at the beginning on stream but it was an exception of the conversion. Therefore, hexene would be more preferable as a feedstock to reduce unnecessary by-products, especially C_1-C_3 hydrocarbons which would seldom be aromatic formation [15].

3.5.2 Ga loaded HZSM-5 catalyst

Hexane reacted with Ga-HZSM-5 as a catalyst at 400-550℃ of reaction temperatures and various W/F ratios. Then, products of the reactions would be hydrogen, methane, ethane, ethene, propane, propene, butane, butene 1-Pentene, cyclohexane, cyclohexene and aromatics. Selectivity of the products, was affected by increased conversion, is demonstrated in figure 10. From the research, aromatization steps that were divided into two conditions are demonstrated. Firstly, Ga on HSZM-5 was activated by protonic acidic sites [15].

$$C_6H_{14} \longrightarrow C_6H_{12} + H_2$$
$$nC_6H_{12} \longrightarrow C_6H_6 + 3H_2$$
$$C_6H_{14} \longrightarrow C_6H_{10} + H_2$$
$$C_6H_{10} \longrightarrow C_6H_6 + 2H_2$$
$$C_6H_{14} \longrightarrow C_2H_4 + C_4H_{10}$$
$$C_4H_{10} \longrightarrow C_3H_6 + CH_4$$
$$nC_3H_6 \longrightarrow aromatics$$
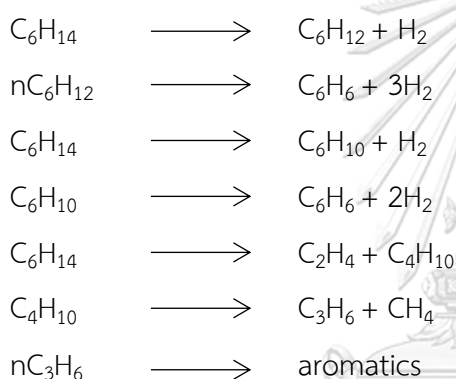
Secondly, Ga affected to the dehydrogenation of hexane directly without the protonic sites. It appears that the protonic sites would be desired for aromatization. From the involvement of the protonic sites, oligomers of formed hexene could be cracked into smaller molecules [17,18]. However, Ga loaded on HZSM-5 would significantly enhance aromatization. In detail, a very large majority of hexane molecules was influenced by Ga for dehydrogenation accelerating [15]. They are presented in figure 8 and figure 9 [15].
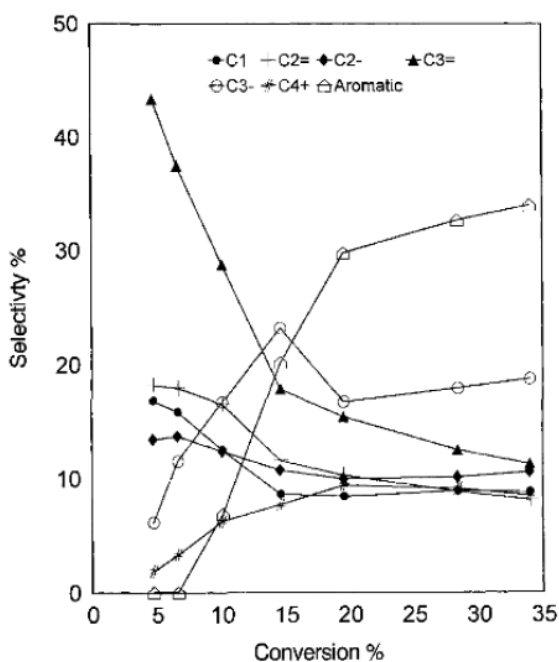
Figure10: Effect of increased conversion on product selectivity on Ga-HZSM-5 at different W/F ratios. Reaction temperature 550 ºC process time 1 hour.

Temperature could be quite affected to the results, for instance, conversion and product selectivity from table 2 [18].

Table 2: The effect of temperature on the product selectivity at low conversion level over Ga-HZSM-5 (Si/Al = 50)

	Reaction temperature, °C				
	300	350	400	450	500
Conversion (%)	0.2	1.0	6.3	12.1	29.3
Products selectivity (%)					
C1–C5	1.4	1.4	4.2	9.4	28.9
Hexenes	3.9	16.8	7.0	5.5	1.5
Benzene	0.0	0.0	3.0	5.9	22.7
Toluene	0.0	18.2	19.0	24.0	25.5
Heptenes	66.6	45.2	24.9	22.4	4.5
Octenes	28.1	15.2	7.6	9.2	3.1
Ethylbenzene	0.0	0.0	20.6	15.7	8.6
m- and p-xylene	0.0	3.3	2.8	1.9	1.4
o-Xylene	0.0	0.0	11.0	6.1	3.8

Reaction conditions: H_2/n-C8 molar ratio 6 : 1, WHSV 5 h^{-1}, 10 h on stream.

3.5.3 Mo₂C/ HZSM-5 catalyst

The aromatization was operated from n-hexane over Mo$_2$C /HZSM-5 with different concentration at 540 $^\circ$C and 1 atm for 1 hour. The products and conversion demonstrate in table 3. Moreover, temperature influence of the reaction illustrates in table 4.[19]

Table 3: Effect of Mo loading on the aromatization on n-C$_6$H$_{14}$ at 540 $^\circ$C over Mo$_2$C /HZSM-5 catalyst (SiO$_2$/Al$_2$O$_3$ = 80), the data were taken at 60 min on stream)

Mo (wt%)	0	0.5	3	10	15	20	40
Conversion (%)	77.5	58.6	70.4	71.3	64.1	61.7	50.1
Yield of aromatics (%)	10.4	9.6	26.8	28.5	23.6	23.2	17.1
Product distribution (%)							
CH4	9.5	10.0	12.3	12.3	11.4	10.0	10.1
C2H6	17.3	19.3	17.3	16.6	14.5	15.6	11.9
C2H4	20.1	17.6	9.5	8.6	11.0	11.7	11.9
C3H8	14.4	10.7	4.5	4.6	4.6	4.5	3.4
C3H6	17.5	17.0	10.2	9.7	11.5	11.9	14.1
C4H10	1.2	1.6	1.8	1.7	1.5	1.6	2.1
C4H8	5.7	6.1	5.9	6.0	5.5	7.3	11.9
C5	0.9	0.8	0.4	0.3	0.5	0.5	0.4
Aromatics	13.4	16.4	38.1	40.0	36.0	36.8	34.1
Aromatics distribution (%)							
C6H6	32.1	33.1	39.3	42.2	43.6	39.0	45.2
C7H8	47.0	46.2	38.7	36.9	35.4	38.4	36.3
C8H10	18.4	17.6	14.3	14.0	13.6	14.1	13.4
C9+	2.8	3.1	7.7	6.8	7.5	8.6	5.2

Table 4: Effect of reaction temperature on the product distribution during the reaction of n-hexane over Mo_2C /HZSM-5 (10wt.% Mo, SiO_2/Al_2O_3 = 30, the data were taken at 60 min on stream)

Temperature (^oC)	380	420	460	500	540
Conversion (%)	17.5	35.1	56.2	84.5	99.1
Product distribution (%)					
CH4	1.1	2.5	6.0	14.8	27.1
C2H6	8.7	15.1	21.9	22.8	16.1
C2H4	2.4	2.4	2.0	2.5	1.4
C3H8	36.4	26.2	14.8	5.1	1.1
C3H6	6.4	5.8	4.6	2.6	0.4
C4H10	6.6	3.8	2.2	0.4	0.0
C4H8	4.7	5.4	3.3	1.4	0.1
C5	4.4	1.6	0.2	0.0	0.0
Aromatics	29.2	37.2	45.0	50.4	53.8
Aromatics distribution (%)					
C6H6	11.4	16.2	25.1	39.6	50.8
C7H8	43.9	46.8	43.6	32.6	23.7
C8H10	34.0	27.1	19.6	11.8	5.2
C9+	10.8	9.8	11.6	16.0	20.3

3.5.4 H-GaAlMFI catalyst

Aromatization from n-paraffins were performed at 400 ^oC over H-GaAlMFI zeolite with different space velocities from 3100 to 58100 CM^3/g.h. Certain products appear in figure 11 and 12 which also show product selectivity and distribution [22].
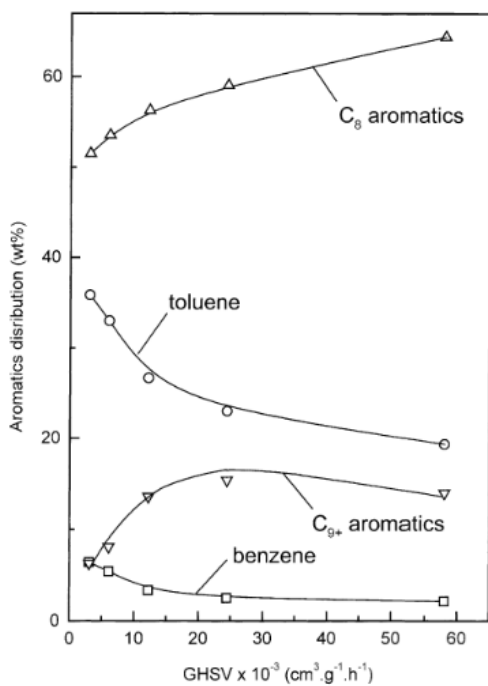
Figure 11: Dependence on the space velocity of the aromatics formed in the n-hexane aromatization.
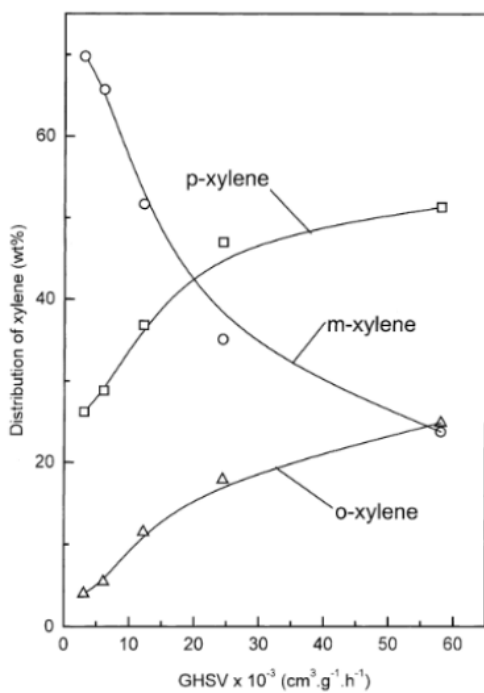
Figure 12: Dependence on the space velocity of the distribution of xylene isomers formed in the n-hexane aromatization.

3.5.5 Pt/KL-VPI, Pt/KL-IWI, and Pt/SiO$_2$ catalysts

Ajao และ Akande (2009) studied the production of aromatic from n-Octane on a Pt/KL catalyst prepared by vapor-phase impregnation. The activity for *n*-octane aromatization at 500 °C and 1 atm was low and it quickly dropped after a few hours on stream. The product distribution obtained from the n-octane conversion showed benzene and toluene as the dominant aromatic compounds, with small quantities of ethylbenzene (EB) and o-xylene (OX), which are the expected products from the direct closure of the six-member ring. The analysis of the product evolution as a function of conversion indicated that the benzene and toluene are secondary products resulting from the hydrogenolysis of ethylbenzene and o-xylene.
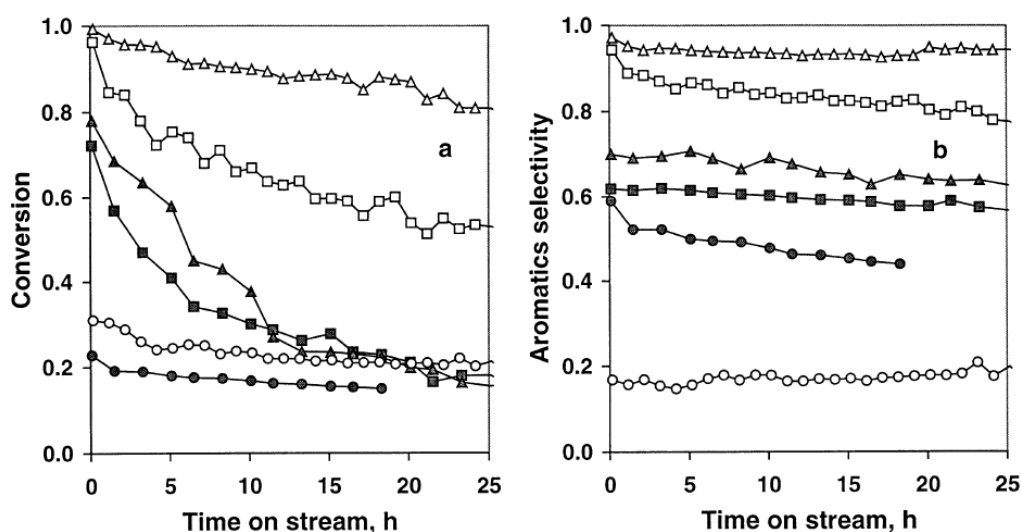
Figure 13: (a) Total conversion of n-hexane (open symbols) and n-octane (full symbols) as a function of time on stream. (b) Selectivity to total aromatics as a function of time on stream. Reaction conditions: 500 °C, H$_2$/n-C6 (n-C8) molar ratio 6: 1, WHSV 5 h^{-1}.

The Pt/KL-VPI, Pt/KL-IWI, and Pt/SiO2 catalysts were tested for the aromatization of *n*-octane and compared to that of *n*-hexane. The evolution of the conversion and total aromatics selectivity are shown in Figs. 13a and 13b, respectively. In agreement with previous reports [27,28,30], the VPI Pt/KL exhibited

the highest *n*-hexane aromatization conversion, benzene selectivity, and stability. Contrasting with the excellent performance obtained on this catalyst with *n*-hexane, the selectivity and stability were disappointingly low when the feed was changed to *n*-octane. In fact, Fig. 13a shows that for the *n*-octane aromatization the stability of Pt⁄SiO2 was somewhat better than that of Pt⁄KL, although the overall conversion was very low. Interestingly, over the Pt⁄SiO2 catalyst, the aromatic selectivity with *n*-octane was considerably higher than that with *n*-hexane, which contrasts with the behavior observed over the Pt⁄KL catalysts [40].

Table 5: Product distribution from n-hexane and n-octane aromatization

Product distribution from *n*-hexane and *n*-octane aromatization

	Feed: *n*-hexane			Feed: *n*-octane			
	Pt/SiO$_2$	Pt/KL-IWI	Pt/KL-VPI	Pt/SiO$_2$	Pt/KL-IWI	Pt/KL-VPI	Pt/KL-VPI-KOH
Coniversion (%) (after 10 h on stream)	18.8	71.1	90.6	16.8	30.1	37.7	14.3
Products (%)							
C1–C5	8.8	22.4	12.2	7.1	34.0	29.4	32.6
Hexenes	78.7	5.9	0.7	3.5	1.2	0.7	5.4
Benzene	15.1	85.6	93.6	0.0	27.4	27.7	19.2
Toluene	–	–	–	0.9	22.8	28.3	26.0
Heptenes	–	–	–	34.8	2.6	3.0	1.8
Octenes	–	–	–	5.4	1.4	1.9	1.4
Ethylbenzene	–	–	–	21.5	5.9	6.5	9.2
m-Xylene	–	–	–	1.2	1.1	1.2	1.2
p-Xylene	–	–	–	0.4	0.3	0.2	0.2
o-Xylene	–	–	–	24.8	2.8	3.0	3.0
Total aromatics	15.1	85.6	93.6	48.8	60.2	69.2	58.7

Reaction conditions: 500 °C, H_2/n-C6 (or *n*-C8) 6 : 1 molar ratio, WHSV 5 h^{-1}, 10 h on stream.

Table 5 summarizes the product distribution obtained after 10 h on stream over the Pt⁄SiO2, Pt⁄KL-IWI, Pt⁄KLVPI, and Pt⁄KL-VPI-KOH catalysts for *n*-hexane and *n*-octane aromatization. As mentioned above, when *n*-hexane was the feed, the Pt⁄KL catalysts, particularly the one prepared by VPI, exhibited high conversion and high benzene selectivity while the Pt⁄SiO2 showed much lower ability to produce aromatics [38]. In fact, its main product was hexene from direct dehydrogenation. A different result was obtained when *n*-octane was used as feed. Although the selectivity to total aromatics was higher over Pt⁄KL than on Pt⁄SiO2, the aromatics obtained with Pt⁄KL were mostly benzene and toluene. By contrast, the Pt⁄SiO2 catalyst produced mostly ethylbenzene (EB) and *o*-xylene (OX) as its dominant

aromatization products, but no benzene was produced at any time [41]. The differences in the aromatic product distribution obtained over Pt/KL and Pt/SiO2 are better illustrated in figure 14, which shows the ratio of benzene to C8 aromatics produced from n-octane as a function of time on stream. This ratio was initially very high for the two Pt/KL catalysts. Although it decreased with time on stream, the amount of benzene was at any time higher than three times that of the n-octane aromatics.
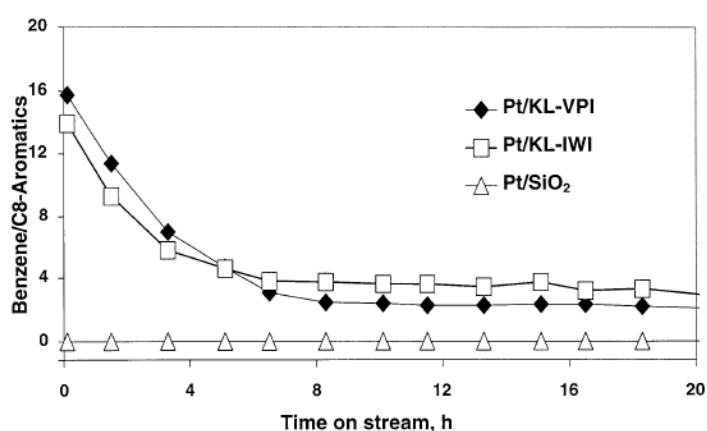
Figure 14: Benzene to C8-aromatics product ratio during n-octane aromatization as a function of time on stream over Pt/KL-VPI, Pt/KL-IWI, and Pt/SiO2 catalysts. Reaction conditions: 500 °C, H2/n-C8 molar ratio 6: 1, WHSV 5 h^{-1}.

Another important difference between Pt/KL and Pt/SiO2 is interesting to note. As shown in Table 5, over Pt/SiO2 the production of OX was only slightly higher than that of EB. The decay of both products as a function of time was almost parallel. As a result, the EB/OX ratio remained constant with time on stream. On the other hand, Pt/KL exhibited a much higher production of EB than OX. The drop in OX production was much more rapid than that of EB [29]. As illustrated in figure 15, the EB/OX product ratio obtained on the VPI Pt/KL catalyst rapidly increased during the first 7h and stayed at a value of about 2.5, much higher than that reported for other Pt catalysts supported on nonacidic materials without microporosity [34]. A slight but clear difference between the IWI and VPI Pt/KL catalysts can be noted here. On the IWI catalyst, the EB/OX ratio started at a high value of about 2.0 from the very first

moments on stream. After about 7 h, this ratio was about the same for both catalysts. As discussed below, it is important to note that high EB/OX ratios have only been observed on Pt/zeolite catalysts [35], which reveal the role that shape-selectivity may have in this reaction. Therefore, the difference observed on the two Pt/KL catalysts before coke deposition might be related to slight differences in the molecular transit inside the zeolite pores related to the different metal particle sizes. After several hours on stream, the coke deposits that partially block the pores may erase the initial differences.
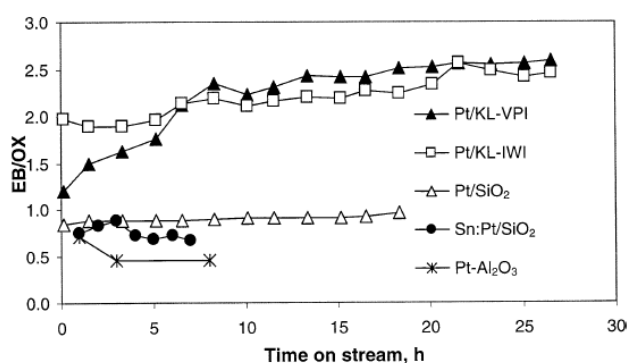
Figure 15: Ethylbenzene: o-xylene (EB/OX) ratio during n-octane aromatization over Pt/KL-VPI, Pt/KL-IWI, and Pt/SiO2 catalysts.

Reaction conditions: 500 °C, H2/n-C8 molar ratio 6:1, WHSV 5 h^{-1}.
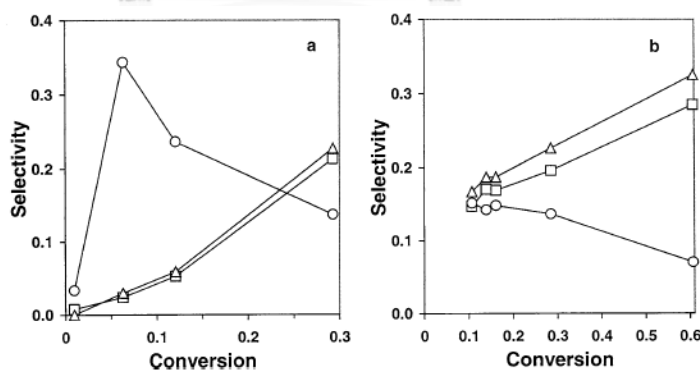
Figure 16: Steady-state product selectivity as a function of conversion during n-octane aromatization.

(a) Conversion varied by increasing temperature from 300 to 500 °C, at a fixed WHSV = 5 h^{-1}. (b) Conversion varied by changing the WHSV from 9 to 1 h^{-1}, at a fixed temperature 500 °C. Circles: C8-aromatics; triangles: toluene; squares: methane.

Figure 16(a) shows the variation of the steady-state product selectivity with conversion as the reaction temperature was varied from 300 to 500 °C, at a fixed WHSV = 5 h^{-1}. It can be observed that the selectivity to methane continuously increased with conversion. The selectivity to C8 aromatics exhibited a maximum at about 6.5% conversion and then it decreased. This decrease is accompanied by an increase in the production of benzene, indicating that benzene is a secondary product, which results from hydrogenolysis of C8 aromatics, rather than from cyclization of previously hydrogenolyzed *n*-octane [42]. The detailed product distribution and the corresponding temperatures and conversions are shown in Table 6, which clearly illustrates the enhanced hydrogenolysis of EB and OX to benzene and toluene at higher temperatures.

Figure 6(b) shows a similar graph of steady-state selectivity vs conversion, but in this case, the conversion was varied by changing the WHSV from 9 to 1 h^{-1}, at a fixed temperature (500 °C). In line with the results obtained by varying the temperature, the data shows that at higher conversions the selectivity to C8 aromatics dropped while the amount of benzene and methane increased [44]. The detailed product distribution is reported in Table 7. An interesting trend in the EB/OX ratio as a function of space velocity is clearly apparent. As illustrated in figure 17, EB/OX ratio markedly drops approaching a value of about one as the space velocity decreases.

Table 6: Product distribution of n-octane aromatization over Pt/KL-VPI at various reaction temperatures

	Reaction temperature, °C				
	300	350	400	450	500
Conversion (%)	0.2	1.0	6.3	12.1	29.3
Products selectivity (%)					
C1–C5	1.4	1.4	4.2	9.4	28.9
Hexenes	3.9	16.8	7.0	5.5	1.5
Benzene	0.0	0.0	3.0	5.9	22.7
Toluene	0.0	18.2	19.0	24.0	25.5
Heptenes	66.6	45.2	24.9	22.4	4.5
Octenes	28.1	15.2	7.6	9.2	3.1
Ethylbenzene	0.0	0.0	20.6	15.7	8.6
m- and *p*-xylene	0.0	3.3	2.8	1.9	1.4
o-Xylene	0.0	0.0	11.0	6.1	3.8

Reaction conditions: H$_2$/*n*-C8 molar ratio 6 : 1, WHSV 5 h^{-1}, 10 h on stream.

Table 7: Product distribution of n-octane aromatization over Pt/KL-VPI at various WHSV

	WHSV, h^{-1}				
	1.0	3.0	5.0	7.0	9.0
Conversion (%)	60.7	28.5	16.1	14.0	10.7
Products selectivity (%)					
C1–C5	34.5	28.5	26.4	26.7	24.1
Hexenes	0.65	1.9	2.7	2.8	3.1
Benzene	32.5	22.6	18.7	18.7	16.7
Toluene	23.3	26.1	25.1	24.8	25.1
Heptenes	1.0	3.1	4.6	4.3	5.1
Octenes	1.0	4.0	7.4	8.2	10.4
Ethylbenzene	3.5	8.2	9.6	9.2	10.0
m- and *p*-xylene	1.1	1.6	1.6	1.6	1.6
o-Xylene	2.4	3.9	3.7	3.5	3.6

Reaction conditions: 500 °C, H_2/n-C8 molar ratio 6 : 1, 10 h on stream.
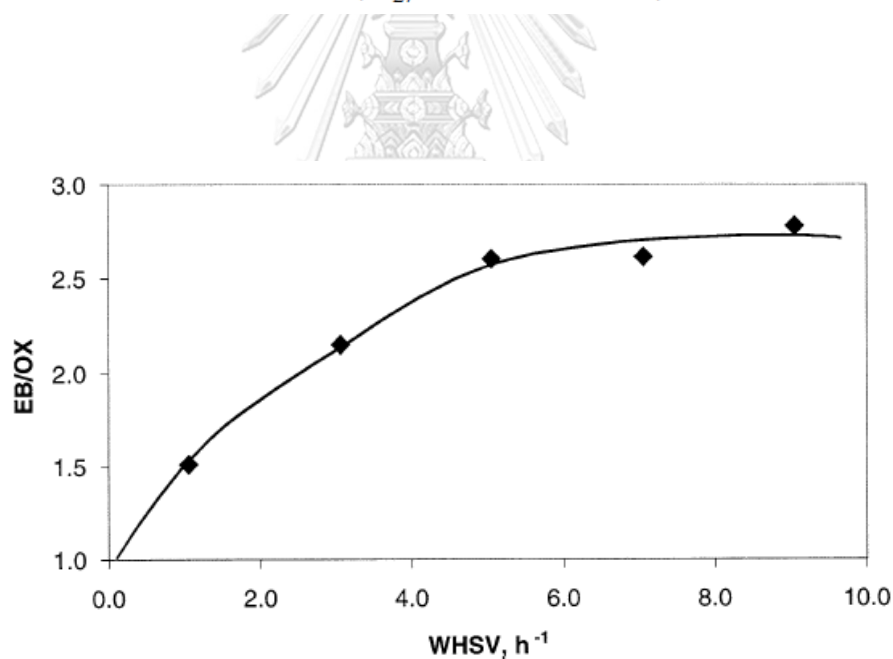
Figure 17: Ethylbenzene: o-xylene (EB/OX) ratio during n-octane aromatization over the Pt/KL-VPI catalyst as a function of space velocity.

Reaction conditions: 500 °C, H2/n-C8 molar ratio 6 : 1, 10 h on stream.

An aspect that in some studies of Pt/KL catalysts has been neglected is the role of residual acidity on the zeolite, but it may have very detrimental effects on selectivity and catalyst life. It has been shown [45,46] that the C1–C5 products greatly increase when residual acidity is present on the zeolite. We may ask whether, in our case, the presence of residual acidity has an effect on the secondary hydrogenolysis of EB and OX to benzene and toluene. To analyze the effect of residual acidity we may compare the product distribution of the Pt/KL catalysts with that of the KOH-treated catalyst, which should have any residual acidity eliminated. The first difference is the drop in conversion observed on the KOH-treated catalyst. This drop may be due to the loss of metal area caused either by leaching or pore plugging during the treatment in the KOH solution [49]. However, the most important comparison is the production of the secondary products benzene/toluene relative to the C8 aromatics. The benzene/EB ratio obtained on the KOH-treated catalyst was about half of that obtained on the untreated Pt/KL catalysts, indicating that some residual acidity may have existed on the untreated catalysts and it may enhance the EB-to-benzene conversion. However, it is important to note that, even when all possible residual acidity has been removed, the catalyst still had a high level of EB and OX secondary hydrogenolysis activity [51]. Therefore, the high conversion of EB and OX into benzene and toluene is mostly due to the geometric constraints of the zeolite channels.

Table 8: Product distribution of different feeds over Pt/KL-VPI catalysts

	Reactant				
	n-Octane	Ethylbenzene	*o*-Xylene	Toluene	*n*-Heptane
Conversion (%)	37.7	71.5	16.7	64.9	36.4
Products selectivity (%)					
C1–C2	27.0	20.1	11.8	15.4	21.6
C3–C5	2.4	0.0	0.0	0.0	6.2
Hexenes	0.7	0.00	0.0	0.0	7.5
Benzene	27.7	46.5	6.4	84.3	28.5
Toluene	28.3	32.9	78.9	–	33.1
Heptenes	3.0	0.0	0.0	0.0	2.3
Octenes	1.9	0.0	0.2	0.0	0.0
Ethylbenzene	6.5	–	0.2	0.0	0.0
m- and *p*-xylene	1.4	0.0	1.8	0.0	0.0
o-Xylene	3.0	0.2	–	0.0	0.0

Reaction conditions: 500 °C, H_2/reactant molar ratio 6 : 1, WHSV 5 h^{-1}, 10 h on stream.

To further investigate the effect of secondary reactions on the product distribution, we conducted activity measurements using n-C_7 as well as C_7 and C_8 aromatics as feed, keeping the same H_2: reactant molar ratio of 6: 1 as for the n-octane activity measurements. The results obtained at 500 °C and at a WHSV of 5 h^{-1} are summarized in Table 8. The vast majority of the products of C_8 aromatics come from hydrogenolysis of the alkyl groups attached to the aromatic ring. The conversion of EB and OX only resulted in C_1, C_2, benzene, and toluene. No ring-opening products and very small amounts of isomerization products were observed. Very different deactivation patterns were exhibited by the different aromatic compounds. As illustrated in figure 18, the OX conversion dropped much more rapidly than the EB conversion, which could be explained in terms of the different diffusion rates of the two aromatics through the zeolite channels. To illustrate this difference, the interaction of EB, OX, and toluene with the KL zeolite was further investigated using the static volumetric adsorption apparatus. The uptakes of EB, OX, and toluene after the bare zeolite was exposed to the same initial pressure of hydrocarbon vapor is summarized in Table 9. It is seen that the OX uptake was significantly lower than those of EB and toluene, which can be rationalized in terms of the critical molecular diameters relative to the zeolite pore size. The pore size of the KL zeolite is 0.71 nm [47], which is larger than the critical diameters of EB and toluene but smaller than that of OX. Therefore, one can expect that the mobility of OX inside the channels of the zeolite will be very much restrained.
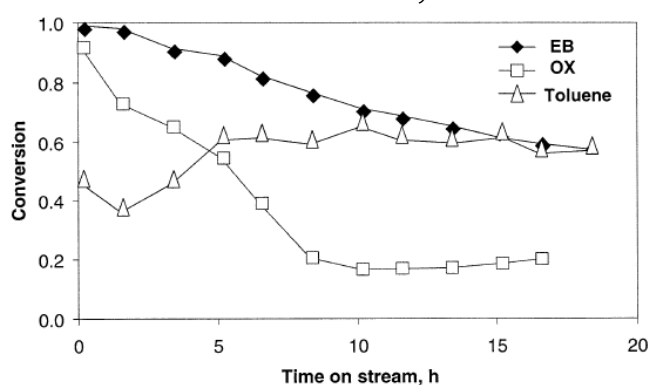
Figure 18: Total conversion of different hydrocarbons over the Pt/KL-VPI catalyst as a function of time on stream.

Reaction conditions: 500 °C, H2/hydrocarbon molar ratio 6 :1 WHSV5 h^{-1}.

Table 9: Hydrocarbon uptakes on the KL zeolite as measured in a static volumetric apparatus

	Toluene	Ethylbenzene	*ortho*-Xylene
Temperature (°C)	180	180	180
Initial moles in cell	7.6×10^{-5}	7.1×10^{-5}	6.9×10^{-5}
Equilibrium pressure (Torr)	1.7	2.5	5.9
Moles adsorbed	5.7×10^{-5}	4.4×10^{-5}	0.6×10^{-5}
Critical molecular diameter (nm)	0.67	0.67	0.74

In the experiments conducted at low space velocities one may expect that EB would have the time to come out of the zeolite and reenter, so eventually the secondary conversion erases the differences as it is experimentally verified (see figure 17). As the space velocity increases, the EB that diffuses out of the zeolite is removed more quickly from the catalyst bed and does not have time to continue reacting.

The more rapid deactivation displayed when the reactant was OX than when it was EB (see figure 18) also reflects the longer residence time that the OX molecule may have inside the zeolite. Another evidence for the important role of diffusion in selectivity is the variation of the EB/OX ratio as a function of time on stream. As shown in figure 15, the ratio on the very clean VPI Pt/KL catalyst is initially near unity, but very rapidly starts increasing as coke begins to make the diffusion of OX through the pores more difficult. On the IWI catalyst, the presence of larger Pt clusters makes the diffusion of OX slower, even on the clean catalyst. As a result, the EB/OX ratio on this catalyst is higher from the start.

It is highly possible that the C8 aromatics produced inside the channels of the zeolite are responsible for the rapid deactivation observed during n-octane aromatization, as opposed to the high stability displayed during n-hexane aromatization. As mentioned above, they may spend more time inside the zeolite and they are the only new species that appear in the system, compared to the

situation in n-hexane aromatization [49]. The other species that could result in coke formation are benzene and olefins, but they are also present during the n-hexane aromatization, but they cause no significant deactivation if when the Pt/KL catalyst is well prepared.

A final comment on the effect of pressure is important. The rapid deactivation observed with C_8 feed at atmospheric pressure may not be necessarily the same at the higher pressures typically used in industrial operations [48]. Differences in product distribution and catalyst lifetime have been observed between the lab and industrial operations in this process.

3.5.6 Mo_2C-containing catalysts

Róbert Barthos and Frigyes Solymosi. [53] studied Aromatization of n-heptane on Mo_2C-containing catalysts. The reaction pathways of n-heptane were studied on various Mo2C-containing catalysts. Unsupported Mo_2C catalyzed the dehydrogenation and cracking of n-heptane even at 573–623 K. The catalytic performance of Mo_2C was improved when Mo_2C was deposited in a highly dispersed state on various supports, like silica, alumina, and ZSM-5. The best yield of the formation of aromatics (48.7%) was obtained for 5% Mo_2C /ZSM-5 (SiO_2/Al_2O_3 = 80) at 873 K. The results obtained were interpreted by the monofunctional (pure Mo_2C), and bifunctional mechanism (supported Mo_2C) of the aromatization of n-heptane.

The direct conversion of alkanes into aromatics is an important industrial process that has been the subject of extensive research. The results obtained on various catalysts and the possible mechanisms of this complex process are well documented in several excellent reviews [51,52,53]. Early studies focused mainly on supported Pt catalysts, which exhibited outstanding catalytic performance among the metals [57,58]. Two mechanisms were proposed: a bifunctional mechanism involving both the metal and the acid sites of the support, and a monofunctional mechanism involving only the metallic sites [55]. Coke formation in the hydrocarbon transformation reactions over Pt metals caused a serious problem, however; L-type

zeolites, then later ZSM-5, loaded with Pt were found to be more active and selective for the aromatization of n-heptane [52–56,59]. The formation of coke in this case is severely restricted in the channels of ZSM- 5 zeolite. But the high acidity of H-form zeolite led to increased cracking activity [55]. Therefore, it appeared necessary to balance the zeolite acidity and to compensate for its decrease with some additives, which greatly improved the catalytic performance of ZSM-5 [50].

All of these studies were exclusively restricted to the reactions of C_2–C_7 compounds, because no catalyst combination could convert methane into aromatics [51–55]. A milestone in this area occurred when a Chinese group observed that MoO_3/ZSM-5 catalyst can transform methane into benzene with 80–100% selectivity at a 10–12% conversion level [51]. Subsequent studies revealed that MoO_3 is reduced and converted into Mo_2C during the early phase of the reaction, and that Mo2C activates methane, resulting in the formation of benzene on ZSM-5 [52–56]. Further investigations showed that Mo_2C is also an active catalyst toward the reaction of C_2–C_4 alkanes into aromatic compounds. However, its effect was mainly exhibited when it was deposited on ZSM-5 or on silica surface containing acidic centers. Pure Mo_2C catalyzed only the decomposition and dehydrogenation of alkanes, but aromatics were produced only in trace amounts [51–53]. An exception was the hexane, the aromatization of which occurred on pure Mo2C with a selectivity of ∼65% at a conversion of ∼25% [54]. Here we report on the aromatization of n-heptane on unsupported and supported Mo_2C catalysts. n-Heptane is one of the components of natural gas liquids (NGL), and its reforming to olefins and aromatics is of practical importance [53–55].

3.5.6.1 Reaction on pure Mo_2C

Mo_2C prepared by the C_2H_6/H_2 gas mixture exhibited relatively high activity. The decomposition of heptane started at 573 K, and the conversion reached an initial value of 20–23% at 823 K (figure 19A). To obtain more information on the initial performance of the catalysts and to avoid the effect of its deactivation, the

reacting gases were replaced by argon during the product analysis in the first 30–60 min. Further increases in temperature led to a very fast deterioration of the catalyst, likely as a result of carbon deposition. At lower temperatures (573–623 K), the main process is the dehydrogenation with some cracking. Various types of heptenes were formed in this reaction. At 673–823 K, the dehydroaromatization of heptane became the dominant reaction, yielding toluene and benzene, with selectivity increasing with increasing temperature. At 823 K, these values were ~43% for toluene and ~8% for benzene, with heptene selectivity of ~26–28%. Note that CO was also observed during the reaction at 823–873 K, indicating that the Mo oxide was not fully converted into Mo2C [48]. Another possibility was that the partial oxidation of Mo_2C occurred in the passivation of freshly prepared Mo_2C. To exclude the possible role of Mo oxycarbide, the preparation was made in situ without treatment with a 1% O2/He stream at 300 K. Although the production of a small amount of CO was seen at 823 K at the beginning of the heptane reaction, the catalytic performance of Mo_2C was practically the same as that shown in the figure 19A.
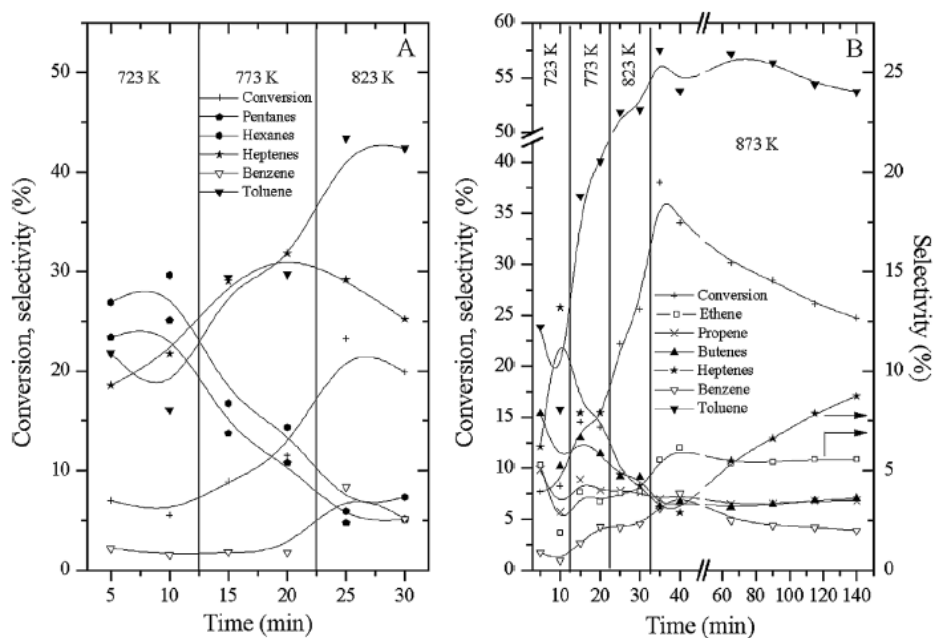
Figure 19: Reaction of n-heptane over Mo_2C

(A) and 2% Mo_2C/Al_2O_3 (B) catalysts at different temperatures.

3.5.6.2 Reaction on supported Mo$_2$C

Somewhat different behavior was seen when Mo$_2$C was prepared on an alumina surface. Both the conversion and selectivity of toluene increased with increasing temperature. In this case, fast deactivation at 873 K was not observed; the heptane reaction was measurable for a longer period [55]. The selectivity of toluene was 57% and that of benzene was 5–7% at 35–30% conversion on 2% Mo$_2$C/Al$_2$O$_3$. The selectivity of heptenes was low (<15%) throughout the measurements at 723–873 K (figure 19B). Nearly the same values were calculated for butene and propene. 2% Mo$_2$C on silica exhibited similar catalytic performance. But at 873 K, the selectivity of toluene and benzene was lower, 15 and 5%, respectively, at a conversion of 34%. With a greater amount of Mo$_2$C (10%), toluene selectivity reached its maximum value, 55–65% at 823 K with a conversion of 10–14%. At 873 K, the initial conversion was 26.5–22.0%, but toluene selectivity decayed to 32% and then to 17–12%. On both catalysts, heptenes formed with a selectivity of 6–15%. Similar to the pure Mo$_2$C, the silica-based catalysts rapidly lost their catalytic efficiency at 823–873 K; some data are given in Table 10.

Table 10: Characteristic data for the reaction of n-heptane on different catalysts at 873 K[a]

Catalyst	Conversion (%)	Selectivity (%)									Yield of aromatics
		Methane	Ethene	Propene	Propane	Butenes	Heptenes	Benzene	Toluene	Xylenes	
Mo$_2$C	18.8	2.6	4.1	5.0	0.4	2.8	23.9	3.0	19.7	0.1	3.9
Mo$_2$C[b]	21.5	1.0	0.5	1.9	0.2	4.0	31.4	6.0	43.0	0.0	8.6
2% Mo$_2$C/Al$_2$O$_3$	34.1	3.3	6.1	7.4	1.7	6.7	2.9	7.5	53.8	0.3	21.0
2% Mo$_2$C/SiO$_2$	34.4	3.4	10.2	25.5	0.8	27.4	5.5	5.4	15.4	0.8	7.4
10% Mo$_2$C/SiO$_2$	22.5	6.9	1.7	3.2	0.3	7.2	15.3	6.2	18.7	0.5	5.8
10% Mo$_2$C/SiO$_2$[b]	12.5	1.0	0.5	1.0	0.1	1.6	20.0	4.0	60.0	0.9	7.9
H-ZSM-5(80)	96.7	5.8	24.0	20.0	9.8	5.9	–	8.4	9.3	2.9	20.2
2% Mo$_2$C/ZSM-5(80)	99.6	11.0	14.2	7.3	8.9	1.7	–	22.7	20.2	5.7	48.7
5% Mo$_2$C/ZSM-5(80)	99.9	14.1	11.4	4.9	5.4	0.6	–	27.4	23.3	6.0	57.2
10% Mo$_2$C/ZSM-5(80)	80.6	5.7	15.5	31.3	5.9	14.6	0.2	8.5	8.8	0.4	14.3
ZSM-5(280)	91.5	3.3	19.9	28.4	11.2	11.3	–	2.6	3.4	1.8	7.2
2% Mo$_2$C/ZSM-5(280)	82.6	2.5	14.6	27.6	10.0	13.3	0.1	4.5	8.8	1.6	12.4

[a] Data were taken at 10 min of time on stream.
[b] At 823 K.

More attractive results were obtained when Mo$_2$C was combined with zeolites. We choose two ZSM-5 samples with SiO2/Al2O3 ratios of 80 and 280,

respectively. In harmony with previous studies [51,53,54], even in a pure state the ZSM-5(80) is active toward the conversion of heptane into other compounds. The reaction on ZSM-5(80) was observed at very low temperature (～523 K), but the formation of aromatics, xylene, and benzene occurred to a measurable extent only above 573 K. At 773 K, the main products were propane, propene, ethene, butanes, and butenes. The conversion reached ～92% at 823 K and ～96% at 873 K. At the latter temperature, propene (S = 20%), ethylene (S = 24%) formed with the highest selectivity; this value was ～9% for both the xylene and benzene. ZSM-5(280) was less active and its aromatizing property was also lower. The total selectivity of aromatics was <4–5% even at 873 K. Heptenes were not identified on these zeolites at 450–873 K.

Deposition of 2% Mo_2C on the ZSM-5(80) samples enhanced the rate of heptane decomposition measured on pure ZSM-5(80). The formation of cracking products, hexane, pentane, propane, propene, butane, and butenes was observed even at 473–523 K. With increasing temperature, their evolution increased up to 673 K, then decreased. Hexane was an exception, because its production above 673 K decreased. At the same time, dehydrogenation set in at 573 K, as indicated by the formation of H_2 and heptenes with a very low selectivity of 2%. Heptenes disappeared from the products at 623–673 K, when the formation of toluene, benzene, and xylene became prominent. In contrast to the previously studied catalysts, in which toluene was the main aromatic compound on 2% Mo_2C /ZSM-5, the selectivity of benzene approached that of toluene at 823 K and became even higher at 873 K. At 873 K, the total selectivity of aromatics reached a value of ～49%. This catalyst exhibited a very stable activity, with conversion decaying by only a few percentage points even after 10 h and the aromatizing capability remaining high. These findings are illustrated in figure 20.
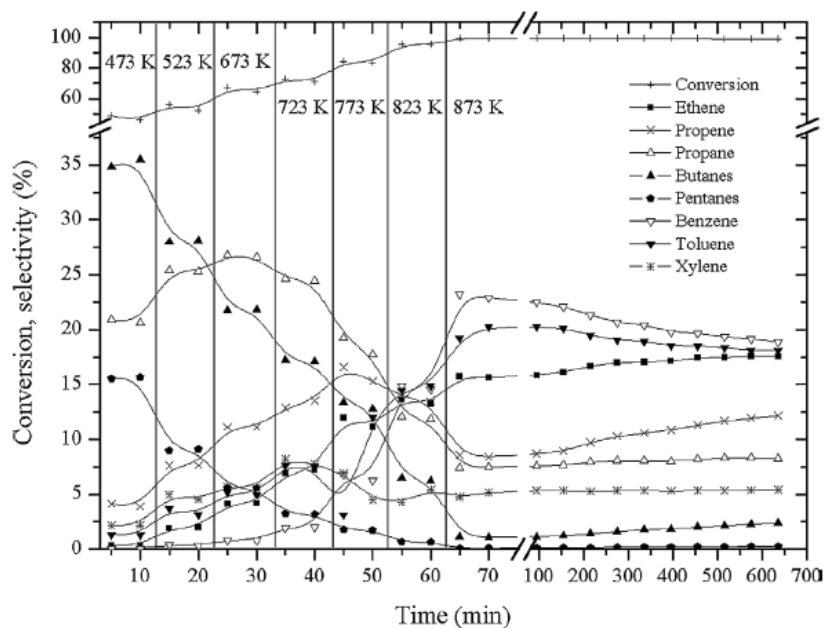
Figure 20: Reaction of n-heptane over 2% Mo$_2$C /ZSM-5(80) at different temperatures.

Higher loading of Mo$_2$C (5%) further increased the selectivity of aromatics to ～57%, while decreasing the selectivity of ethylene, propene, butene, and butane. Heptenes were practically absent. Less activity was exhibited by 10% Mo$_2$C /ZSM-5. The effects of loading of Mo$_2$C are displayed in Figure 21. The promoting effect of Mo$_2$C was experienced in the case of less-active ZSM-5(280), when it enhanced both the conversion and selectivity of aromatics (Table 10). We performed some kinetic measurements on Mo$_2$C /ZSM- 5(80) and found that the concentration of n-heptane varied between 1.3 and 8.0% and the decomposition rate of heptane followed first-order kinetics. The same results were found for the formation of benzene and toluene, which assumedly did not undergo secondary reactions. We obtained an activation energy of 83 kJ/mol for the heptane decomposition.
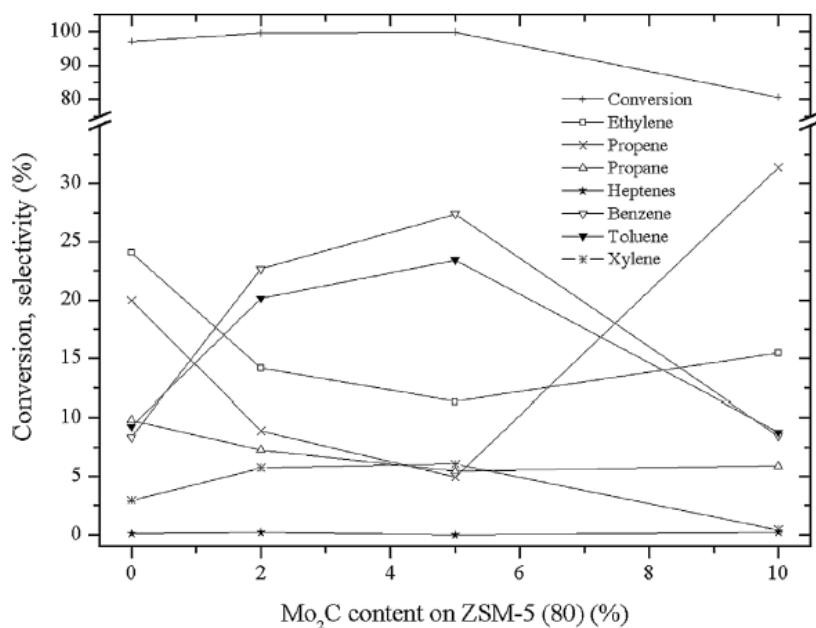
Figure 21: Effects of Mo$_2$C content of ZSM-5(80) on the conversion of n-heptane and selectivity of various products formed at 823 K.
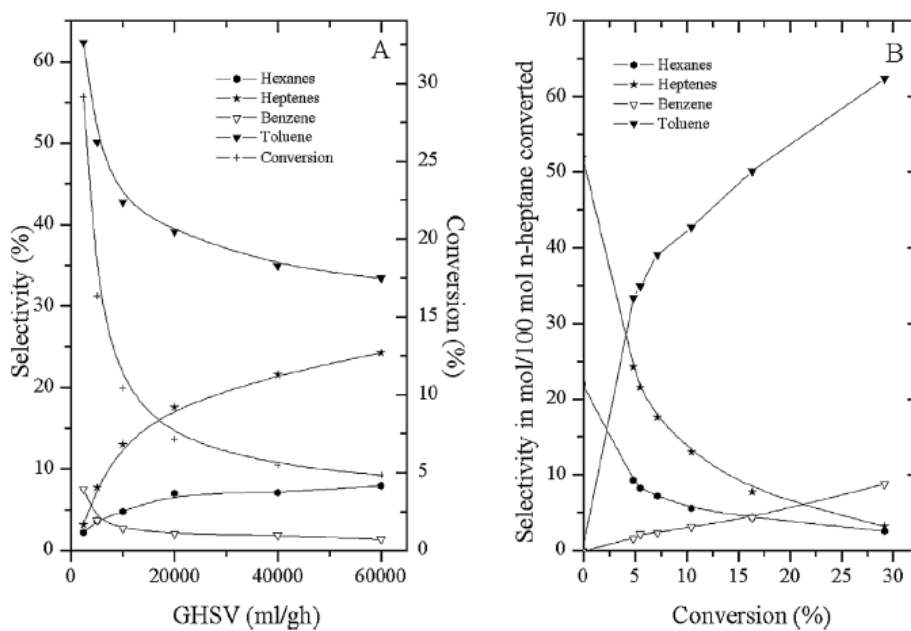
Figure 22: Effects of space velocity on the reaction of n-heptane

(A) and product selectivity as a function of n-heptane conversion

(B) over 2% Mo$_2$C/Al$_2$O$_3$ at 873 K.

The results showing the effect of space velocity on the conversion and selectivity of the important compounds for 2% Mo_2C/Al_2O_3 are displayed in figure 22A. As shown, the conversion and selectivity of aromatics decreased, whereas the selectivity of heptenes and hexanes increased with increasing space velocity.

High conversion values (55–95%) were measured for alumina- and silica-supported Mo_2C samples at 773–873 K. Butenes, ethene, ethane, and propene were the main products. On 2% Mo_2C/Al_2O_3 at 873 K, toluene selectivity was 27% and benzene selectivity was 6%; xylene formation was also observed. On Mo_2C /SiO_2, aromatics were produced with lower selectivity. The maximum value 11% was attained at 873 K. The catalytic behavior of pure ZSM-5(80) and 5% Mo_2C /ZSM-5(80) was also tested. The conversion of heptene was near 100% on both solids at 723–873 K; the aromatic selectivity values were similar. The positive influence of Mo_2C was exhibited at lower temperatures (723–773 K), where it increased the selectivity and yield of aromatics (Table 11).

Table 11: Characteristic data for the reaction of 1-heptene on different catalysts

Catalyst	Temperature (K)	Conversion (%)	Selectivity (%)										Yield of aromatics
			Methane	Ethene	Ethane	Propene	Propane	Butenes	Benzene	Toluene	Xylenes	
Mo_2C	773	34.3	0.8	2.8	1.5	10.3	1.0	17.4	2.0	33.8	0.1	12.3
	873	70.4	7.0	4.3	7.8	8.4	2.7	20.2	4.9	15.8	0.1	14.6
2% Mo_2C/Al_2O_3	773	54.1	0.8	2.6	0.6	10.2	0.5	22.4	1.0	27.7	0.4	17.4
	873	94.6	5.7	10.4	5.1	11.6	2.1	18.5	5.8	27.3	0.2	33.0
2% Mo_2C/SiO_2	773	72.5	0.1	0.6	0.1	38.4	0.1	55.6	0.5	0.8	0.3	1.1
	873	73.7	4.5	5.8	6.1	18.5	1.3	30.2	2.6	7.3	0.9	8.4
H-ZSM-5(80)	723	99.5	0.5	8.5	1.1	13.8	20.2	8.9	3.8	8.4	0.1	12.3
	773	99.7	1.3	14.9	2.0	19.1	18.1	9.5	4.5	12.7	0.1	17.2
	873	99.9	5.3	26.5	4.7	18.3	5.9	5.0	9.4	16.3	6.0	32.0
5% Mo_2C/ZSM-5(80)	723	99.2	0.3	9.6	0.7	18.3	9.8	12.8	3.4	13.3	3.4	20.3
	773	99.6	0.5	15.7	0.7	23.6	9.2	12.6	4.2	13.2	4.2	21.8
	873	99.9	2.1	21.7	1.7	29.5	3.7	10.7	10.2	15.8	1.4	27.4

a Average data determined during gradual heating from 723 K.

3.5.6.3 Reaction of n-heptane on pure Mo_2C

The reaction of heptane on different catalysts has been the subject of extensive research [55,59]. Supported Pt was found to be an active catalyst for the dehydrocyclization process. Significant progress was made in this area when zeolite

was used as a catalyst and/or as a support. A bifunctional mechanism involving both the metal and the acid sites of the support and a monofunctional mechanism involving only the metallic sites were assumed [55,59,60]. The results obtained in the present study show that pure Mo_2C can catalyze the aromatization of heptane with a maximum selectivity of ∼51% at 823 K. This suggests the action of the monofunctional mechanism. Accordingly, Mo_2C can activate the heptane molecule, catalyze its dehydrogenation, and affect subsequent processes leading to the production of aromatics. The catalytic performance of Mo_2C remained the same when the presence of Mo–O was completely eliminated, suggesting that Mo oxycarbide is not required for the activation of heptane and the subsequent processes. We delineate the following main steps:

with cracking and dehydrogenation,

$$C_7H_{16} \longrightarrow C_3H_6 + C_4H_{10}, \tag{1}$$

$$C_7H_{16} \longrightarrow C_7H_{14} + H_2, \tag{2}$$

with cracking and dehydrocyclization of heptene,

$$C_7H_{14} \longrightarrow 2C_2H_4 + C_3H_6, \tag{3}$$

$$C_7H_{14} \longrightarrow C_6H_5- CH_3 + 3H_2. \tag{4}$$

Studying the reaction of 1-heptene shows that Mo_2C can convert this compound into aromatics, mainly to toluene. Nevertheless, a significant fraction of heptene formed in the reaction of n-heptane remained unreacted (Table 10), likely because pure Mo_2C contains no acidic sites advantageous for these processes.

At higher temperature (873 K), the unsupported Mo_2C lost its catalytic activity very rapidly, likely due to the deposition of coke. TPR measurements revealed that its reactivity toward hydrogen is relatively low, with a peak temperature, $T_p = 948$ K, higher than that measured for the hydrogenation of excess carbon produced during the preparation of Mo_2C (Figure 23A).
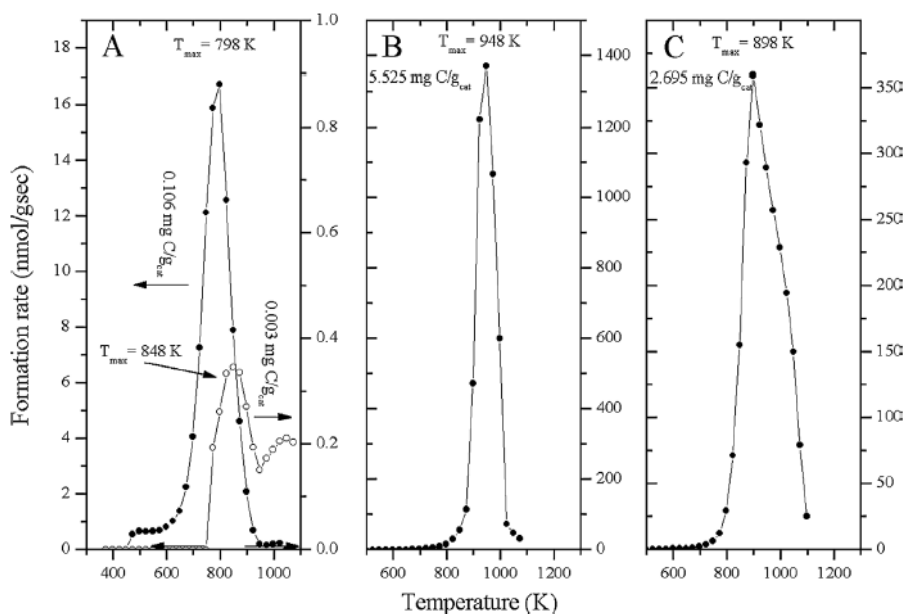
Figure 23: Formation of methane in the TPR measurements for unused and unreduced Mo$_2$C (●) and after repeating the measurement with the same sample (○) (A), and following n-heptane reaction at 823 K for 120 min on Mo$_2$C (B) and 2% Mo$_2$C /ZSM-5(80) (C).

5.5.6.4 Effects of supported Mo$_2$C

The conversion of heptane was markedly increased when Mo$_2$C was deposited on alumina and silica of high surface area (Table 10). The formation of toluene and benzene occurred with enhanced selectivity, particularly on 2% Mo$_2$C/Al$_2$O$_3$ (Figure 1 9 B). In these cases, we may assume the operation of a bifunctional mechanism. Mo$_2$C is mainly responsible for the dehydrogenation reaction, whereas the Lewis acidic sites of the supports facilitate the dehydrocyclization of heptene into toluene (Eq. (4)). In accordance with this picture, heptene was formed with much lower selectivity (6–20%) on supported Mo$_2$C than on pure Mo$_2$C (Table 10). Separate studies on the reaction of 1-heptene confirmed that the Mo2C-containing catalysts were effective in converting hexene into aromatics (Table 11). From the extrapolation of the selectivity to zero percent

conversion, we determined the primary products of the reaction on 2% Mo_2C/Al_2O_3 to be hydrogen, heptene, and hexane (Figure 2 2 B). This finding suggests that dehydrogenation is the primary process on Mo_2C/Al_2O_3 and that all of the other reactions, including aromatization, occur subsequently.

The role of acidic sites is clearly exhibited by the results obtained using ZSM-5, which contained even Bronsted sites in high concentration. Depending on the number of this site, ZSM-5 alone catalyzed the aromatization of heptane [55]. In this case, the first step is the formation of carbonium ions,

$$C_7H_{16(a)} + H_{(a)}^+ \longrightarrow C_7H_{17(a)}^+, \tag{5}$$

which undergo dehydrogenation and cracking, followed by the dehydrocyclization of olefins into different aromatics. Deposition of Mo_2C on ZSM-5, particularly on ZSM-5(80), markedly increased the selectivity and yield of aromatics at the expense of the formation of alkene. In this sample, heptene was completely absent from the reaction products at temperatures >673–723 K, indicating that it reacted rapidly after its formation [56]. The better aromatization property of Mo_2C /ZSM-5(80) compared with pure ZSM-5 suggests that a fraction of the intermediate formed at the Mo_2C/ZSM-5 interface, or, more precisely, on the highly dispersed Mo_2C interacting with the acid sites of ZSM-5, was effectively converted into aromatics before being transformed into other molecules. This intermediate is very likely a hexyl species formed in the activation of n-hexane on Mo_2C,

$$C_7H_{16(a)} \longrightarrow C_7H_{15(a)} + H_{(a)}. \tag{6}$$

We mention that an alternative route for the formation of aromatics was also considered on supported Pt [55]. Accordingly, the first main step in the aromatization of heptane is its dehydrocylization into C_7 cycloalkane,

$$C_7H_{16} \quad \longrightarrow \quad C_6H_{11}- CH_3 + H_2, \tag{7}$$

followed by dehydrogenation of the cycloalkane into aromatics,

$$C_6H_{11}- CH_3 \longrightarrow C_6H_5- CH_3 + 3 H_2. \tag{8}$$

However, C_7 cycloalkane has not been identified in the products using Mo_2C-containing catalysts.

3.6 Equilibrium modeling

In process simulation literatures, computer aid simulations were viral to use as representative of real process. Simulation could predict outcome of the process with reliable results. The simulation for chemical reactor was divided into two categories; kinetic model and chemical equilibrium model.

Generally, kinetic model was commonly used in process simulation due to its reliability in prediction. However, equilibrium model was also used in many process simulations. Most of the processes were equilibrium limit reactions or reaction with easily reached equilibrium [41].

Process literature which used equilibrium model to represent reactor were summarized in table 12. In table, there were the main reactions that reaction producing benzene toluene and xylene directly while the side reactions were unexpected reactions, particularly thermal cracking, dehydrogenation and hydrocracking. One of advantages for simulation with equilibrium model was ease in utilization. It did not require much parameter as kinetic to represent the model.

Table 12: Equilibrium model in process simulation

System	Reactions	Reference
Dehydrogenation	n - C6H14 $\longrightarrow$ C6H12 + H2	[52,53,54]
Hydrocracking	C8H10 (e) + H2 $\longrightarrow$ C7H8 + CH4	[52]
Dimerization	2C4H8 (e) $\longrightarrow$ C8H16 (ethyl cyclohexane)	[52,53]
Aromatization	C8H16 $\longrightarrow$ C8H10 (ethylbenzene) + 3H2	[51,52,53,54]
Thermal cracking	C8H10 (e) $\longrightarrow$ C6H6 + C2H4	[51,52]
Isomerization	C8H10 (e) $\longrightarrow$ C8H10 (p)	[51,53]
	C8H10 (e) $\longrightarrow$ C8H10 (o)	
	C8H10 (e) $\longrightarrow$ C8H10 (m)	

However, there was a limitation for equilibrium model. This model could not predict outcome of reactor that did not reach equilibrium.

As described above, the development of the better aromatization property of Mo_2C /ZSM-5(80) is the key element to produce high-quality aromatic production. There are many researches focused on the production of BTX by using normal paraffins. In contrast, in this study c6-c8 was selected for the process preparation, which was interested alternative and can be helped contribute to develop modeling to produce BTX productions.

3.7 Extension from literature

As aromatization simply reached equilibrium, it fulfilled concept of chemical equilibrium that could predict reactor effluence composition at equilibrium time. So, this research intended to model the aromatization in chemical equilibrium aspect which expected to give the same result as experiment at complete conversion of BTX as show in figure 24.
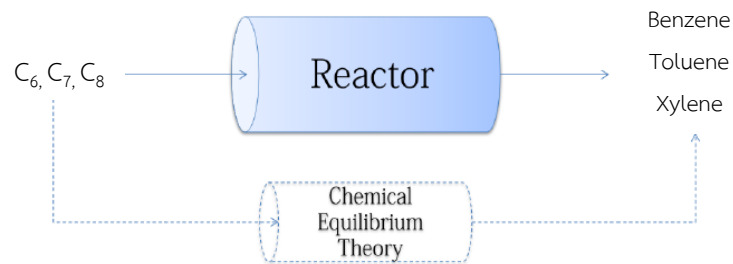
Figure 24: Concept of aromatics modeling by chemical equilibrium

However, competitive of catalytic reaction in aromatization led modeling for equilibrium very complex. Integration chemical equilibrium with reactor configuration in modeling such as catalytic density, void fraction etc. was an idea for this modeling which shall be verified the result of developed model with experiment.

CHAPTER 4

SIMULATION

This chapter described methodology to develop appropriate equilibrium model of aromatics production starting with specifying elementary inputs of model. Then, the equilibrium models were explained. After that the validation methodology were discussed and followed by utilization of the models.

4.1 Concept of Chemical Equilibrium Modeling

Aromatics production was the reaction that feed normal paraffins include C_6, C_7, C_8 into reactor to form BTX product. With the operating condition at very high temperature (450-500℃), the reaction rate was very fast. Therefore, the concentration of reactant i.e. hydrogen in reactor decreased very rapidly and remained only small amount. After the concentration of hydrogen was very low, the concentrations of all components were stable. It could be compiled that the very small amount of hydrogen left in effluence was in equilibrium with concentration of others products i.e. CH_4, C_2H_6, C_2H_4 and H_2. Thus, concentration of components should be explained by chemical equilibrium theory [62].

Therefore, this research intended to simulate and predict aromatics production results with chemical equilibrium theory. The simulation results were then compared to the previous literatures.

4.2 Elementary parameters for beginning of simulation

Simulations of aromatics production in this research were done with Aspen Plus program. In order to start simulation, there were many elementary parameters were required before calculation.

4.2.1 Influent components

Components that fed into reactor were consisted of normal paraffins include C_6, C_7, C_8. Normal paraffins were at ultrapure condition because it would be easy to analyze the effluence of reactor. The ultrapure feed condition was taken from the laboratory literatures [60, 61].

4.2.2 Reactions in aromatic production

Specifying the reactions available for the system was one of the important input parameters for simulation. The available reactions were depending on type of catalyst used in reactor. In this research, there were three types of catalysts Mo_2C/Al_2O_3, Mo_2C/SiO_2 and $Mo_2C/ZSM-5(80)$. The properties of each catalyst were shown in table 13.

Table 13: Some properties of catalysts studied in this research.

Model	Catalyst	Catalyst Properties		Operating Condition	
		Density	Void fraction	Temp (^{0}C)	Alkane/H2
Hinsen et al [62]	Mo_2C/Al_2O_3	1,100	0.4	500-775	3-10
Stransch et al [60]	Mo_2C/SiO_2	3,600	0.8	500-775	3-10
Danashpayeh et al [61]	$Mo_2C/ZSM-5(80)$	2,000	0.7	650-750	3-10

From the various literatures [60-63, 65, 68], there were many proposed reactions in the system which was shown in table 13. They were classified into three groups; catalytic reactions.

Table 14: All Possible reactions of aromatics production from literatures

No.	Reaction	K equilibrium 500 C	K equilibrium 600 C	K equilibrium 700 C
Catalytic Reaction				
	Dehydrogenation			
1	$n - C_6H_{14}$ (hexane) $\rightarrow C_6H_{12} + H_2$	1.98×10^4	4.69×10^6	6.89×10^7
2	$n - C_7H_{16}$ (heptane) $\rightarrow C_7H_{14} + H_2$	4.41×10^7	3.73×10^7	5.00×10^5
3	$n - C_8H_{18}$ (octane) $\rightarrow C_8H_{16} + H_2$	2.60×10^{10}	5.97×10^9	1.79×10^9
	Hydrocracking			
4	$C_6H_{14} + H_2 \rightarrow C_4H_8 + 2CH_4$	1.98×10^4	7.05×10^3	3.02×10^3
5	$C_6H_{14} + H_2 \rightarrow 2C_3H_8$	6.61×10^5	3.11×10^4	2.55×10^3
6	$C_7H_{16} + H_2 \rightarrow C_6H_{14} + CH_4$	1.65×10^4	5.14×10^3	2.49×10^3
7	$C_7H_{16} + H_2 \rightarrow C_5H_{10} + 2CH_4$	2.81×10^5	3.62×10^4	3.15×10^3
8	$C_7H_{16} + H_2 \rightarrow C_3H_6 + 2C_2H_6$	7.32×10^5	5.92×10^3	4.65×10^4
9	$C_8H_{18} + H_2 \rightarrow C_7H_{16} + CH_4$	5.31×10^6	4.65×10^5	1.35×10^2
10	$C_8H_{18} + H_2 \rightarrow C_6H_{12} + 2CH_4$	2.75×10^5	1.14×10^4	2.85×10^3
11	C_8H_{10} (e) $+ H_2 \rightarrow C_7H_8 + CH_4$	4.79×10^5	3.85×10^4	2.15×10^3
12	$C_7H_8 + H_2 \rightarrow C_6H_6 + CH_4$	6.75×10^5	3.21×10^4	1.95×10^3
	Dimerization			
13	$2C_4H_8 \rightarrow C_8H_{16}$ (ethylxyclohexane)	3.98×10^{27}	7.36×10^{26}	1.87×10^{26}
	Aromatization			
14	$C_8H_{16} \rightarrow C_8H_{10}$ (ethylbenzene) $+ 3H_2$	4.49×10^{11}	3.23×10^{11}	2.49×10^{11}
	Thermal cracking			
15	$C_6H_{12} \rightarrow C_4H_8 + C_2H_4$	2.99×10^{-2}	2.27×10^{-1}	1.19×10^{-1}
16	$C_7H_{14} \rightarrow C_4H_8 + C_3H_6$	7.59×10^{-2}	1.92×10^{-2}	1.51×10^{-1}
17	$2C_7H_8 \rightarrow 2C_6H_6 + C_2H_4$	7.29×10^2	4.06×10^5	6.92×10^7
18	C_8H_{10} (e) $\rightarrow C_6H_6 + C_2H_4$	3.41×10^4	2.23×10^3	5.69×10^2
19	C_8H_{10} (p) $\rightarrow C_6H_6 + C_2H_4$	7.95×10^3	9.51×10^2	9.35×10^2
20	C_8H_{10} (o) $\rightarrow C_6H_6 + C_2H_4$	2.34×10^5	4.26×10^4	1.64×10^2
21	C_8H_{10} (m) $\rightarrow C_6H_6 + C_2H_4$	2.63×10^4	1.34×10^3	6.47×10^2
22	$2C_8H_{10}$ (m) $\rightarrow 2C_7H_8 + C_2H_4$	1.43×10^4	2.43×10^3	1.75×10^2
23	$2C_8H_{10}$ (o) $\rightarrow 2C_7H_8 + C_2H_4$	1.01×10^5	2.24×10^4	3.60×10^3
24	$2C_8H_{10}$ (p) $\rightarrow 2C_7H_8 + C_2H_4$	5.51×10^5	4.06×10^4	9.73×10^2
25	C_8H_{10} (p) $+ C_8H_{10}$ (o) $\rightarrow 2C_7H_8 + C_2H_4$	7.29×10^6	4.06×10^5	6.92×10^3
26	C_8H_{10} (p) $+ C_8H_{10}$ (m) $\rightarrow 2C_7H_8 + C_2H_4$	5.25×10^6	1.07×10^5	8.19×10^3
27	C_8H_{10} (o) $+ C_8H_{10}$ (m) $\rightarrow 2C_7H_8 + C_2H_4$	1.75×10^6	4.69×10^5	6.89×10^3
	Isomerization			
28	C_8H_{10} (e) $\rightarrow C_8H_{10}$ (p)	2.44×10^4	1.79×10^6	5.84×10^7
29	C_8H_{10} (e) $\rightarrow C_8H_{10}$ (o)	1.98×10^4	7.05×10^3	3.02×10^3
30	C_8H_{10} (e) $\rightarrow C_8H_{10}$ (m)	6.61×10^5	3.11×10^4	2.55×10^3

Table 14 showed the possible reactions in aromatics/BTX production summarized from many published literatures. The Eq. 1 , 2 and 3 were the main catalytic reactions of aromatics production and dehydrogenation of normal paraffins [45 , 4 9] , respectively. The hydrocracking, Thermal cracking were the hydrogen consumed reactions which performed as the side reactions in the process.

To complete the reaction in aromatics/BTX, this research proposed the hydrocracking reaction into possible reactions because some metal in catalyst was used in hydrocracking reaction. Tungsten (W) [63, 64].

4.2.3 Effluent Components

From various aromatization literatures [61, 62, 6 5], the effluence of reactors was consisted of hydrogen, methane, ethane, ethene, propane, propene, butane, butene 1-Pentene, cyclohexane, cyclohexene and aromatics. These components were the same as the products from the possible reactions mentioned in previous section.

4.2.4 Operating Conditions

Temperature reactor and amount of feed were the important input parameters. From aromatics production experiments, most reactors were operating isothermally in the range of 450-500^{0}C while the feed of normal paraffins ratio was around 3- 10 [60-62].

4.2.5 Thermodynamic property calculation method

Thermodynamic property calculation method was one of input factors in calculation. This method calculated the component properties and their interaction with each other at given temperature and pressure. The selection of thermodynamic property calculation method was based on two guidelines, Aspen plus components guideline [66] shown in figure 25 and industrial guideline.
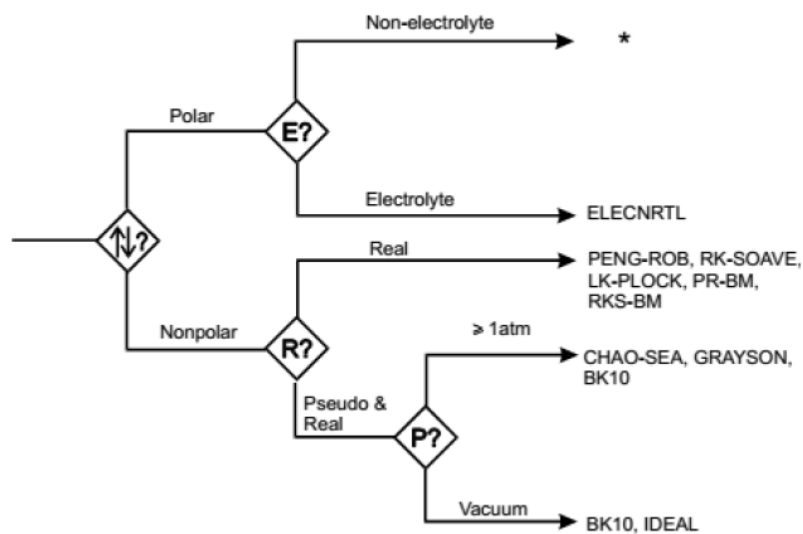
Figure 25: Selection guideline of the thermodynamic property calculation method

However, operating temperature in the simulation was more than 500^0C and all components were in gas state including water. Moreover, because all products were known, pathway for real components was selected. Therefore, with respect to the Aspen plus guideline, the suggestions for suitable thermodynamic properties were PENG-ROB, RK-Soave, PR-BM, LK-PLOCK and RKS-BM.

The others industrial guideline [66] for petrochemical process recommended CHAO-SEA, Grayson, PENG-ROB, RK-Soave, NRTL, UNIQUAC and REFPROP. It should be noticed that NRTL and UNIQUAC were liquid activity prediction which were not suitable in this research because all components state was gas phase.

From the two guidelines, the coincident suggestion methods were PENG-ROB and RK-Soave. To select the appropriate method, the simulation at temperature 500^0C and pressure 1 atm of normal paraffins were simulated and expressed in table 15 In the table, volume, enthalpy and other properties were calculated with RK-Soave and PENG-ROB and compared the results. It could be clearly seen that difference between the calculation methods was less than 0.01%.

Thus, both methods could be used in this work without any insignificant difference. For the simulation in this work, PENG-ROB was selected.

Table 15: Difference of property calculation using RK-Soave and PENG-ROB*

Property	RK-Soave	PENG-ROB	Difference (%)
Vapor Frac	1.00	1.00	0.000
Total Flow l/hr	11473900.00	11472900.00	0.009
Enthalpy cal/mol	-23674.02	-23674.31	-0.001
Entropy cal/mol-K	2.86	2.85	0.004
Density gm/cc	0.00	0.00	-0.008
Average MW	19.76	19.76	0.000
Liq Vol 60F l/hr	5858.44	5858.44	0.000

*Calculation with Aspen Plus program

4.3 Proposed models / Propose all possible chemical reactions

After the elementary parameters were selected, the construction of simulation model was then figured out. For mathematic calculation, it could split calculation in the reactor into many sections. For example, in figure 26, one real reactor could be split into three sub-reactors and calculated the efflux result.
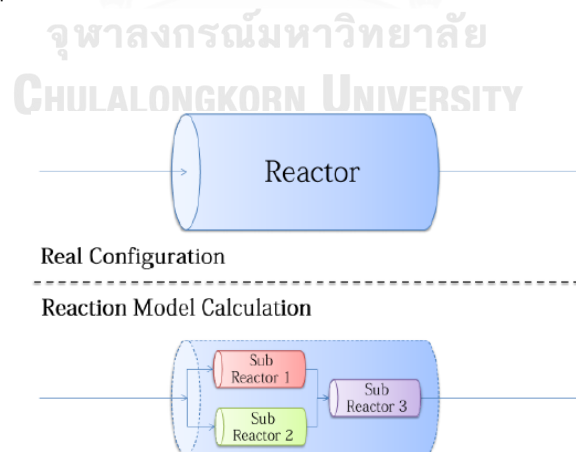
Figure 26: Reaction model calculation scheme

The reactions were from Aspen Plus V9 simulation for more accuracy and approaching actual value as possible as. The reactions would be divided into main reactions and side reactions. The main reactions were reaction producing benzene toluene and xylene directly while the side reactions were unexpected reactions, particularly thermal cracking, dehydrogenation and hydrocracking. Then, all possible chemical reactions were proposed.

Conversion of each reaction that possibly occur in the reactor is important in the analysis of product quantity which was represented in terms of partial pressure and it is a key variable for the model test and result prediction.

4.3.1 Uni-equilibrium reaction model

Uni-equilibrium reaction model, figure 27, was the simplest model imitated real configuration of reactor. Simulation was run under the assumption that all reactions were reacted in the same phase and the equilibrium of every reaction was reached. In this model, there were three trials to be simulated. First, all possible 30 reactions in table 14 were available. Second, some reactions were selective with respected to the literature corresponding to type of catalysts. Finally, the reactions selective to catalysts were chosen by researcher.
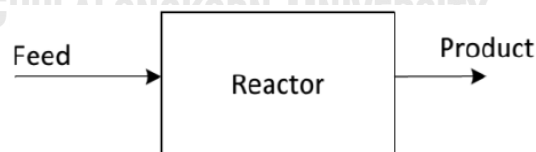
Figure 27: Single Equilibrium Reactor model

4.3.2 Duo-equilibrium reaction model

Duo-equilibrium reaction model was developed under the assumption that catalytic reaction (main reaction) took place at the catalyst surface while noncatalytic reaction (side reaction) occurred in the gas phase of void space among catalyst

particle. The effluents from both parts were the end products. This model was shown in figure 28.
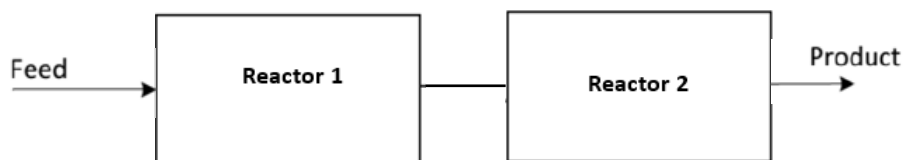
Figure 28: Duo-equilibrium reaction model

In the catalytic reactor, the simulation was run with the catalytic reactions in table 13, i.e. the main reactions were reaction producing benzene toluene and xylene directly while the side reactions were unexpected reactions, particularly thermal cracking, dehydrogenation and hydrocracking. Both reactors were assumed to run at the same temperature and pressure until getting the equilibrium. Ratio of catalytic and dependent on type of catalyst.

4.3.3 Trio-equilibrium reaction model

The trio-equilibrium reaction model was modified from previous model under the assumption that products from both catalytic and non-catalytic reaction would react further in the consequent reaction others reactions. Then, model consisted of three sub-reactors, shown in figure 29, first two sub reactors were similar to that of the previous model. Another reactor was connected allowing the combined effluents other reactions before the products were final yielded.
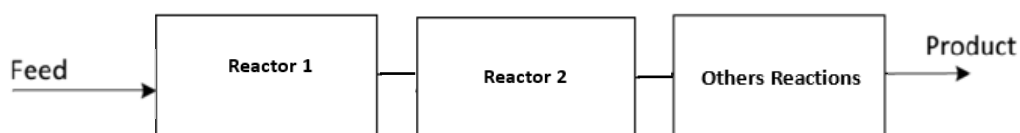
Figure 29: Trio-equilibrium reaction model

4.4 Verification of models using statistics

After simulating with the same influents, product components and concentrations from each model were compared to the previous literatures. However, the effluent data reported from literatures were different in two styles. Some reported all components efflux in system and the other described only the reactor performance, such as percent conversion. In this work, each information was utilized to validate the proposed model.

4.4.1 Verification using components in effluence.

For literature reporting all effluent component data, model validation utilizing Residue Sum Square (RSS) shown in equation 4.1 was chosen. RSS value was the value of deviations calculated from summation of square difference between effluent mole flow of chemical equilibrium model (M_{model}) and the experiment (M_{exp}) divided by the experiment mole flow. The small RSS value indicated accuracy of model of all components.

$$RSS = \sum_{i=1}^{N} \left[\frac{M_{exp} - M_{model}}{M_{exp}} \right]^2 \qquad [4.1]$$

4.4.2 Verification using reactor performance

For literatures reporting the reactor performance in system, the accuracy of model was tested with respected to variety information. such as conversion, yield and selectivity as a variable for performance evaluation were represented in terms of average absolute relative deviation (AARD) which is statistical information:

$$AARD = \frac{1}{N} \sum_{i=1}^{N} \left| \frac{(P_{exp} - P_{model})}{P_{exp}} \right| \qquad [4.2]$$

Where P_{exp} and P_{model} are the variable from the experiment and the equilibrium model, respectively. [59]

It should be notice that deviations of all variables could be totally shown in value of AARD. Small value of AARD suggested the validity of model.

After statistic variable showed precision of each model, the best model could be selected. The selected model would be validated further at others operating condition to ensure that the model could be predict the outcome at various conditions.

4.5 Advantage of developed models

After developing the appropriate model for aromatics production, the model would be utilized in process simulation. The used of equilibrium model would be an optional for the simulation of aromatics production and helps to save more lab expenses.
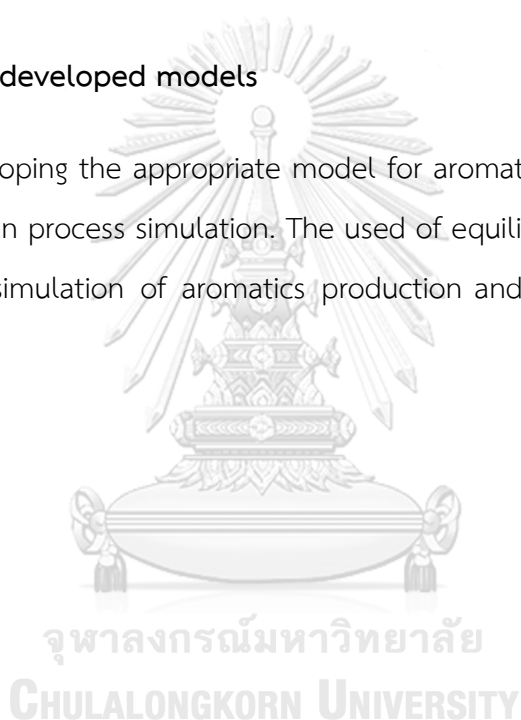
CHAPTER 5
RESULT AND DISCUSSION

Explanation and discussion of results from this study are included in this chapter. Major highlights contained in this chapter includes simulation of aromatics production using ASPEN PLUS. This chapter consisted of 5 categories: Equilibrium of aromatization from normal paraffins, chemical Equilibrium modeling, model manipulation, model validation and advantage of developed model. The first category explained the system at the equilibrium. Chemical Equilibrium modeling reported the construction and development of each model. Model manipulation was to modify the model to get more accuracy. Model Validation discussed and analyzed the accuracy of models via statistics. Finally, model advantages were implied. Moreover, other suggestions related to this research, which useful for future studies will be described in this chapter.

5.1 Equilibrium of aromatization from normal paraffins

In this research, with the help of Aspen Plus, n-Hexane, n-Heptane and n-Octane were feed into reactor at the variety conditions based on the condition published in the literatures. In the reactor, hydrogen was consumed by various reactions (e.g. hydrogenation etc.).

Most kinetic works were generally studied aromatization by varying the principle factors such as flow rate, reactor temperature and fraction of catalysts followed by determining the effects of the factors on the effluent components.

However, aim of this research is to study aromatics production using chemical equilibrium principle, then, operating space time must reach equilibrium. Thus, the kinetic studied were simulated further extending the residence time till the system got the equilibrium and the results were used as a reference data (the expected

data). The comparison between the reference data and the results calculated from the proposed equilibrium model would suggest the precision of model.

To demonstrate, simulation was set with the condition employed in the previous work of Daneshpayeh et al [9] using Mo_2C as a catalyst. Normal paraffins to aromatics feed was at 3 and reactor temperature was 500°C. Both of the results from kinetic model and the experimental data were plotted and shown in part I of figure 30 The simulation was allowed to run further till the concentration of each components got equilibrium. The percent conversion of hydrogen and alkanes as well as yield of aromatic products were shown in figure 30 part II.
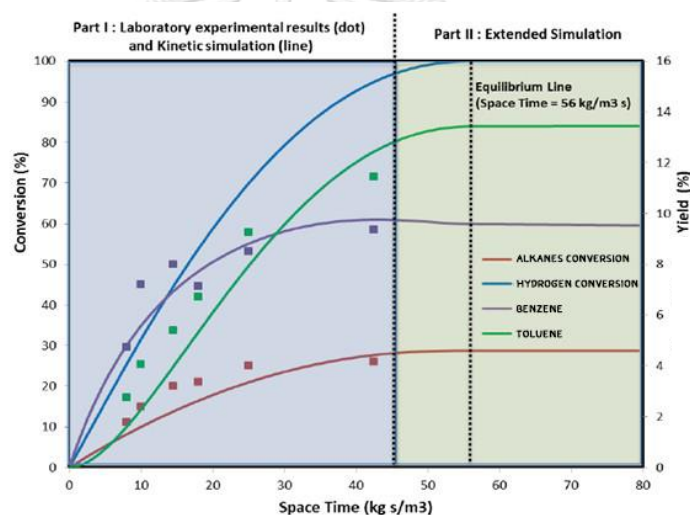
Figure 30: Percent conversions of effluents simulated by kinetic model with respect to the space time

In figure 30 part I, results from laboratory experiments (dots) and kinetic model (lines) were plotted versus the space time up to 46 kg s/m³ (41.8milliseconds). After extending the residence time further with kinetic simulation, it showed the system was reach the equilibrium at the space time of 56 kg s/m³ (50.9 milliseconds). It was shown the very short times of 9.1 milliseconds where the products yield between experiment and kinetic simulation at equilibrium was not significantly different. Thus, data from experiment was reasonable assumed as the reference data.

5.2 Chemical equilibrium modeling

Chemical equilibrium modeling procedure was constructed as described in chapter 4. In this research, there were three catalysts to be studied: Mo_2C/Al_2O_3, Mo_2C/SiO_2 and $Mo_2C/ZSM-5(80)$. Some properties of catalysts used in this research were listed in table 13

Three models mentioned in chapter 4 were consecutively studied for each catalyst, starting from uni-reactor to trio-equilibrium reaction model. The precision of models (difference between data from the proposed model and the data from the reference data) were determined to verify the best model. The chosen model was then validated to find the validation regions.

5.2.1 Uni-equilibrium reaction model

The uni-equilibrium reaction model detailed in chapter 4.2.1 was tested with three types of catalysts, Mo_2C/Al_2O_3, Mo_2C/SiO_2 and $Mo_2C/ZSM-5(80)$. Operating conditions were the picked up from the corresponding literatures which was listed in table 13. The results were compared to the reference data which was called "the equilibrium composition" to verify the capability of models.

5.2.1.1 The test of aromatics production over Mo_2C/Al_2O_3 catalyst

Simulations were run with the feed conditions taken from Hinsen et al [62] who study aromatics production over Mo_2C/Al_2O_3 catalyst. All reactions presented in table 14 were input for the competition in the reactor. Simulations were tested with the temperatures 500^0C and 550^0C. Feed ratios at a given temperature were varied from 3 to 10. Reaction pressure was fixed at ambient pressure. After the simulation was complete at equilibrium, the effluent yield in mole fractions were plotted against the feed ratio compared shown in figure 31.

Dots were the equilibrium composition (the reference data) and line represented the data from the proposed uni-equilibrium reaction model.
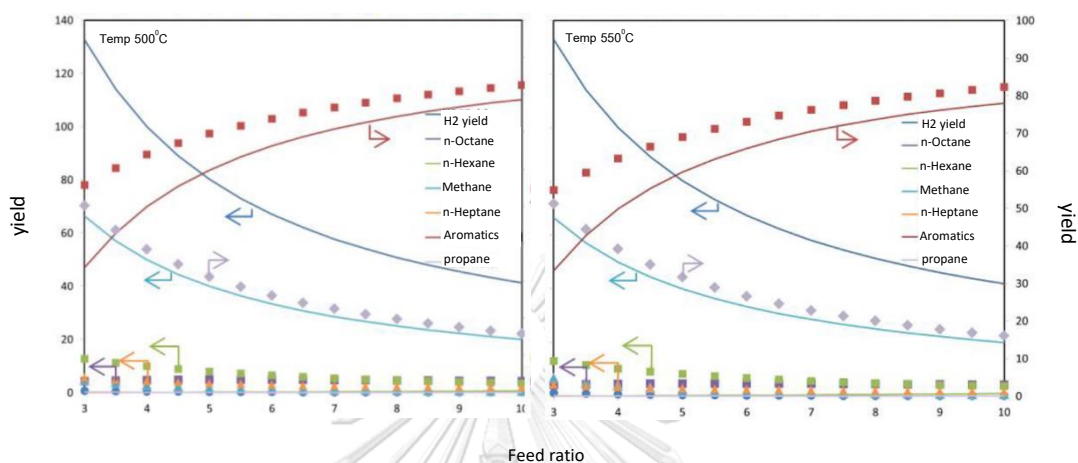
Figure 31: Simulation results from the uni-equilibrium reaction model and equilibrium composition versus the feed ratio of normal paraffins for Mo_2C/Al_2O_3 catalyst at a variety given temperatures

Data from uni-equilibrium reaction model. Equilibrium composition from figure 31, red plot of dots and line represented the aromatics in equilibrium. It could be described that the higher the feed ratio, the more aromatics left in the effluent while the other effluents (other colors data) showed conversely. For temperature effect, it was clearly shown that the higher temperature, the closer between two calculated data of aromatics (red dots versus red line) which suggested the better precision of the proposed model at high temperature. The plots at 500 or 550^0C were both determine as the best fit for this case. To magnify and show the comparison clearly, data at 500^0C and the feed ratio = 5 was drawn in bar chart and shown in figure 32.
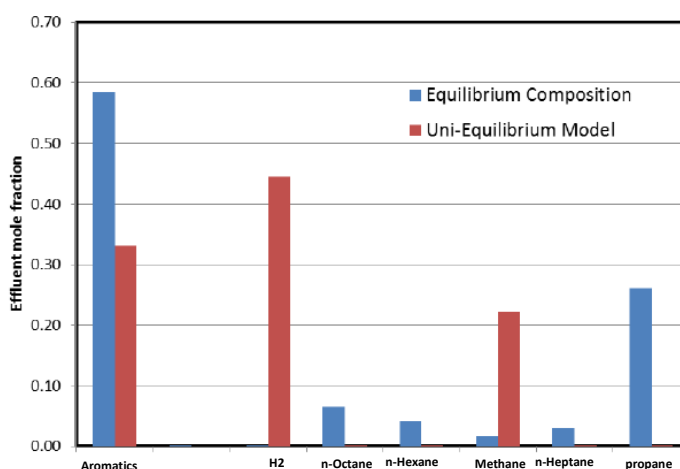
Figure 32: Simulation results from uni-equilibrium reaction model and equilibrium composition at equilibrium for Mo_2C/Al_2O_3 catalyst.
(Conditions: T = 550^0C)

From figure 32, the blue and red bars represented the equilibrium composition and the uni-equilibrium reaction model, respectively. The results showed the far difference between those two calculation methods. It suggested the low precision of this proposed model. One important point was that effluents of equilibrium composition consisted of n-hexane, n-heptane, n-octane, hydrogen and aromatics.

The absent of other products including the low precision of these results allowed to conclude that the uni-equilibrium reaction model could not explain the behavior of the aromatics reaction. It should be notified here that the bar plots at other temperatures were ignored according to their similar results to figure 32.

5.2.1.2 The test of aromatics production over Mo_2C/SiO_2 catalyst

This section, simulations using uni-equilibrium reaction model were tested in the same way to section 5.2.1.1. The operating conditions were substituted with the Stransch et.al. [10] model studied over the catalytic of Mo_2C/SiO. After the simulation was completed at equilibrium, the effluent yield in mole fractions were plotted against the feed ratio compared shown in figure 33.
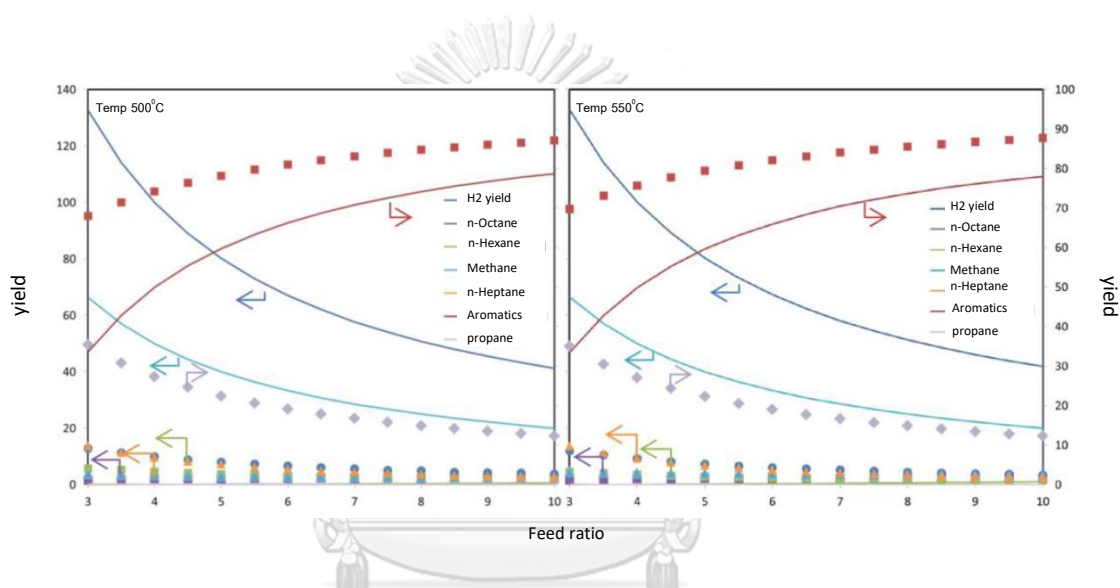
Figure 33: Simulation results from the uni-equilibrium reaction model and equilibrium composition versus the feed ratio of H_2/n-alkanes for Mo_2C/SiO_2 catalyst at a variety given temperatures

--- Data from uni-equilibrium reaction model. Equilibrium composition from figure 33, deviations between two calculation methods were still as high as that of the previous catalyst. The result at 500^0C was chosen to plot with bars of effluents mole. The result was depicted in figure 34.
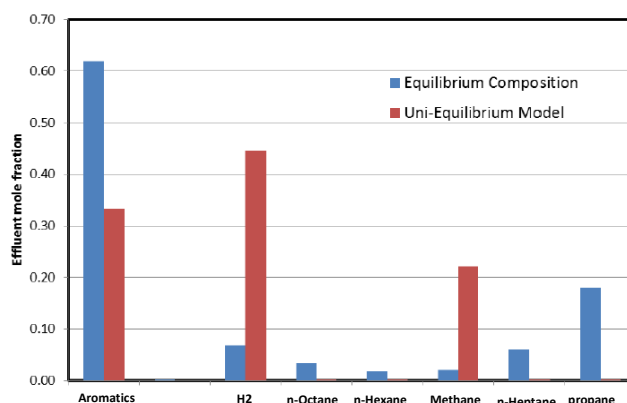
Figure 34: Simulation results from uni-equilibrium reaction model and equilibrium composition for Mo_2C/SiO_2 catalyst.

Form figure 34, the calculated effluent components showed large deviation from the expected results as the same as that of the previous test using Mo_2C/Al_2O_3. The products components were H_2 indicated that main reaction in the system was dehydrogenation.

5.2.1.3 The test of aromatics production over $Mo_2C/ZSM-5(80)$ catalyst.

The simulation method was repeated with the information from Daneshpayeh et al [9] tested over $Mo_2C/ZSM-5(80)$ catalyst. Reaction temperature range was 500 – 550°C. The plots of effluent yields as the functions of feed ratio were illustrated in figure 35.
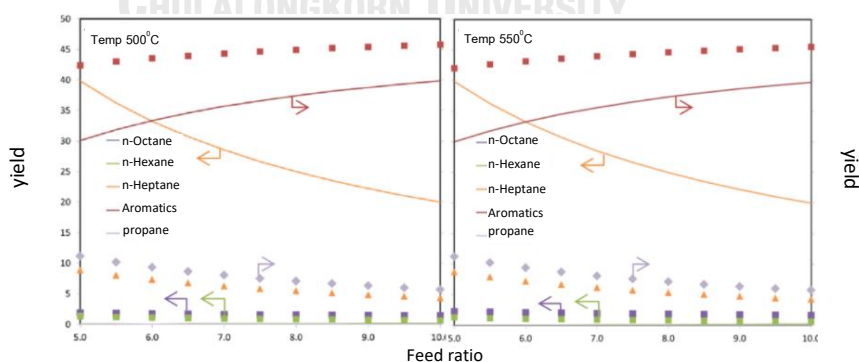
Figure 35: Simulation results from the uni-equilibrium reaction model and equilibrium composition versus the feed ratio of H_2/n-alkanes for $Mo_2C/ZSM-5(80)$ catalyst at a variety given temperatures

Data from uni-equilibrium reaction model. Equilibrium composition There were large deviations found in this simulation too. The result at 500^{0}C was chosen to represent the comparison with bar plot and shown in figure 36.
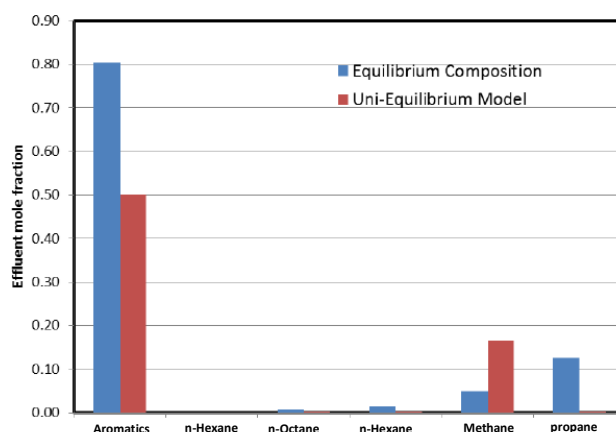
Figure 36: Simulation results from uni-equilibrium reaction model and equilibrium composition for Mo$_2$C/ZSM-5(80) catalyst.

Again, with the Mo$_2$C/ZSM-5(80) catalyst, It should be mentioned here that bar of mole fraction of H2 was not shown because there was no information of H$_2$ concentration in the literature. Bar of H$_2$ mole found from the simulation could make the misunderstanding without the comparative quantity from equilibrium composition. Moreover, methane components were summarized reported form in literature. Therefore, the model results were also reported in the same pattern.

According to the large deviations from uni-equilibrium reaction model over the three catalysts, Mo$_2$C/Al$_2$O$_3$, Mo$_2$C/SiO$_2$ and Mo$_2$C/ZSM-5(80), It can be concluded that this simulation model could not explain the behaviors of some reaction of aromatics production. It was attributed to the limitation of feed hydrogen concentration that led dehydrogenation dominate the other reactions such as hydrocracking, dimerization etc.

To prove that only the main reaction is aromatization and side reaction are dehydrogenation, hydrocracking, thermal cracking reacted in the system while other reactions were inactive, new simulation was set with the same feed condition but selecting only the partial reaction to be the available reaction computing in the system. This test was run under the hypothesis that the system was run with the solely aromatization if the number of products were identical to that done with all available reaction.

More attempts were tested on the uni-equilibrium reaction model. One was based on the postulate that catalyst selected the occurring reactions. The selectivity of catalysts led to the limitation of available reactions in the process. The summarizations of the catalyst selectivity were based on literatures published The comparison of bar plots resulted from the uni-equilibrium reactions (all 30 reaction) were depicted in figure 37.
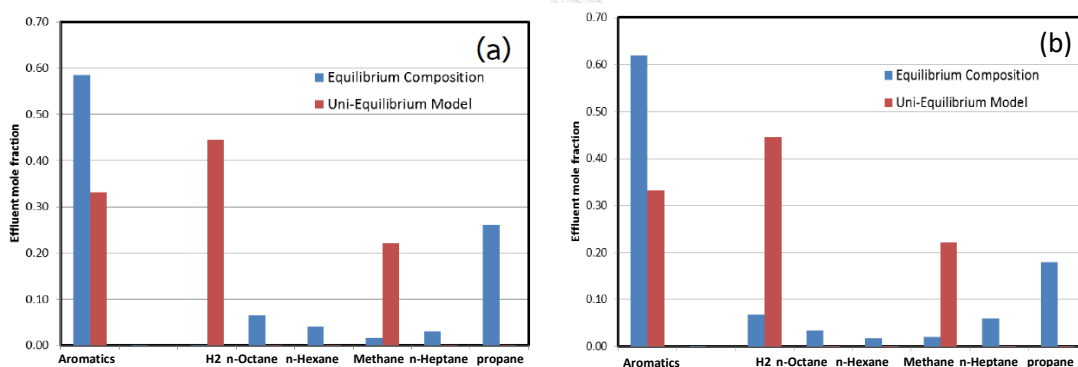
Figure 37: The simulation results from the uni-equilibrium reaction model all 30 reactions available (a) Mo_2C/Al_2O_3 catalyst (b) Mo_2C/SiO_2 catalyst. (Conditions: T =500°C and feed ratio = 5)

Figure 37 showed the comparison of the simulation results from the uni-equilibrium reaction model for Mo_2C/Al_2O_3 and Mo_2C/SiO_2 catalyst, respectively.

Surprisingly, two different simulations with limited reaction using Mo_2C/Al_2O_3, and Mo_2C/SiO_2 catalyst showed the identical bars comparing to those with the aromatization reaction solely. However, products from the simulation did not match to equilibrium compositions. Those suggested that the uni-equilibrium reaction model was the unsatisfactory model for describing the results.

Another attempt was run for $Mo_2C/ZSM-5(80)$ catalyst. The comparison of the simulation results was shown in figure 38.
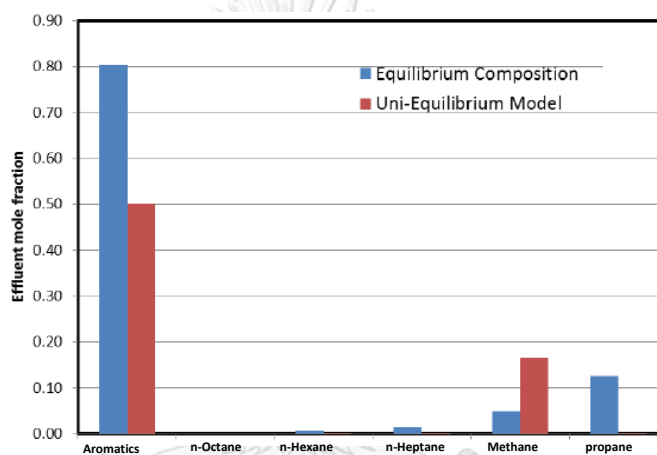
Figure 38: Comparison of the simulation results from the uni-equilibrium reaction model for $Mo_2C/ZSM-5(80)$ catalyst.

From figure 38, the limitation of available reactions input in the simulation impacted the products composition. However, the products i.e. hydrogen were not found. Those confirmed that the uni-equilibrium reaction model with limited selective reactions was not an appropriate model for describing. However, this result suggested the good point that the limitation of reactions helped to get better fit.

5.2.2 Duo-equilibrium reaction model

From previous section, the single equilibrium calculation could not predict competitive reactions between non-equilibrium reactions. Then, model was developed to allow the competition between the reactions. From one single reactor that all reactions were calculated in the same stage, it was split the calculation to two different parts, catalytic and gas phase, total products of those two parts were the output of the simulation. Each spitted part was specified the reaction to competition. The fraction volume input in catalytic was assumed to be equal to the void and solid fraction of catalyst which was a specific property of catalyst as shown in table 13.

The model was regarded as equilibrium state which the forward reaction rate and the reverse reaction rate are equivalent. However, the reactions in the model were grouped by splitting reactors, so there was more than one reactor connected in series to classify which reactions occurred before and after.

The duo-equilibrium reaction model was studied with two different specified reactions as described below.

5.2.2.1 The duo-equilibrium reaction model A
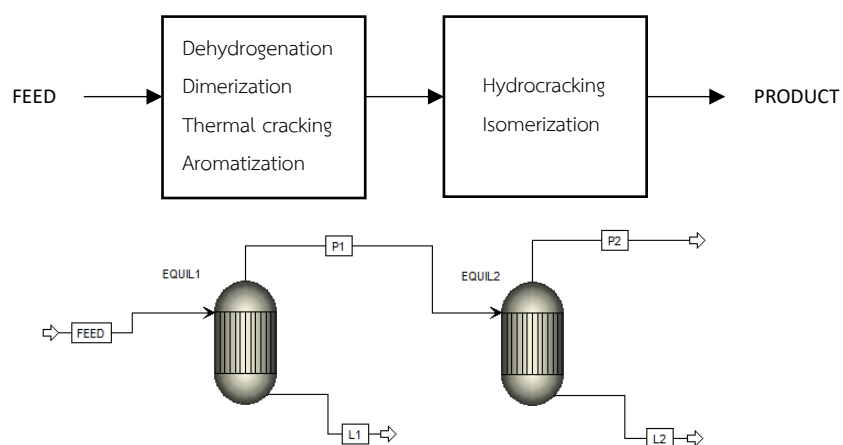
Figure 39: The duo-equilibrium reaction model A

Table 16 : The duo-equilibrium reaction model A

Reactor 1	Reactor 2
$n - C_6H_{14}$ (hexane) $\rightarrow C_6H_{12} + H_2$	C_8H_{10} (e) $+ H_2 \rightarrow C_7H_8 + CH_4$
$C_6H_{12} \rightarrow C_4H_8 + C_2H_4$	$C_7H_8 + H_2 \rightarrow C_6H_6 + CH_4$
$2C_4H_8 \rightarrow C_8H_{16}$ (ethylxyclohexane)	$C_6H_{14} + H_2 \rightarrow C_4H_8 + 2CH_4$
$C_8H_{16} \rightarrow C_8H_{10}$ (ethylbenzene) $+ 3H_2$	$C_6H_{14} + H_2 \rightarrow 2C_3H_8$
$n - C_7H_{16}$ (heptane) $\rightarrow C_7H_{14} + H_2$	$C_7H_{16} + H_2 \rightarrow C_6H_{14} + CH_4$
$C_7H_{14} \rightarrow C_4H_8 + C_3H_6$	$C_7H_{16} + H_2 \rightarrow C_5H_{10} + 2CH_4$
$2C_4H_8 \rightarrow C_8H_{16}$ (ethylxyclohexane)	$C_7H_{16} + H_2 \rightarrow C_3H_6 + 2C_2H_6$
$C_8H_{16} \rightarrow C_8H_{10}$ (ethylbenzene) $+ 3H_2$	$C_8H_{18} + H_2 \rightarrow C_7H_{16} + CH_4$
$n - C_8H_{18}$ (octane) $\rightarrow C_8H_{16} + H_2$	$C_8H_{18} + H_2 \rightarrow C_6H_{12} + 2CH_4$
$C_8H_{16} \rightarrow C_8H_{10}$ (ethylbenzene) $+ 3H_2$	
	C_8H_{10} (e) $\rightarrow C_8H_{10}$ (p)
	C_8H_{10} (e) $\rightarrow C_8H_{10}$ (o)
	C_8H_{10} (e) $\rightarrow C_8H_{10}$ (m)
Total = 22 reactions	

Model A

The model 1 shows two reactors connected in series. Firstly, normal alkanes were dehydrogenated to alkenes before dimerization to ethylcyclohexane in order to aromatize to be ethylbenzene. Likewise, the first aromatic was formed is ethylbenzene in the reactor 1, including thermal cracking to aromatization, hydrogenation and isomerization. Since aromatics production from n-hexane, n-heptane and n-octane is an interesting model, there are dehydrogenation of n-hexane, n-heptane and n-octane in the reactor 1 in order to find equilibrium between them before converting to ethylcyclohexane and ethylbenzene, respectively. Secondly, toluene and benzene were produced from hydrocracking of ethylbenzene and toluene in reactor 2, respectively. In addition, alkanes also were cracked by hydrogen to be propane, ethane and methane. In the reactor 2, by-product of both toluene and benzene production reactions was methane because different by-product strongly influenced reaction equilibrium shifting and aromatics

production, especially toluene and benzene fractions. Finally, ethylbenzene remaining converted to the three isomers of xylene, including para-xylene, ortho-xylene and meta-xylene.

5.2.2.2 The duo-equilibrium reaction model B for Mo_2C/Al_2O_3
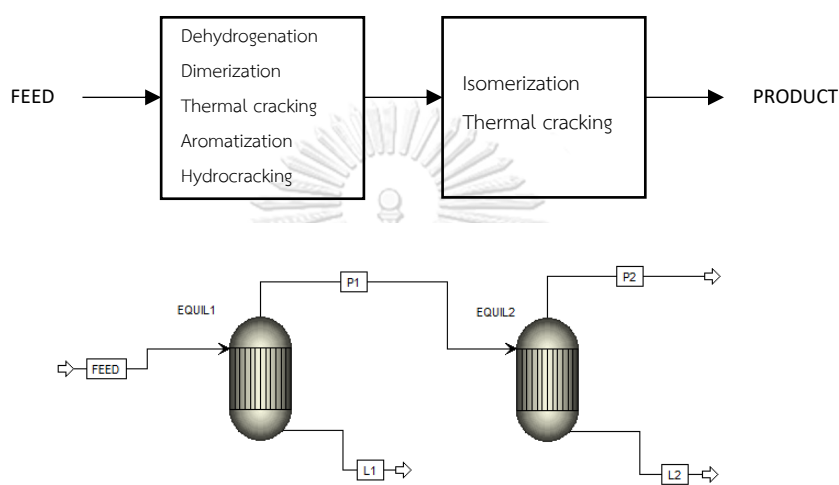
Figure 40: The duo-equilibrium reaction model B

Table 17: The duo-equilibrium reaction model B

Reactor 1	Reactor 2
$n - C_6H_{14}$ (hexane) $\rightarrow C_6H_{12} + H_2$ $C_6H_{12} \rightarrow C_4H_8 + C_2H_4$ $2C_4H_8 \rightarrow C_8H_{16}$ (ethylxyclohexane) $C_8H_{16} \rightarrow C_8H_{10}$ (ethylbenzene) $+ 3H_2$ $n - C_7H_{16}$ (heptane) $\rightarrow C_7H_{14} + H_2$ $C_7H_{14} \rightarrow C_4H_8 + C_3H_6$ $2C_4H_8 \rightarrow C_8H_{16}$ (ethylxyclohexane) $C_8H_{16} \rightarrow C_8H_{10}$ (ethylbenzene) $+ 3H_2$ $n - C_8H_{18}$ (octane) $\rightarrow C_8H_{16} + H_2$ $C_8H_{16} \rightarrow C_8H_{10}$ (ethylbenzene) $+ 3H_2$ $C_6H_{14} + H_2 \rightarrow C_4H_8 + 2CH_4$ $C_6H_{14} + H_2 \rightarrow 2C_3H_8$ $C_7H_{16} + H_2 \rightarrow C_6H_{14} + CH_4$ $C_7H_{16} + H_2 \rightarrow C_5H_{10} + 2CH_4$ $C_7H_{16} + H_2 \rightarrow C_3H_6 + 2C_2H_6$ $C_8H_{18} + H_2 \rightarrow C_7H_{16} + CH_4$ $C_8H_{18} + H_2 \rightarrow C_6H_{12} + 2CH_4$	C_8H_{10} (e) $+ H_2 \rightarrow C_7H_8 + CH_4$ $C_7H_8 + H_2 \rightarrow C_6H_6 + CH_4$ C_8H_{10} (e) $\rightarrow C_8H_{10}$ (p) C_8H_{10} (e) $\rightarrow C_8H_{10}$ (o) C_8H_{10} (e) $\rightarrow C_8H_{10}$ (m) $2C_8H_{10}$ (m) $\rightarrow 2C_7H_8 + C_2H_4$ $2C_8H_{10}$ (o) $\rightarrow 2C_7H_8 + C_2H_4$ $2C_8H_{10}$ (p) $\rightarrow 2C_7H_8 + C_2H_4$ C_8H_{10} (p) $+ C_8H_{10}$ (o) $\rightarrow 2C_7H_8 + C_2H_4$ C_8H_{10} (p) $+ C_8H_{10}$ (m) $\rightarrow 2C_7H_8 + C_2H_4$ C_8H_{10} (o) $+ C_8H_{10}$ (m) $\rightarrow 2C_7H_8 + C_2H_4$ $2C_7H_8 \rightarrow 2C_6H_6 + C_2H_4$
Total = 29 reactions	

Model B

Hydrocracking of n-hexane, n-heptane and n-octane in the reactor 2 were moved to the reactor 1 in the model 2, and it has seen that aromatics fractions are more similar to the experimental result as shown in figure 40 since ethylbenzene production which would be converted to other aromatics halved approximately. The hydrogenations are competitive reaction, which Mo_2C loaded on alumina silica and zeolite socony mobil–5 (ZSM-5) catalyst could not wholly eliminate, the experimental products were lower. Therefore, the desired product will be higher if another catalyst has functional elimination of the reactions from the reactor 1; however, the reactions are proper in the reactor 1 for the catalyst. Moreover, ethylcyclohexane from all models were close to zero, it could be as an intermediate of the mechanism.

Significantly different xylene amounts of the model 1 and 2 depend on remaining hydrogen from the reactor 1 because of xylene production from existing ethylbenzene in the reactor 2, which certain part was converted to toluene by the remaining hydrogen. Therefore, hydrocracking reactions of alkanes are necessary in the reactor 1 to reduce the hydrogen, reacting with ethylbenzene and toluene in the reactor 2 in order to continue to produce greater xylene amount in the reactor 3

5.2.3 Trio-equilibrium reaction model

This model was developed from the duo-equilibrium reaction model A and B. The simulation results from the duo-equilibrium reaction model B show that the amounts of toluene and xylene were similar to the experimental values, quantity of benzene was extremely lower. Then, the next model would be created to improve and more accuracy. The model was developed by adding a new calculation for adjusting the benzene yield by adding one more calculation just after the duo-equilibrium reaction model. The reactions in the model were grouped by splitting

reactors, so there was more than one reactor connected in series to classify which reactions occurred before and after.

5.2.3.1 Trio-equilibrium reaction model A

Since the results from the duo-equilibrium reaction model A showed much deviation from equilibrium composition. The scheme of the developed model was looked like the series connection between the duo-equilibrium reactions model connected to the one new reactor as shown in figure 41.

FEED →

| Dehydrogenation |
| Dimerization |
| Thermal cracking |
| Aromatization |
| Hydrocracking |

→

| Isomerization |
| Hydrocracking |
| Thermal cracking |

→

| Isomerization |

→ PRODUCT
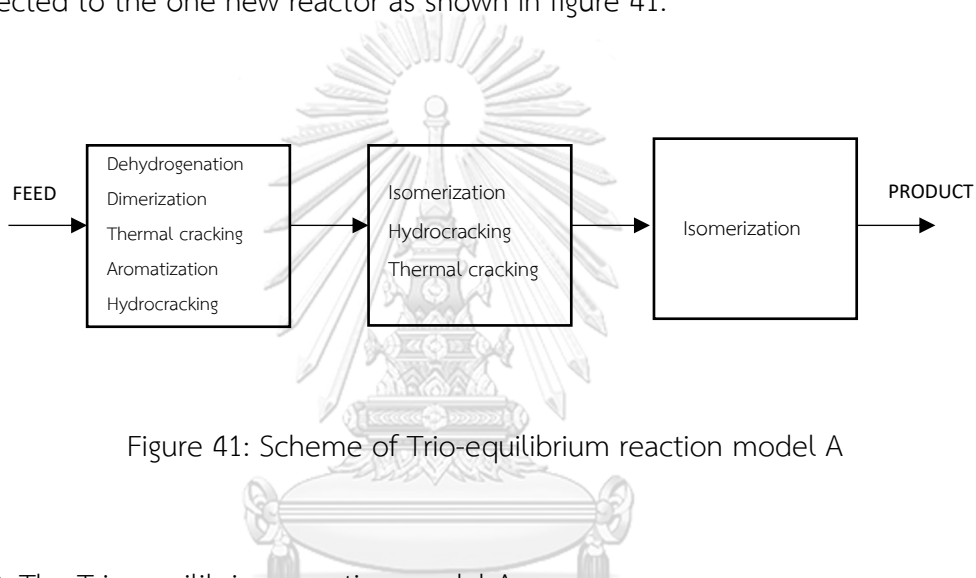
Figure 41: Scheme of Trio-equilibrium reaction model A

Table 18: The Trio-equilibrium reaction model A

Reactor 1	Reactor 2	Reactor 3
$n - C_6H_{14}$ (hexane) $\rightarrow C_6H_{12} + H_2$	C_8H_{10} (e) $+ H_2 \rightarrow C_7H_8 + CH_4$	C_8H_{10} (e) $\rightarrow C_8H_{10}$ (p)
$C_6H_{12} \rightarrow C_4H_8 + C_2H_4$	$C_7H_8 + H_2 \rightarrow C_6H_6 + CH_4$	C_8H_{10} (e) $\rightarrow C_8H_{10}$ (o)
$2C_4H_8 \rightarrow C_8H_{16}$ (ethylxyclohexane)	$C_6H_{14} + H_2 \rightarrow C_4H_8 + 2CH_4$	C_8H_{10} (e) $\rightarrow C_8H_{10}$ (m)
$C_8H_{16} \rightarrow C_8H_{10}$ (ethylbenzene) $+ 3H_2$	$C_6H_{14} + H_2 \rightarrow 2C_3H_8$	
$n - C_7H_{16}$ (heptane) $\rightarrow C_7H_{14} + H_2$	$C_7H_{16} + H_2 \rightarrow C_6H_{14} + CH_4$	
$C_7H_{14} \rightarrow C_4H_8 + C_3H_6$	$C_7H_{16} + H_2 \rightarrow C_5H_{10} + 2CH_4$	
$2C_4H_8 \rightarrow C_8H_{16}$ (ethylxyclohexane)	$C_7H_{16} + H_2 \rightarrow C_3H_6 + 2C_2H_6$	
$C_8H_{16} \rightarrow C_8H_{10}$ (ethylbenzene) $+ 3H_2$	$C_8H_{18} + H_2 \rightarrow C_7H_{16} + CH_4$	
$n - C_8H_{18}$ (octane) $\rightarrow C_8H_{16} + H_2$	$C_8H_{18} + H_2 \rightarrow C_6H_{12} + 2CH_4$	
$C_8H_{16} \rightarrow C_8H_{10}$ (ethylbenzene) $+ 3H_2$		

Total = 22 reactions

The Trio-equilibrium reaction model A

The reactor 3 represented isomerization, was added in the model in order to adjust aromatic proportions to the experimental result, which isomerization moved to the reactor 3 in the Trio-equilibrium reaction model A from the original the reactor 2 in the Duo-equilibrium reaction model A.

5.2.3.2 Trio-equilibrium reaction model B
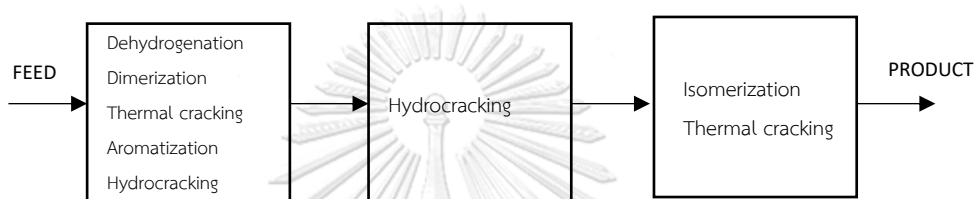
Figure 42: Scheme of Trio-equilibrium reaction model B

Table 19: The Trio-equilibrium reaction model B

Reactor 1	Reactor 2	Reactor 3
$n - C_6H_{14}$ (hexane) $\rightarrow$ $C_6H_{12} + H_2$ $C_6H_{12} \rightarrow C_4H_8 + C_2H_4$ $2C_4H_8 \rightarrow C_8H_{16}$ (ethylxyclohexane) $C_8H_{16} \rightarrow C_8H_{10}$ (ethylbenzene) $+ 3H_2$ $n - C_7H_{16}$ (heptane) $\rightarrow$ $C_7H_{14} + H_2$ $C_7H_{14} \rightarrow C_4H_8 + C_3H_6$ $2C_4H_8 \rightarrow C_8H_{16}$ (ethylxyclohexane) $C_8H_{16} \rightarrow C_8H_{10}$ (ethylbenzene) $+ 3H_2$ $n - C_8H_{18}$ (octane) $\rightarrow$ $C_8H_{16} + H_2$ $C_8H_{16} \rightarrow C_8H_{10}$ (ethylbenzene) $+ 3H_2$ $C_6H_{14} + H_2 \rightarrow$ $C_4H_8 + 2CH_4$ $C_6H_{14} + H_2 \rightarrow 2C_3H_8$ $C_7H_{16} + H_2 \rightarrow$ $C_6H_{14} + CH_4$ $C_7H_{16} + H_2 \rightarrow$ $C_5H_{10} + 2CH_4$ $C_7H_{16} + H_2 \rightarrow$ $C_3H_6 + 2C_2H_6$ $C_8H_{18} + H_2 \rightarrow$ $C_7H_{16} + CH_4$ $C_8H_{18} + H_2 \rightarrow$ $C_6H_{12} + 2CH_4$	C_8H_{10} (e) $+ H_2 \rightarrow$ $C_7H_8 + CH_4$ $C_7H_8 + H_2 \rightarrow$ $C_6H_6 + CH_4$	$2C_8H_{10}$ (m) $\rightarrow 2C_7H_8 + C_2H_4$ $2C_8H_{10}$ (o) $\rightarrow$ $2C_7H_8 + C_2H_4$ $2C_8H_{10}$ (p) $\rightarrow 2C_7H_8 + C_2H_4$ C_8H_{10} (p) $+ C_8H_{10}$ (o) $\rightarrow 2C_7H_8 + C_2H_4$ C_8H_{10} (p) $+ C_8H_{10}$ (m) $\rightarrow 2C_7H_8 + C_2H_4$ C_8H_{10} (o) $+ C_8H_{10}$ (m) $\rightarrow 2C_7H_8 + C_2H_4$ $2C_7H_8 \rightarrow$ $2C_6H_6 + C_2H_4$ C_8H_{10} (m) $\rightarrow C_6H_6 + C_2H_4$ C_8H_{10} (o) $\rightarrow$ $C_6H_6 + C_2H_4$ C_8H_{10} (p) $\rightarrow$ $C_6H_6 + C_2H_4$ C_8H_{10} (e) $\rightarrow$ C_8H_{10} (p) C_8H_{10} (e) $\rightarrow$ C_8H_{10} (o) C_8H_{10} (e) $\rightarrow$ C_8H_{10} (m)

Total = 32 reactions

The Trio-equilibrium reaction model B

The reactor 3, represented thermal cracking, was added in The Trio-equilibrium reaction model B in order to adjust aromatic proportions to the experimental result, especially increasing benzene. Besides, there was no hydrogen in the reactor 3 because it had been extremely depleted since reactor 2, then hydrocracking disappeared. Likewise, ethylbenzene, xylene and toluene in the model is the same production method as the reactor 2, excepting benzene because of adding the reactor 3. Xylene and toluene were cracked by heat to be benzene, so it was found a larger deal of benzene in the reactor 3. Then, it illustrates that xylenes would be cracked by high heat to be toluene before it would be also cracked to be benzene.

In conclusion, the development of the proposed model got better and better results from the uni-equilibrium reaction model through the Trio-equilibrium reaction model. The best fit model was selective to the catalyst types, i.e. the trio-equilibrium reaction model B was suit to both Mo_2C/Al_2O_3 and Mo_2C/ZSM-5(80) catalysts while the duo-equilibrium reaction model A was the best for Mo_2C/SiO_2 catalyst, so an exact model should be defined. Thus, this research proposed the methodology to manipulate equilibrium model by adding the parameter into the model. This parameter was acquired from experiment data. Hence, Residua Sum Square (RSS) was applied to indicate the most suitable model as shown in next section.

5.3 Model manipulation

Before the explanation of the manipulation of model, the discussion on C_2H_6 component must be clarified for understanding the role of C_2H_6 in aromatic reaction.

5.3.1 Discussion on the role of C_2H_6 in aromatic reaction.

In simulation process, C_2H_6 was the product of the hydrocracking reaction; $C_6H_{14} + 2H_2 \longrightarrow 3C_2H_6$. Produced C_2H_6 was then consumed by the dehydrogenation reaction; $C_2H_6 \longrightarrow C_2H_4 + H_2$ as shown in figure 43.
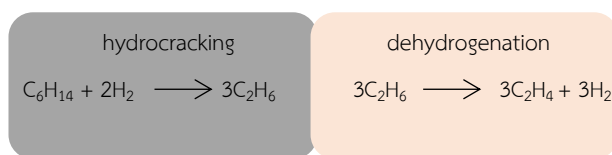
Figure 43: Scheme of ethane formation and consumption

At the equilibrium, all components must be in equilibrium and left in the reactor. The absence of C_2H_6 in the calculation under the equilibrium concept might be explained as followed. The pathway of the C_2H_4 production was formed via two elementary reactions hydrocracking and dehydrogenation as followed.

HDC: $C_6H_{14} + 2H_2 \rightleftharpoons 3C_2H_6$ K_1

DHD: $3C_2H_6 \rightleftharpoons 3C_2H_4 + 3H_2$ K_2

Overall reaction: $C_6H_{14} \rightleftharpoons 3C_2H_4 + H_2$ $K_{overall} = K_1.K_2$

Because C_2H_6 functioned as the intermediate in the process, theoretically of chemical equilibrium, intermediate would not exist in the final products because the reactions were already combined to form the overall reaction. The calculation of products at equilibrium could be done with the overall reaction. Simulations in this pathway led to the nearly zero of C_2H_6 at the end.

In fact, C_2H_6 should still remain with a substantial amount to maintain the production of C_2H_4 via dehydrogenation reaction. This concept was respected to the method calculating the amount of intermediate at steady state which published elsewhere. [70,72]

There were many reports for ethane yield which was summarized in table 20 for variety of catalysts.[69,71,73,74] Moreover, there was an interested issue that yield of ethane were almost constant with small standard deviation at any range of operating condition (i.e. temperature and CH_4/H_2 feed ratio).

Table 20: Yield of ethane for each catalyst [69,71,73,74]

Catalyst	Temperature ($^\circ$C)	CH_4/H_2	Average ethane yield (%mole)	Standard deviation
$Mn/Na_2WO_4/SiO_2$	775-875	4-10	9.07	0.41
La_2O_3/CaO	750-875	5-10	4.16	0.60
PbO/Al_2O_3	700-750	5-10	3.22	0.62
La/MgO	750-850	4	7.75	0.48
Li/MgO	700-820	4	4.14	0.54
$Sn-Ba-TiO_3$	725-775	2-4.5	5.32	0.60

5.3.2 Manipulation of Duo-equilibrium reaction model

As mention in previous section, the existence of intermediate of the chemical reaction was accepted and the chemical equilibrium concept could not describe the intermediate behavior because the combination reaction did not suggest the existence of intermediate. In this section, the manipulation for running the program was described and verified the results.

Up to this section, the best fit model of the simulation for Mo_2C/Al_2O_3 and $Mo_2C/ZSM-5(80)$ was the Trio-equilibrium reaction model type B which was the connection between the three reactors in series. The model shown best fit for Mo_2C/SiO_2 was the duo-equilibrium reaction model which was the set of two reactors in series. The comparison results between the duo-equilibrium reaction model for Mo_2C/SiO_2 was shown in figure 44.
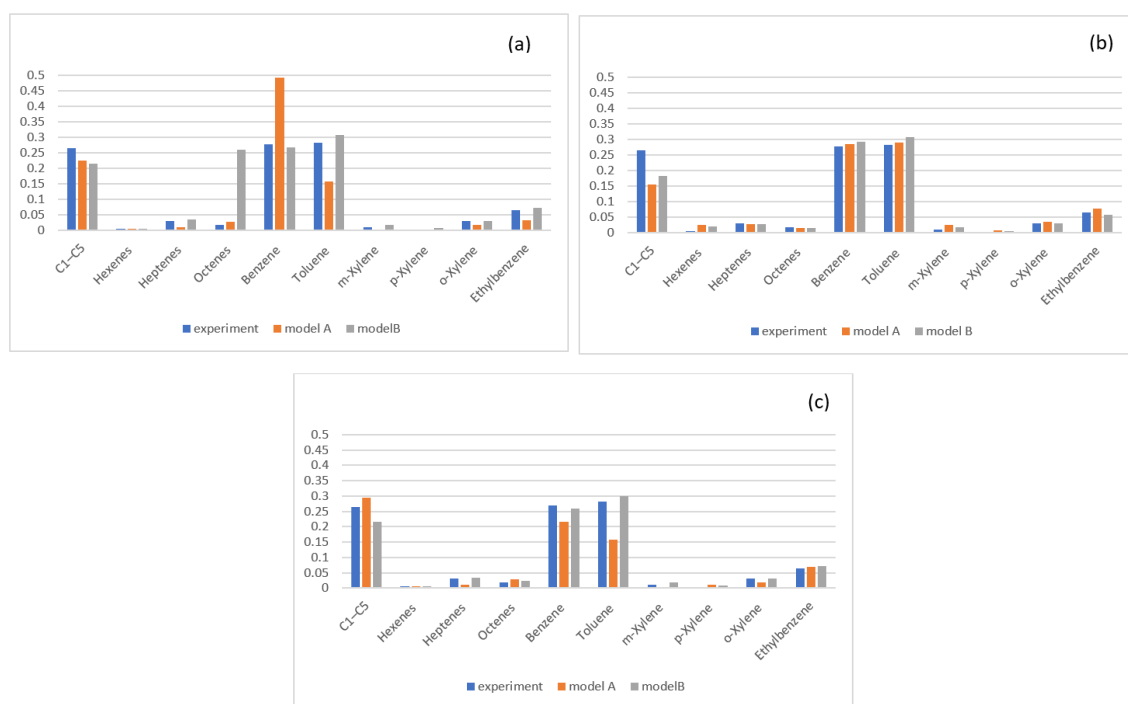
Figure 44: Comparison of results from the duo-equilibrium reaction

model A and model B for Three catalyst

(Conditions: T = 550°C and feed ratio of H$_2$/n-alkanes = 3)

(a) The duo-equilibrium reaction model for Mo$_2$C/Al$_2$O$_3$

(b) The duo-equilibrium reaction model for Mo$_2$C/SiO$_2$

(C) The duo-equilibrium reaction model for Mo$_2$C/ZSM-5(80)

From figure 44, it is clearly shown that after the manipulation, the prediction results from the duo-equilibrium reaction model B showed almost identical to the expected results. Thus, this model was appropriate. Thus, this model was appropriate for Mo$_2$C/SiO$_2$ catalyst.

The comparison of results from the duo-equilibrium reaction model A and B for Mo$_2$C/Al$_2$O$_3$ and Mo$_2$C/ZSM-5(80) catalyst were shown in figure 44 (a) and 44 (b), respectively.

From figure 44 (a) and 44 (b), the manipulated duo-equilibrium reaction model B could provide better outcome of effluents for Mo_2C/Al_2O_3 and Mo_2C/ZSM-5(80). However, there were still deviation of benzene and toluene. Hence, the manipulation technique used in duo-equilibrium reactors model did not suit for Mo_2C/Al_2O_3 and Mo_2C/ZSM-5(80). More tests were tried with the trio-equilibrium reactions model.

5.3.3 Manipulation of Trio-equilibrium reaction model

This model was developed from the trio-equilibrium reaction model B mentioned in section 5.2.3.2. This model gave good result for Mo_2C/Al_2O_3 and Mo_2C/ZSM-5(80). After the model was manipulated as mentioned above, the simulations were tested and the results were shown in figure 4 5 for Mo_2C/Al_2O_3 catalyst and figure 46 for Mo_2C/ZSM-5(80).
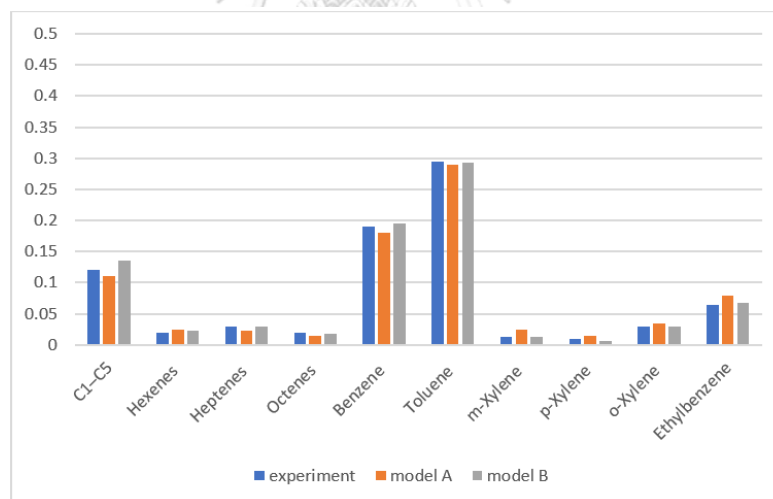
Figure 45: Comparison of results from the Trio-equilibrium reaction model A and B

for Mo_2C/Al_2O_3

(Conditions: T = 550°C and feed ratio of H_2/n-alkanes = 3)

(Blue) Results of the literature review experiment

(Orange) Results of the Trio-equilibrium reaction model A

(Gray) Results of the Trio-equilibrium reaction model B
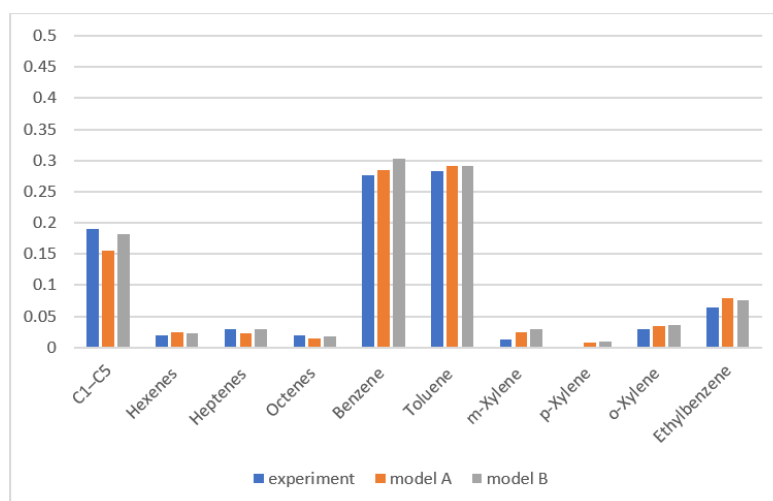
Figure 46: Comparison of results from the Trio-equilibrium reaction model A and B

for Mo$_2$C/ZSM-5(80)

(Conditions: T = 550°C and feed ratio of H$_2$/n-alkanes = 3)

(Blue) Results of the literature review experiment

(Orange) Results of the Trio-equilibrium reaction model A

(Gray) Results of the Trio-equilibrium reaction model B

Figure 45 showed the comparison results of the trio-equilibrium reaction model A and B for Mo$_2$C/Al$_2$O$_3$ catalyst and figure 46 was for Mo$_2$C/ZSM-5(80). The results from the manipulating techniques were shown that both simulations for Mo$_2$C/Al$_2$O$_3$ and Mo$_2$C/ZSM-5(80) were best fit. Concentrations of all components are quite close to the expected results. The deviations of benzene, toluene as well as xylenes from the previous duo-equilibrium model were diminished with the manipulation technique. It could be concluded that the suitable model for both Mo$_2$C/Al$_2$O$_3$ and Mo$_2$C/ZSM-5(80) catalyst was the trio-equilibrium reaction model B.

In summary, the best fit equilibrium model gave better results for BTX productions. By manipulating the duo-equilibrium model B, BTX component as well as other products were reasonably matched with equilibrium composition. Then, for the Mo$_2$C/SiO$_2$ catalyst, the best model was the duo-equilibrium model for the

catalysts of Mo_2C/Al_2O_3 and Mo_2C/ZSM-5(80), the best fit was the trio-equilibrium reactors model with three reactors connected in series.

Moreover, these manipulation models could fit the equilibrium composition at various temperature and feed ratio of H_2/n-alkanes. The validation was then described in next section.

5.3.4 Verification and Validation of Manipulation Model

In this section, the verification and validations of the best fit models were accessed. The best fit developed models were simulated with the operating condition similar to equilibrium composition of the same catalyst. For 2% Mo_2C/Al_2O_3 2% Mo_2C /SiO_2 and 5% Mo_2C /ZSM-5(80), the temperature range of 450 – 600°C and feed H_2/n-alkanes of 3 – 10.

Plots for effluent fractions at the four temperatures with respect to the feed ratio of H_2/n-alkanes were shown in figure 47-49. It should be mentioned here that results from other temperatures were not plotted.
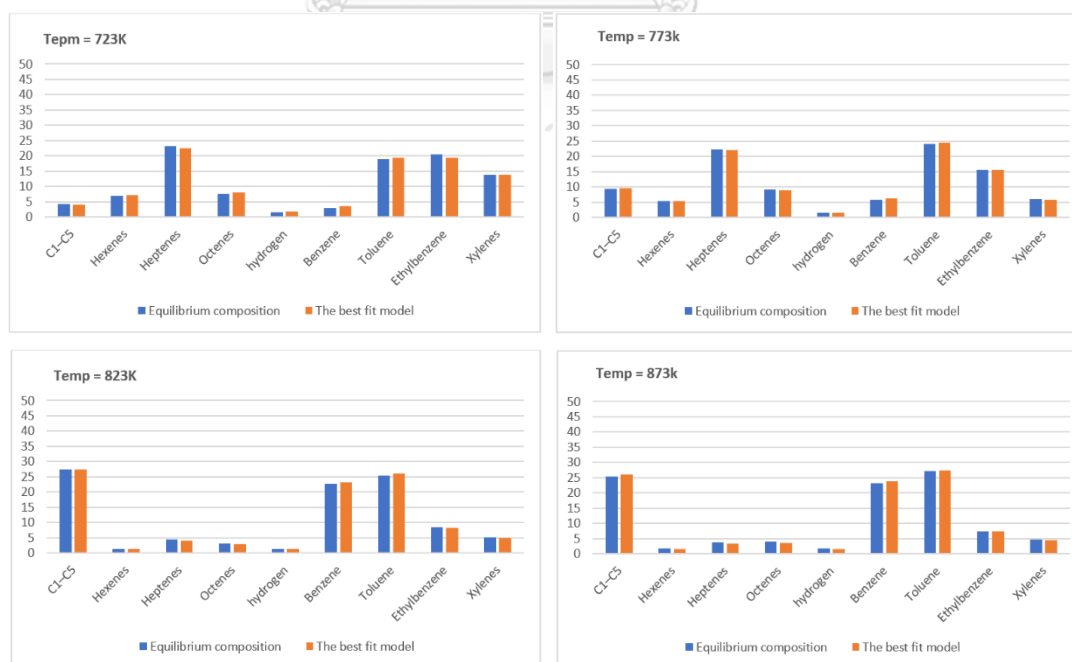
Figure 47: Simulation results from the best fit developed model (Orange) and the equilibrium composition (Blue) for Mo_2C/Al_2O_3 catalyst
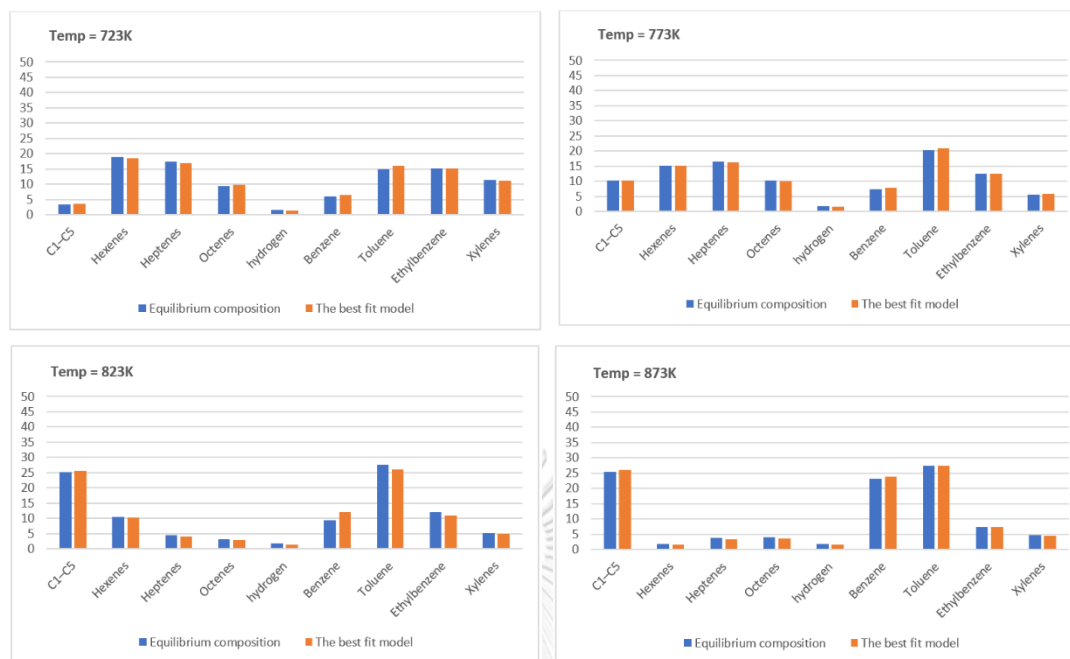
Figure 48: Simulation results from the best fit developed model (Orange) and the equilibrium composition (Blue) for Mo_2C/SiO_2 catalyst
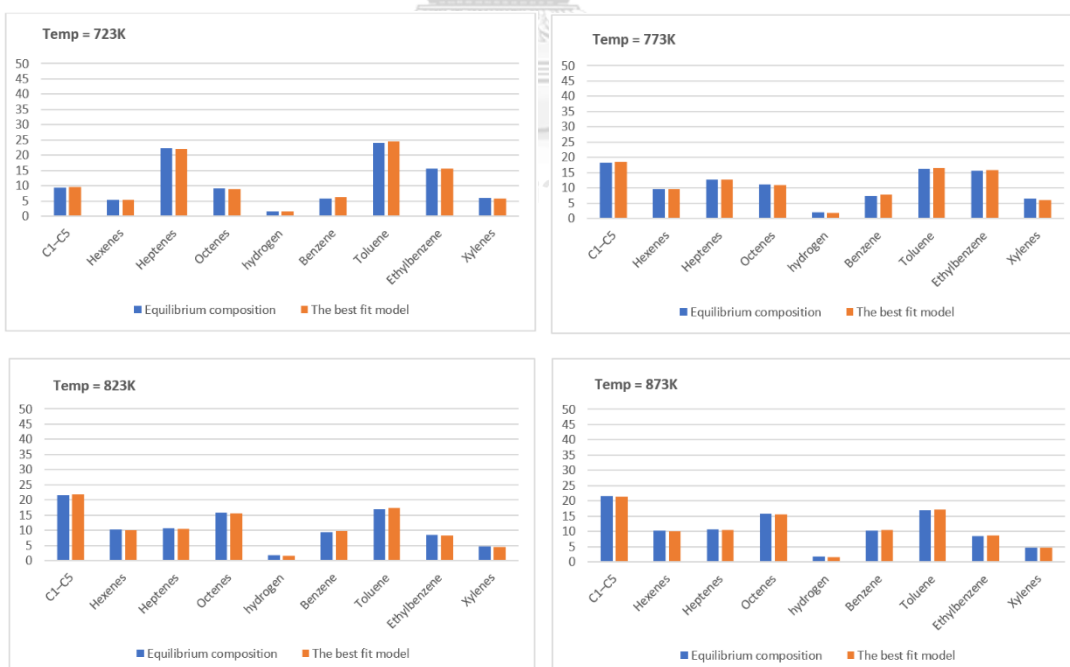
Figure 49: Simulation results from the best fit developed model (Orange) and the equilibrium composition (Blue) for $Mo_2C/ZSM-5(80)$ catalyst

From figure 47-49 showed the simulation results from the best fit developed model (Orange) and the equilibrium composition (Blue) for three catalysts. All components showed the good agreement of simulation data between orange bar and blue bar. The model showed the accurately predict the variation of hydrogen to n-alkanes (n-C_6, n-C_7, n-C_8) feed ratio with small deviation. However, it should be noticed that the accuracy of the model was depended on temperature. The higher the temperature, the closer the prediction of results.

In conclusion, the manipulated models could predict the aromatics reaction at various operating conditions. The validity range of the models would be discussed further in section 5.4.2.2.

5.4 Verification of models

5.4.1 Verification of models using statistics RSS

In this chapter, the statistic of Residua Sum Square (RSS) was used to verify the precision of simulation. The verification was done by running the aromatics reaction in the suitable developed models with the condition similar to that of literatures. The RSS of the differences between data from developed model and the reference data were calculated. Table 21 summarized the RSS value of studied model for all three catalysts. Because the tight fit of the model to the data was suggested with the small value of RSS, then models with best fit for a catalyst were labeled with superscript of alphabet "A" for normal equilibrium models and "B" for manipulated models.

Table 21: RSS of the developed models for three catalysts

Model	RSS		
	Mo_2C/Al_2O_3	Mo_2C/SiO_2	$Mo_2C/ZSM-5(80)$
Equilibrium Models			
Uni-equilibrium reaction model	171.10	124.75	8.84
Uni-equilibrium reaction model with selected reactions	8.34	4.23	3.80
Duo-equilibrium reaction model A	1.24	0.95[a]	12.04
Duo-equilibrium reaction model B	4.79	3.31	32.9
Trio-equilibrium reaction model A	4.17	3.71	14.67
Trio-equilibrium reaction model B	1.09[a]	2.23	1.50[a]
Manipulated Equilibrium Models			
Manipulated Duo-equilibrium reaction model A	0.14	0.03[b]	6.67
Manipulated Trio-equilibrium reaction model B	0.09[b]	1.46	0.01[b]

[a] Best fit model for equilibrium model

[b] Best fit model for manipulated model

As seen in the table 21, the best models over Mo_2C/Al_2O_3 and $Mo_2C/ZSM-5(80)$ were the trio-equilibrium reaction model. While the model reaction over the catalyst of Mo_2C/SiO_2 was used to predict well with the duo-equilibrium reaction model. Thus, it could be concluded that the base reactions in system were the same pattern in any types of catalysts. However, the difference between types of catalysts depended on the composition of the catalyst. The catalysts which contained element that supported hydrocracking reaction, such as Si and Al, were selective to hydrocracking reaction as well.

However, the equilibrium model could not predict the ethane composition correctly. The results for manipulated models gave the better results comparing to normal equilibrium models. Table 22 showed the conclusion of catalysts properties and the best model for predicting the behavior of reaction including its parameters.

Table 22: Catalyst properties and its appropriate proposed models

Category	Catalyst		
	Mo_2C/Al_2O_2	Mo_2C/SiO_2	$Mo_2C/ZSM\text{-}5(80)$
Type of catalyst	Post-Transition	Transition	Rare Earth Metal
Void fraction	0.7	0.4	0.78
Catalyst Density (kg/m³)	2000	1100	3600
Best fit Model	Trio-equilibrium reaction model	Duo-equilibrium reaction model	Trio-equilibrium reaction model

5.4.2 Validation of the developed models by reactor performance

In this section, the precision of the models was determined by comparing results with reactor performances reported from literatures. Reactor performances to be compared in this section were n-alkanes (n-C6, n-C7, n-C8) conversion, aromatics selectivity including Benzene, Toluene, Xylenes (called in this case BTX and other products selectivity. The definitions of these variables were expressed in section 4.4.

5.4.2.1 Validation by comparing with laboratory experiment

The trio-equilibrium reaction model was run over $Mo_2C/ZSM\text{-}5(80)$ catalyst with the conditions used in Daneshpayeh et al [61]. Conversion of n-alkanes (n-C_6, n-C_7, n-C_8) and products selectivity from both trials were calculated and compared to the reactor performances reported from laboratory experimental results.

The simulations were tested at both 550°C and 600°C for confirmation of results. The results were shown in figure 50 (a) and (b), respectively.
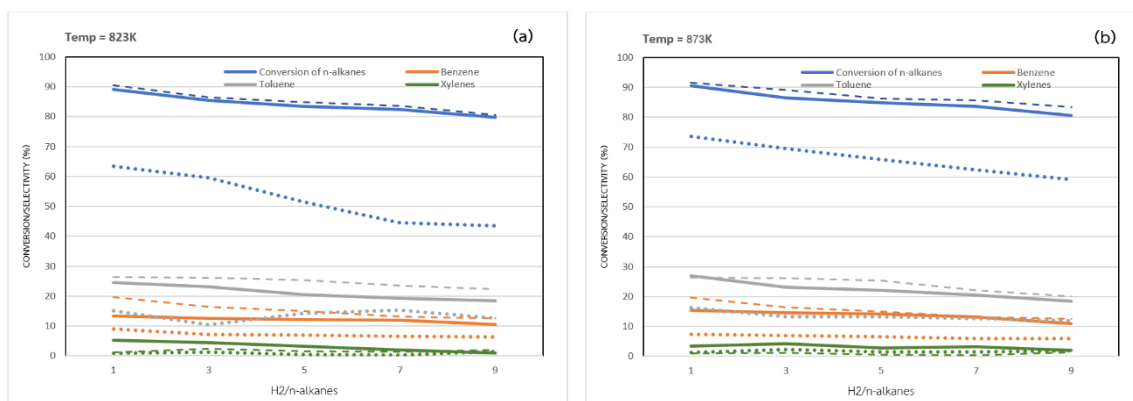
Figure 50: The performance plots with respect to feed ratio (H_2/n-alkanes) for
Mo$_2$C/ZSM-5(80) catalyst (a) 550°C (b) 600°C
(Solid) experimental results
(Dash) the manipulated trio-equilibrium model B
(Dot) the manipulated Duo-equilibrium model B

From figure 50, the reactor performances to be compared were n-alkanes (n-C6, n-C7, n-C8) conversion (Blue), benzene selectivity (Orange) and toluene selectivity (Gray) xylenes selectivity (Green). In figure 50 (a), it was clearly shown all performance calculated from the trio-equilibrium reaction model (dash line) were close to that of the experimental results (solid line). While the calculations from the duo-equilibrium reaction model (dots line) showed quite far from the expected results (solid line). The same results for all performances were shown at 600°C of simulation test (figure 50 (b)). Thus, the equilibrium reaction model without manipulation could not accurately predict the outcome of aromatics reaction.

Take a closer look to the trio-equilibrium reaction model which was manipulated, the side reaction occurred at high temperature and caused the formation of coke [75]. The reaction was supposed to be the decomposition of methane which converted methane into carbon and hydrogen (Eq 5.4).

$$CH_4 \quad \rightarrow \quad C + 2H_2 \quad\quad\quad\quad (5.4)$$
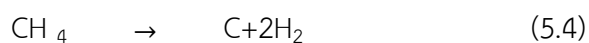
It was believed that this side reaction brought about the deviation occurring for both kinetic model and the equilibrium model. Since, the product of this reaction was solid of coke, it could not be put as the available reaction in the simulation program. However, the percentage error caused by this side reaction was in the acceptable range which could be ignored.

For Mo_2C/SiO_2 catalyst, the duo-equilibrium reaction model was used for simulation. Conditions were imitated from Stransch et al [60]. The results compared with that from the experiments were expressed in figure 51.
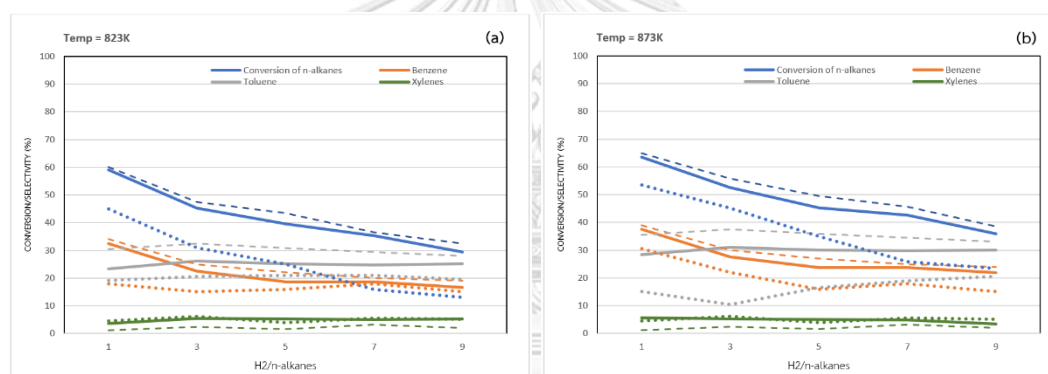
Figure 51: The performance plots with respect to feed ratio (H_2/n-alkanes)
for Mo_2C/SiO_2 catalyst at (a) 550°C (b) 600°C
(Solid) experimental results
(Dot) the manipulated duo-equilibrium reaction model A
(Dash) the manipulated duo-equilibrium model B

The reported reactor performances over Mo_2C/SiO_2 catalyst of Stransch et al [60] were n-alkanes conversion and yield of BTX. The blue line showed n-alkanes conversion of model which was considerable close to experiment. Benzene selectivity (Orange) and toluene selectivity (Gray) xylenes selectivity (Green) which acceptable deviate from experiment. Thus, the manipulated duo-equilibrium reaction

model could predict the results that fit with the experiment. It should be notice that the dots line of the manipulated duo-equilibrium reaction model B showed the same trend as the experimental results but with large deviation. Thus, without manipulation, the duo-equilibrium reaction model could roughly predict the outcome of OCM for ethane and ethylene components.

In summary, the equilibrium model without manipulation could roughly predict reactor performance while the manipulation of the model could predict with better accuracy. However, the model had some limitation in prediction of decomposition reaction which did not including in calculation system.

5.4.2.2 Validity region of developed model at variety of operating conditions

The comparisons of reactor performance calculated from best manipulated model and equilibrium composition at various operating conditions were shown in this section. It was aimed to find the validity region based on the performance of process within 20% deviation. The interest performances were n-alkanes conversion, selectivity of BTX. The studied operating conditions for Mo_2C/Al_2O_3, Mo_2C/SiO_2 and $Mo_2C/ZSM-5(80)$ were at temperature 450-700°C and H_2/n-alkanes feed ratio 3-10.

The validity region was determined using the AARD. The validity of the developed model was strong accepted at the 15% lower of AARD and accepted under the considerable at 20% lower of AARD.

The best fit developed models were written again below; the trio equilibrium model for Mo_2C/Al_2O_3 and $Mo_2C/ZSM-5(80)$, the duo-equilibrium reaction model for Mo_2C/SiO_2 catalyst

Table 23: indicated operating conditions of $Mo_2 C/Al_2 O_3$ catalyst which provided the AARD lower than 10% (+), AARD between 10-15% (•), AARD between 15 – 20% (O) and AARD more than 20% (x).

Table 23: AARD with respect to H_2/n-alkanes feed ratios at variety of reaction temperatures for Mo_2C/Al_2O_3.

H_2/n-alkanes Feed Ratio	Temperature (°C)									
	450	475	500	525	550	575	600	625	675	700
3	X	X	X	X	O	•	+	+	X	X
3.5	X	X	X	O	•	+	+	+	X	X
4	X	X	X	O	•	+	+	+	X	X
4.5	X	X	X	O	+	+	+	+	X	X
5	X	X	O	•	+	+	+	+	X	X
5.5	X	X	O	•	+	+	+	+	X	X
6	X	X	O	•	+	+	+	+	X	X
6.5	X	X	O	+	+	+	+	+	X	X
7	X	X	O	+	+	+	+	+	X	X
7.5	X	X	•	+	+	+	+	+	X	X
8	X	X	•	+	+	+	+	+	X	X
8.5	X	X	•	+	+	+	+	+	X	X
9	X	X	•	+	+	+	+	+	X	X
9.5	X	X	•	+	+	+	+	+	X	X
10	X	X	•	+	+	+	+	+	X	X
11	X	X	X	X	X	X	X	X	X	X
12	X	X	X	X	X	X	X	X	X	X

+ AARD less than 10%   • AARD between 10-15%   O AARD between 15-20%   X AARD more than 20%

As seen in the table, the operating conditions which the manipulated trio-equilibrium reaction model could predict effluence of Mo_2C/Al_2O_3 catalyst with the AARD less than 15% were at temperature 525-625°C and H_2/n-alkanes feed ratio were 4-10. It should be noticed that at higher temperature than 625°C or H_2/n-alkanes feed ratio more than 10, all of the AARD values were excess than 20%. The deviations were caused by the reference value that simulated from kinetic were deviated. The kinetic model of Hinsen et al [62] was confirmed their accuracy only at temperature 500-600°C and H_2/n-alkanes feed ratio 3-10.

With respect to AARD calculation, for Mo_2C/SiO_2 catalyst, the accuracy of the developed model at the variety of temperature and feed ratio of H_2/n-alkanes were shown in table 24.

Table 24: AARD with respect to H_2/n-alkanes feed ratios at variety of reaction temperatures for Mo_2C/SiO_2.

H_2/n-alkanes Feed Ratio	Temperature (°C)									
	450	475	500	525	550	575	600	625	675	700
3	X	X	X	X	O	•	•	X	X	X
3.5	X	X	X	X	•	+	+	O	X	X
4	X	X	X	O	•	+	+	O	X	X
4.5	X	X	X	•	•	+	+	O	X	X
5	X	X	O	•	•	+	+	O	X	X
5.5	X	X	O	•	•	+	+	O	X	X
6	X	X	•	+	•	+	+	O	X	X
6.5	X	X	+	•	•	+	+	O	X	X
7	X	X	+	+	•	+	+	O	X	X
7.5	X	X	+	•	•	+	+	O	X	X
8	X	X	+	•	•	+	+	O	X	X
8.5	X	X	+	•	•	+	+	O	X	X
9	X	X	+	+	+	+	+	O	X	X
9.5	X	•	+	•	+	+	+	O	X	X
10	X	O	+	•	•	+	+	O	X	X
11	X	X	X	X	X	X	X	X	X	X
12	X	X	X	X	X	X	X	X	X	X

+ AARD less than 10%   • AARD between 10-15%   O AARD between 15-20%   X AARD more than 20%

As seen in the table, the operating conditions which the manipulated duo-equilibrium reaction model could predict effluence of Mo_2C/SiO_2 with the AARD less than 15% was at temperature 500-600°C and H_2/n-alkanes feed ratio were 5-10. Again, the values of AARD for temperature more than 625°C or H_2/n-alkanes feed ratio more than 10 were deviated more than 20%. It was also caused by deviation of kinetic model which simulated out of literature ranges.

Mo_2 C/ZSM-5(80) could be predicted by the trio equilibrium model with specifying the ethane yield. Table 25 indicated operating condition which had AARD lower than 15%.

Table 25: AARD with respect to H_2/n-alkanes feed ratios at variety of reaction temperatures for Mo_2C/ZSM-5(80).

H_2/n-alkanes Feed Ratio	Temperature (^oC)									
	450	475	500	525	550	575	600	625	675	700
3	X	X	O	O	O	•	•	X	X	X
3.5	X	X	O	O	•	+	+	X	X	X
4	X	X	X	O	•	+	+	X	X	X
4.5	X	X	X	•	•	+	+	X	X	X
5	X	X	O	•	•	+	+	X	X	X
5.5	X	X	O	•	•	+	+	X	X	X
6	X	X	•	+	•	+	+	X	X	X
6.5	X	X	+	•	•	+	+	X	X	X
7	X	X	+	+	•	+	+	X	X	X
7.5	X	X	+	•	•	+	+	X	X	X
8	X	X	+	•	•	O	•	X	X	X
8.5	X	X	+	•	•	O	+	X	X	X
9	X	X	+	+	•	•	+	X	X	X
9.5	X	X	O	+	+	•	+	X	X	X
10	X	X	O	+	+	•	+	X	X	X
11	X	X	X	X	X	X	X	X	X	X
12	X	X	X	X	X	X	X	X	X	X

+ AARD less than 10%   • AARD between 10-15%   O AARD between 15-20%   X AARD more than 20%

As seen in the table, the operating conditions which the manipulated trio-equilibrium reaction model could predict outcome of Mo_2C/ZSM-5(80) with the AARD less than 15% was at temperature 500-600^oC and H_2/n-alkanes feed ratio were 4-10. This type of catalyst also reported AARD value over than 20% at temperature more than 625 ^oC or H_2/n-alkanes feed ratio more than 10. It was corresponding to reference data which simulated by kinetic simulation were out of range suggested by literature.

In summary, each model had its individual accuracy range. Table 2 6 concluded ranges of operations for each model and catalyst. It should be noticed that, for all models, the best conditions were at high temperature.

Table 26: The validity for the developed equilibrium model.

Catalyst	Mo_2C/Al_2O_3	Mo_2C/SiO_2	$Mo_2C/ZSM-5(80)$
Pressure (atm)	1	1	1
Temperature (^oC)	525-625	500-600	500-625
H_2/n-alkanes mole ratio	3-10	5-10	4-10

5.5 The advantage of the proposed model

According to the results explained previously, this research succeeded to construct and develop the competitive model for predicting the aromatics production. The models were able to predict the components composition and performances correctly. The models were proposed with confidence to be an alternative tool for predicting the outcomes as required. This section described the advantages of the proposed models which were two categories, the ease in prediction and extrapolated prediction.

5.5.1 Ease in prediction

The comparison of some utility responses was summarized in table 27. [73,75]

Table 27: Comparison between kinetic model and the proposed model.

Topic	Kinetic Model	Equilibrium Model
Number of Parameters	a lot	small
Accuracy	High	High
Limitation	within regression range of experiments	only at the equilibrium
Iteration time	fast	Very fast
Data required for Construction	a lot of data from experiment	A few data from experiment
Reactor Design Availability	Yes	No

As kinetic model was developed from regression of the experiment data into rate law equations, a lot of experiment data were required to construct the model. The accuracy of the kinetic model within the range of regression was high.

For the equilibrium model, it was developed from theory with some manipulations which required only a few data to determine the parameters. The calculation procedure for equilibrium was simple. Nevertheless, equilibrium model had the limitation to predict only at equilibrium time while kinetic model could predict the effluence as a function of time and able to use for reactor design.

Table 28 summarized the comparison of parameters of both models, kinetic model and equilibrium model (EB) for three catalyst. It was obviously seen that equilibrium model have lower parameters than that of kinetic model with average error slightly more than kinetic model but still less than 20%. Thus, the use of equilibrium model was more convenient because it required less parameter than kinetic model with the same level of accuracy.

Table 28: Parameters comparison between kinetic and equilibrium model

Catalyst	Mo_2C/Al_2O_3		Mo_2C/SiO_2		$Mo_2C/ZSM\text{-}5(80)$	
	Kinetic	EB	Kinetic	EB	Kinetic	EB
Number of Reactions	10	5	10	4	4	5
Number of Parameters	42	2	54	2	16	2
Number of reactors	1	3	1	2	1	3
AARD (%)	9.15	9.74[*]	14	15.56[*]	-	15.17[*]

*Range of operating conditions in table 26

In conclusion, the ease of use was the advantage of the proposed equilibrium model. To predict the aromatics production, only two parameters were required to input for simulation. The results would be obtained in a few seconds. However, this model could not be used in reactor design and was limited to predict only at the equilibrium. However, aromatics production model reached equilibrium in very short time (milliseconds). Therefore, these equilibrium models could be defined an alternative in process simulation.

5.5.2 The extrapolated prediction

One of the interesting of the equilibrium model was its capable to extrapolate the results for another aromatic reactions catalyzed by the other catalysts. Generally, the simulation of the aromatic reactions was obtained after the kinetic study which must take many laboratory experiments. Therefore, a new prediction method with much more convenient would be valued for aromatics reaction simulation.

There were 11 more catalysts which were subjected to study the accuracy of extrapolated prediction. Detail for extrapolation results were summarized in Appendix D.

In order to increase extrapolation accuracy, it was suggested to use average split fraction as well as specific BTX yield for each catalyst. However, this research was used one-point extrapolation because the others operating conditions were kept for validation with the results calculated from the reference point.

In summary, equilibrium model had capability in extrapolation prediction of aromatic reactions. After determine model parameters from experiment, the model could predict outcome of reactor within AARD less than 20%.

CHAPTER 6

CONCLUSION

The experimental results reported and described in chapter 5, which consists of reaction study in aromatics production process were summarized. The experimental variables and optimum conditions in this study were collected. Moreover, other suggestions related to this research, which useful for future studies will be described in this chapter.

6.1 Conclusion

1. Equilibrium model could predict aromatics production of normal paraffins model with concept of the reactions in the model were grouped by splitting reactors and various catalyst.

2. For typical catalyst, the duo-equilibrium reaction model which two reactor connected in series to classify which reactions was appropriate for Mo_2C/SiO_2 catalyst while Mo_2C/Al_2O_3 and $Mo_2C/ZSM-5(80)$ catalyst were appropriate for trio-equilibrium reaction model which one reactor connected in series following reactors of the duo-equilibrium reaction model.

3. Equilibrium model had limitation in prediction only at high temperature and conversion reached almost 100 percent.

4. Advantage of equilibrium model compared to kinetic was its ease in utilization due to much lower number of parameters and equations in equilibrium model. However, the equilibrium model could not be used to design the reactor.

5. Equilibrium model could extrapolation predict by fitting n-alkanes conversion, benzene toluene and xylenes of one experiment that reached equilibrium with the model.

6. Catalysts are relatively efficient for the aromatization of n-alkanes at 723–873 K. The main aromatic product was toluene. The greatest selectivity of aromatics (toluene, benzene, and xylene) and conversion measured was similar to a literature review.

7. All of these catalysts effectively promoted the aromatization of BTX assumed to be the main product of n-alkanes.

6.2 Recommendation

This model could be further developed to predict outcome of aromatics production by specified only catalyst type and properties. Unfortunately, without experiment, the data obtained from literature was not sufficed
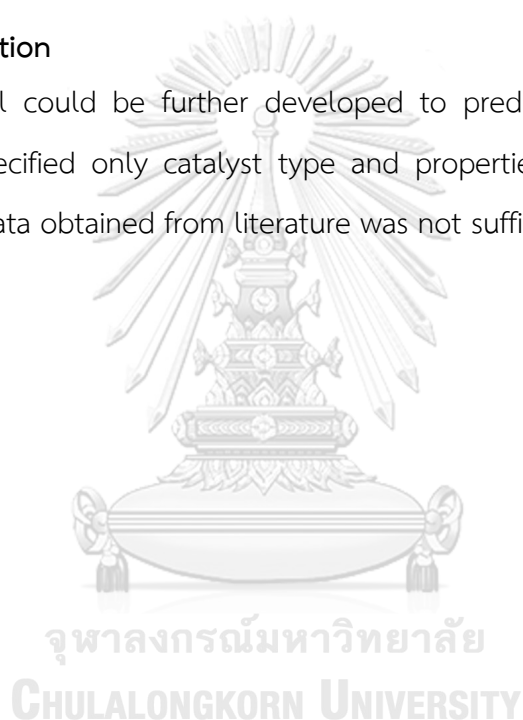
REFERENCE

[1]   P.Meriaudeau, A. Thangaraj, C. Naccache, S. Narayanan, J. Catal. 146 (1994) 579.

[2]   J.R. Bernard, in: L.V.C. Rees (Ed.), Proc. 5th Internat. Zeolite Confer., Heyden, London, 1980, p. 686.

[3]   R.J. Davis, in: HCR Concise Review, Wiley, New York, 1994, p. 41.

[4]   G.A. Somorjai, in: Proceedings of 8th International Congress in Catalysis, Berlin, 1984, Vol.I, Dechema, Frankfurt-am-Main, 1984, p. 113.

[5]   J.T. Miller, N.G.B. Agrawa, G.S. Lane, F.S. Modica, J. Catal. 163 (1996) 106.

[6]   J.E. Germain, Catalytic Conversion of Hydrocarbons, Academic Press, London, 1969.

[7]   P. Mériaudeau, C. Naccache, Catal. Rev.-Sci. Eng. 39 (1997) 5, and references therein.

[8]   N.Y. Chen, T.Y. Yan, Ind. Eng. Chem., Process Des. Dev. 25 (1986) 151.

[9]   E. Iglesia, J.F. Baumgartner, in: L. Guczi, F. Solymosi, P. Tétényi (Eds.), Proc. 10th Int. Congr. Catal., in: New Frontiers in Catalysis, Akad. Kiadó, Budapest, 1993, p. 993.

[10]   P. Wang, S. Yang, J.N. Kondo, K. Domen, T. Yamada, H. Hattori, J. Phys. Chem. B 107 (2003) 11951.

[11]   G.A. Mills, H. Heineman, T.H. Milliken, A.G. Oblad, Ind. Eng. Chem. 45 (1953) 134.

[12]   Ameen, M., et al., (2017). Catalytic hydrodeoxygenation of triglycerides: An approach to clean diesel fuel production.

[13]   Apisit Songsasen, A. S., and S. Bangkedphol (02. 2012). "General chemistry for engineers " Bangkok: Triple education: 205-219.

[14]   Covavisaruch, S., et al., (Editor. 2011). What are petroleum chemicals, in Petrochemical Encyclopedia. K. Bunyakiat, WPS(Thailand) Co..Ltd.: Bangkok: p. 14-67.

[15]   Stacia M Edwards, Stephen J Stanley, and M.M. Shreehan, *Relative economics of mixed C4 processing routes*, in *Digital Refining*. 1998, PTQ Magazine: UK.

[16]   Song, C., et al., *Influence of reaction conditions on the aromatization of cofeeding n-butane with methanol over the Zn loaded ZSM-5/ZSM-11 zeolite catalyst.* Fuel Processing Technology, 2014. 126: p. 60-65.

[17]   Wongwailikhit, K., *Modeling of Oxidative Coupling of Methane to Ethylene with Chemical Equilibria*, in *Chemical Engineering*. 2013, Chulalongkorn University.

[18]   J, B.S.R., *A Review of the Water Gas Shift Reaction Kinetics.* International Journal of Chemical Reactor Engineering, 2010. 8.

[19]   Fogler, H.S., *Elements of Chemical Reaction Engineering, 3rd* 2004.

[20]   V. H. Rane, S.T.C., V. R. Choudhary, *Influence of alkali metal doping on surface properties and catalytic activity/selectivity of CaO catalysts.* Journal of Natural Gas Chemistry 2008. 17: p. 313-320.

[21]   Farooji, N.R., A. Vatani, and S. Mokhtari, *Kinetic simulation of oxidative coupling of methane over perovskite catalyst by genetic algorithm: Mechanistic aspects.* Journal of Natural Gas Chemistry, 2010. 19(4): p. 385-392.

[22]   V. R. Choudhary, S.A.R.M., B.S. Uphade, *aromatization over alkaline earth oxides deposited on commercial support precoated with rare earth oxides.* Fuel 1999. 78: p. 427–437.

[23]   Cantelo, R.C., *The Thermal Decomposition of alkanes.* J. Phys. Chem, 1924. 28(10): p. 1036–1048.

[24]   Ching Thian Tye, A.R.M., Subhash Bhatia, *Modeling of catalytic reactor for aromatization of alkanes using La2O3/CaO catalyst.* Chemical Engineering Journal, 2002. 87: p. 49-59.

[25]   Tock, L., M. Gassner, and F. Maréchal, *Thermochemical production of liquid fuels from biomass: Thermo-economic modeling, process design and process integration analysis.* Biomass and Bioenergy, 2010. 34(12): p. 1838-1854.

[26]   Gutiérrez Ortiz, F.J., P. Ollero, and A. Serrera, *Thermodynamic analysis of the autothermal reforming of glycerol using supercritical water.* International Journal of Hydrogen Energy, 2011. 36(19): p. 12186-12199.

[27]   Zhang, Y., et al., *Process simulation and optimization of methanol production coupled to tri-reforming process.* International Journal of Hydrogen Energy, 2013. 38(31): p. 13617-13630.

[28]   Trippe, F., et al., *Comprehensive techno-economic assessment of dimethyl ether (DME) synthesis and Fischer–Tropsch synthesis as alternative process steps within biomass-to-liquid production.* Fuel Processing Technology, 2013. 106: p. 577- 586.

[29]   Bao, B., M.M. El-Halwagi, and N.O. Elbashir, *Simulation, integration, and economic analysis of gas-to-liquid processes.* Fuel Processing Technology, 2010. 91(7): p. 703-713.

[30]   Trippe, F., et al., *Techno-economic assessment of gasification as a process step within biomass-to-liquid (BtL) fuel and chemicals production.* Fuel Processing Technology, 2011. 92(11): p. 2169-2184.

[31]   Haro, P., et al., *Bio-syngas to gasoline and olefins via DME – A comprehensive techno-economic assessment.* Applied Energy, 2013. 108: p. 54-65.

[32]   Chang S. Hsu, P.R.R., *Practical Advances in Petroleum Processing.* Vol. 1. 2006.

[33]   Kareem, S.A., *SYNERGIC PROMOTION OF CATALYST BY GROUP VIII B ELEMENTS* Journal of Sciences, Islamic Republic of Iran, 2002. 13: p. 237-240.

[34]   Limited, A.P.C., *ASPEN PLUS® User Guide.* 2000.

[35]   Cavani, F., N. Ballarini, and A. Cericola, *dehydrogenation of ethane and propane: How far from commercial implementation?* Catalysis Today, 2007. 127(1-4): p. 113-131.

[36]   Sadeghzadeh Ahari, J., S. Zarrinpashne, and M.T. Sadeghi, *Micro-kinetic modeling of OCM reactions over Mn/Na2WO4/SiO2 catalyst.* Fuel Processing Technology, 2013. 115: p. 79-87.

[37]   Ahari, J.S., M.T. Sadeghi, and S. Zarrinpashne, *Effects of operating parameters on Na-W-Mn/SiO2 catalyst at elevated pressures.* Journal of Natural Gas Chemistry, 2011. 20(2): p. 204-213.

[38]   Ghiasi, M., et al., *Kinetic study of oxidative coupling of methane over Mn and/or W promoted Na2SO4/SiO2 catalysts.* Journal of Natural Gas Chemistry, 2011. 20(4): p. 428-434.

[39]   Kiatkittipong, W., et al., *Comparative study of aromatization of alkanes modeling in various types of reactor.* Chemical Engineering Journal, 2005. 115(1-2): p. 63-71.

[40]   Kruglov, A.V., M.C. Bjorklund, and R.W. Curr, *Optimization of the simulated countercurrent moving-bed chromatographic reactor for aromatization of alkanes.* Chemical Engineering Science, 1996. 51(11): p. 2945-2950.

[41]   Mleczko, U.P.a.l., *Comprehensive model of aromatization of alkanes in a fluidized-bed reactor.* Chemical Engineerin Science, 1996. 51(14): p. 3575-3590.

[42]   Pannek, U. and L. Mleczko, *Effect of scale-up on the performance of a fluidized-bed reactor for aromatization.* Chemical Engineering Science, 1997. 52(14): p. 2429-2434.

[43]   Ng, K.S. and J. Sadhukhan, *Process integration and economic analysis of bio-oil platform for the production of methanol and combined heat and power.* Biomass and Bioenergy, 2011. 35(3): p. 1153-1169.

[44]   Zhang, Y., et al., *Comparative techno-economic analysis of biohydrogen production via bio-oil gasification and bio-oil reforming.* Biomass and Bioenergy, 2013. 51: p. 99-108.

[45]   Freitas, A.C.D. and R. Guirardello, *reforming of alkanes for hydrogen and synthesis gas production: Thermodynamic equilibrium analysis.* Journal of Natural Gas Chemistry, 2012. 21(5): p. 571-580.

[46]   Jones, C.A., J.J. Leonard, and J.A. Sofranko, *The oxidative conversion of alkanes to higher hydrocarbons over alkali-promoted MnSiO2.* Journal of Catalysis, 1987. 103(2): p. 311-319.

[47]   Nelson, P.F., C.A. Lukey, and N.W. Cant, *Isotopic evidence for direct methyl coupling and ethane to ethylene conversion during partial oxidation of methane over lithium/magnesium oxide.* The Journal of Physical Chemistry, 1988. 92(22): p. 6176-6179.

[48]   Morales, E. and J.H. Lunsford, *Dehydrogenation of hexane over a lithium-promoted magnesium oxide catalyst.* Journal of Catalysis, 1989. 118(1): p. 255-265.

[49] M. Kennedy, E. and N. W. Cant, *Comparison of dehydrogenation of octane and oxidative coupling of hexane over rare earth oxides.* Applied Catalysis, 1991. 75(1): p. 321-330.

[50] Miro, E., J. Santamaria, and E.E. Wolf, *Dehydrogenation of octane on alkali metal-promoted nickel titanate: I. Catalyst characterization and transient studies.* Journal of Catalysis, 1990. 124(2): p. 451-464.

[51] Lacombe, S., et al., *Kinetic modelling of aromatization of hydrocarbons over lanthanum oxide in connection with mechanistic studies.* Chemical Engineering & Technology, 1995. 18(3): p. 216-223.

[52] Traykova, M., et al., *aromatization of hydrocarbons – the transition from reaction to transport control over La2O3/MgO catalyst.* Applied Catalysis A: General, 1998. 169(2): p. 237-247.

[53] Shahri, S.M.K. and S.M. Alavi, *Kinetic studies of the aromatization of hydrocarbons over the Mn/Na2WO4/SiO2 catalyst.* Journal of Natural Gas Chemistry, 2009. 18(1): p. 25-34.

[54] Lee, M.R., et al., *A kinetic model for the aromatization of hydrocarbons over Na2WO4/Mn/SiO2.* Fuel Processing Technology, 2012. 96: p. 175-182.

[55] Lee, J.Y., et al., Scaled-up production of C6 hydrocarbons by the aromatization of hydrocarbons over pelletized Na2WO4/Mn/SiO2 catalysts: Observing hot spots for the selective process. Fuel, 2013. 106: p. 851-857.

[56] Jašo, S., et al., aromatization of Octane: Reactor Performance and Operating Conditions. 2010. 28: p. 781-786.

[57] Liu, H., et al., Scale up and stability test for aromatization of hydrocarbons over Na2WO4-Mn/SiO2 catalyst in a 200 ml fixed-bed reactor. Journal of Natural Gas Chemistry, 2008. 17(1): p. 59-63.

[58] Jašo, S., et al., Experimental investigation of fluidized-bed reactor performance for aromatization of alkanes. Journal of Natural Gas Chemistry, 2012. 21(5): p. 534-543.

[59] Klvana, D., Alkanes and its derivatives (Chemical Industries Series/70), by Sunggyu Lee, 1996, 424 + viii pages, illustrated, Marcel Dekker inc, Monticello, NY 12701. ISBN#: 0-8247-9754-X. Price: US $165.00. The Canadian Journal of Chemical Engineering, 1997. 75(5): p. 990-990.

[60] Alvarez-Galvan, M.C., et al., Direct heptane conversion routes to chemicals and fuels. Catalysis Today, 2011. 171(1): p. 15-23.

[61] Rostrup-Nielsen, J.R., Production of synthesis gas. Catalysis Today, 1993. 18(4): p. 305-324.

[62] Ullmann's Encyclopedia of Industrial Chemistry 2003. 10(Cyano Compounds, Inorganic): p. 774.

[63] Oryx GTL plant officially opened. Focus on Catalysts, 2006. 2006(9): p. 4.

[64]   Lobo, W.E., Chemical Process Industries, Third Edition, R. Norris Shreve, McGraw-Hill Book Company, New York (1967). $18.50. AIChE Journal, 1968. 14(2): p. 210-364.

[65]   Driscoll, D.J., et al., Formation of gas-phase methyl radicals over magnesium oxide. Journal of the American Chemical Society, 1985. 107(1): p. 58-63.

[66]   Dissanayake, D., J.H. Lunsford, and M.P. Rosynek, Site Differentiation in Homolytic vs. Heterolytic Activation of Methane over Ba/MgO Catalysts. Journal of Catalysis, 1994. 146(2): p. 613-615.

[67]   Buyevskaya, O.V., et al., Transient Studies on Reaction Steps in the aromatization of heptane over Catalytic Surfaces of MgO and Sm2O3. Journal of Catalysis, 1994. 146(2): p. 346-357.

[68]   Lunsford, J.H., *The Catalytic aromatization of heptane.* Chem. Int. Ed. Engl, 1995. 34: p. 970-980.

[69]   Oosterkamp, P.F.v.d., *Encyclopedia of Catalysis.* I. Horvath (Ed.), 2003. 6: p. 770.

[70]   Holmen, A., *Direct conversion of alkanes to fuels and chemicals.* Catalysis Today, 2009. 142(1-2): p. 2-8.

[71]   Al-Shalchi, W., *Gas to Liquid Technology (GTL).* 2006.

[72]   G.Ertl, H.K., *Handbook of Heterogeneous Catalysis.* Vol. 1. 2008.

[73]   Tiemersma, T.P., et al., *A kinetics study for aromatization of hydrocarbons on a Mn/Na2WO4/SiO2 catalyst.* Applied Catalysis A: General, 2012. 433-434: p. 96-108.

[74]   Arndt, S., et al., *Mn–Na2WO4/SiO2 as catalyst for the aromatization of hydrocarbons. What is really known?* Applied Catalysis A: General, 2012. 425-426: p. 53-61.

[75]   Simon, U., et al., *Fluidized bed processing of sodium tungsten manganese catalysts for the aromatization of hydrocarbons.* Chemical Engineering Journal, 2011. 168(3): p. 1352-1359.

[76]   Sergei Pak, P.Q., and Jack H. Lunsford, *Elementary Reactions in the aromatization of hydrocarbons over Mn/Na2WO4/SiO2 and Mn/Na2WO4/MgO Catalysts.* Journal of catalysis 1998. 179: p. 222-230.

[77]   Z. Stansch, L.M., * and M. Baerns‡, *Comprehensive Kinetics of aromatization of hydrocarbons over the La2O3/CaO Catalyst.* Ind. Eng. Chem. Res., 1997. 36: p. 2568-2579.

[78]   Daneshpayeh, M., et al., *Kinetic modeling of aromatization of hydrocarbons over Mn/Na2WO4/SiO2 catalyst.* Fuel Processing Technology, 2009. 90(3): p. 403-410.

[79]   Hinsen, W.B., W.; Baerns, *Dehydrogenation and Coupling of hydrocarbons.* Proceedings of the 8th International Congress on Catalysis, 1985: p. 251- 283.

[80]   Olsbye, U., et al., *A kinetic study of the aromatization of hydrocarbons over a BaCO3 / La2On(CO3)3-n catalyst: I. Determination of a global reaction scheme and the influence

of heterogeneous and homogeneous reactions. Catalysis Today, 1992. 13(2–3): p. 209-218.

[81]   J.M. Smith, H.C.V.N., M.M. Abbott, *Introduction to Chemical Engineering Thermodynamics.* 2005: McGraw-Hill Companies, Inc.

[82]   Keller, G.E. and M.M. Bhasin, *Synthesis of ethylene via aromatization of hydrocarbons: I. Determination of active catalysts.* Journal of Catalysis, 1982. 73(1): p. 9-

APPENDIX

Appendix A: Kinetic Model Validation

Before invention of equilibrium model, reactor effluent data such as conversion and selectivity were required for verification of the model. Unfortunately, effluent data at equilibrium times (very small amount of oxygen left) was lacked. However, this data could be simulated by kinetic model which also represented the system. Nevertheless, kinetic models need to be validated to ensure their precise and accuracy.

In this research, there were three catalysts being studied, Mo_2C/Al_2O_3, Mo_2C/SiO_2 and $Mo_2C/ZSM-5(80)$. Kinetic model for Mo_2C/SiO_2 of Stranch et al [10] was validated with the experiment result from Ching Thian Tye et al [76]. Table A.1 showed the validation for conversion, selectivity and yield which had slightly deviation from experimental.

Table A.1 Kinetic Model Validation for Mo_2C/SiO_2

	Runs					
	1 (1023K)	2 (1073K)	3 (1103K)	4 (973 K)	5 (1023K)	6 (1103K)
Feed Mole Ratio						
n-alkanes	0.612	0.612	0.612	0.699	0.699	0.699
H_2	0.388	0.388	0.388	0.301	0.301	0.301
Conversion (%)						
Experiment*	4.9	7.9	9.9	4.1	7.1	14.4
Simulated	7.1	11.4	12.2	4.7	8.9	17.3
Selectivity (%)						
Experiment*	55.6	69.2	72.5	35.6	53.7	69.6
Simulated	56.5	67.2	68.1	32.2	47.7	62.2
Yield (%)						
Experiment*	2.7	5.5	7.2	1.5	3.8	10
Simulated	4.0	7.7	8.3	1.5	4.2	10.8

* At m_{cat}/V_{STP} = 3.7 kg s m^{-3}

Validation of Mo$_2$ C/ZSM-5(80) catalyst, validation was compared with experiment as showed in table A.2. In the table, conversion and selectivity were compared and found slightly deviation. Thus, kinetic model could be used as representative of experiments.

Table A.2 Kinetic Validation for Mo$_2$C/ZSM-5(80)

Runs	H$_2$/n-alkanes	Conversion (%)		Selectivity (%)		Yield (%)	
	Ratio	Experiment	Simulated	Experiment	Simulated	Experiment	Simulated
1 (600°C)	1	66	63.5	20	27.1	13.5	17.2
2 (600°C)	3	25	24.7	37	39.5	9	9.7
3 (600°C)	10	8	8.9	50	52.2	4	4.6

Appendix B: Equilibrium Model Results and Validation

Table B.1 Trio-equilibrium reaction model calculation result for Mo_2C/Al_2O_3 catalyst

Temp (°C)	H_2/ n-alkanes	Effluent Composition							RSS
		H_2	heptene	hexene	octene	benzene	toluene	xylene	
450	3	0.0005	0.0479	0.1105	0.0016	0.3322	0.3735	0.0072	4.88
450	3.5	0.0004	0.0431	0.0987	0.0020	0.2988	0.4342	0.0067	4.65
500	4	0.0004	0.0393	0.0892	0.0024	0.2715	0.4838	0.0063	4.60
500	4.5	0.0004	0.0360	0.0814	0.0026	0.2487	0.5251	0.0058	4.66
500	5	0.0004	0.0333	0.0748	0.0027	0.2294	0.5601	0.0055	4.80
500	5.5	0.0003	0.0309	0.0691	0.0028	0.2130	0.5900	0.0052	5.04
500	6	0.0003	0.0289	0.0643	0.0029	0.1987	0.6159	0.0049	5.35
500	6.5	0.0003	0.0271	0.0600	0.0030	0.1862	0.6385	0.0046	5.75
500	7	0.0003	0.0255	0.0563	0.0030	0.1752	0.6585	0.0044	6.22
500	7.5	0.0003	0.0241	0.0530	0.0030	0.1654	0.6762	0.0042	6.73
500	8	0.0003	0.0228	0.0501	0.0030	0.1566	0.6921	0.0040	7.22
500	8.5	0.0003	0.0217	0.0475	0.0030	0.1488	0.7064	0.0038	7.82
500	9	0.0002	0.0207	0.0451	0.0030	0.1416	0.7193	0.0036	8.50
500	9.5	0.0002	0.0197	0.0429	0.0030	0.1352	0.7310	0.0035	9.34
500	10	0.0002	0.0189	0.0410	0.0030	0.1293	0.7417	0.0034	10.02
550	3	0.0007	0.0471	0.1100	0.0014	0.3321	0.3740	0.0086	2.56
550	3.5	0.0006	0.0425	0.0984	0.0018	0.2988	0.4345	0.0079	2.43
550	4	0.0006	0.0386	0.0890	0.0021	0.2715	0.4840	0.0073	2.40
550	4.5	0.0006	0.0354	0.0812	0.0023	0.2488	0.5252	0.0068	2.43
550	5	0.0005	0.0327	0.0747	0.0024	0.2295	0.5600	0.0064	2.52
550	5.5	0.0005	0.0304	0.0691	0.0025	0.2131	0.5899	0.0060	2.66
550	6	0.0005	0.0284	0.0643	0.0026	0.1988	0.6157	0.0056	2.84
550	6.5	0.0004	0.0266	0.0601	0.0027	0.1863	0.6384	0.0053	3.06
550	7	0.0004	0.0251	0.0564	0.0027	0.1753	0.6583	0.0050	3.31
550	7.5	0.0004	0.0237	0.0531	0.0027	0.1655	0.6760	0.0048	3.62
550	8	0.0004	0.0224	0.0502	0.0027	0.1568	0.6919	0.0046	3.97
550	8.5	0.0004	0.0213	0.0476	0.0027	0.1489	0.7062	0.0044	4.36
550	9	0.0003	0.0203	0.0452	0.0027	0.1418	0.7191	0.0042	4.75
550	9.5	0.0003	0.0194	0.0431	0.0027	0.1353	0.7308	0.0040	5.21
550	10	0.0003	0.0185	0.0411	0.0027	0.1294	0.7415	0.0038	5.71
600	3	0.0010	0.0463	0.1097	0.0013	0.3322	0.3738	0.0099	1.70
600	3.5	0.0009	0.0417	0.0983	0.0017	0.2989	0.4342	0.0091	1.61
600	4	0.0008	0.0379	0.0890	0.0019	0.2716	0.4837	0.0084	1.57
600	4.5	0.0008	0.0348	0.0813	0.0021	0.2489	0.5248	0.0078	1.57

Table B.1 Trio-equilibrium reaction model calculation result for Mo_2C/Al_2O_3 catalyst

Temp (^oC)	H_2/ n-alkanes	Effluent Composition							RSS
		H_2	heptene	hexene	octene	benzene	toluene	xylene	
600	5	0.0007	0.0072	0.0748	0.0022	0.2297	0.5596	0.0321	1.61
600	5.5	0.0007	0.0068	0.0692	0.0023	0.2133	0.5895	0.0298	1.68
600	6	0.0006	0.0064	0.0644	0.0024	0.1990	0.6153	0.0278	1.78
600	6.5	0.0006	0.0060	0.0603	0.0024	0.1865	0.6379	0.0261	1.91
600	7	0.0006	0.0057	0.0566	0.0024	0.1755	0.6579	0.0246	2.07
600	7.5	0.0005	0.0054	0.0533	0.0025	0.1657	0.6756	0.0232	2.26
600	8	0.0005	0.0051	0.0504	0.0025	0.1570	0.6914	0.0220	2.47
600	8.5	0.0005	0.0049	0.0478	0.0025	0.1491	0.7057	0.0209	2.71
600	9	0.0005	0.0047	0.0454	0.0025	0.1420	0.7186	0.0199	2.97
600	9.5	0.0004	0.0045	0.0433	0.0025	0.1355	0.7303	0.0190	3.28
600	10	0.0004	0.0043	0.0414	0.0024	0.1296	0.7410	0.0182	3.61
625	3	0.0013	0.0112	0.1097	0.0012	0.3324	0.3732	0.0454	1.39
625	3.5	0.0012	0.0102	0.0983	0.0015	0.2991	0.4336	0.0409	1.30
625	4	0.0011	0.0094	0.0891	0.0017	0.2719	0.4829	0.0371	1.25
625	4.5	0.0010	0.0087	0.0814	0.0019	0.2492	0.5241	0.0341	1.23
625	5	0.0010	0.0081	0.0750	0.0020	0.2300	0.5589	0.0314	1.23
625	5.5	0.0009	0.0075	0.0694	0.0021	0.2135	0.5887	0.0292	1.26
625	6	0.0008	0.0071	0.0647	0.0021	0.1993	0.6146	0.0273	1.31
625	6.5	0.0008	0.0067	0.0605	0.0022	0.1868	0.6372	0.0256	1.38
625	7	0.0007	0.0063	0.0568	0.0022	0.1758	0.6572	0.0240	1.48
625	7.5	0.0007	0.0060	0.0536	0.0022	0.1660	0.6749	0.0227	1.58
625	8	0.0007	0.0057	0.0507	0.0022	0.1572	0.6908	0.0215	1.72
625	8.5	0.0006	0.0054	0.0481	0.0022	0.1494	0.7051	0.0204	1.86
625	9	0.0006	0.0051	0.0457	0.0022	0.1422	0.7180	0.0195	2.04
625	9.5	0.0006	0.0049	0.0436	0.0022	0.1358	0.7297	0.0186	2.22
625	10	0.0006	0.0047	0.0416	0.0022	0.1299	0.7405	0.0178	2.45
650	3	0.0017	0.0124	0.1098	0.0011	0.3326	0.3722	0.0444	1.28
650	3.5	0.0016	0.0113	0.0985	0.0014	0.2994	0.4325	0.0400	1.19
650	4	0.0015	0.0103	0.0893	0.0016	0.2721	0.4819	0.0364	1.14
650	4.5	0.0013	0.0095	0.0817	0.0017	0.2495	0.5231	0.0333	1.10
650	5	0.0012	0.0088	0.0752	0.0018	0.2303	0.5579	0.0308	1.08
650	5.5	0.0012	0.0082	0.0697	0.0019	0.2138	0.5878	0.0286	1.08
650	6	0.0011	0.0077	0.0649	0.0020	0.1995	0.6137	0.0267	1.09
650	6.5	0.0010	0.0073	0.0608	0.0020	0.1871	0.6363	0.0250	1.12
650	7	0.0010	0.0069	0.0571	0.0020	0.1761	0.6563	0.0235	1.17
650	7.5	0.0009	0.0065	0.0539	0.0020	0.1663	0.6741	0.0222	1.23

Table B.1 Trio-equilibrium reaction model calculation result for Mo_2C/Al_2O_3 catalyst

Temp (^{o}C)	$H_2/$ n-alkanes	Effluent Composition							RSS
		H_2	heptene	hexene	octene	benzene	toluene	xylene	
650	8.5	0.0008	0.0059	0.0483	0.0020	0.1496	0.7043	0.0200	1.41
650	9	0.0008	0.0056	0.0460	0.0020	0.1425	0.7172	0.0191	1.51
650	9.5	0.0008	0.0054	0.0438	0.0020	0.1360	0.7290	0.0182	1.64
650	10	0.0007	0.0051	0.0419	0.0020	0.1301	0.7398	0.0174	1.77
675	3	0.0023	0.0135	0.1101	0.0010	0.3329	0.3709	0.0435	1.29
675	3.5	0.0020	0.0123	0.0988	0.0013	0.2996	0.4312	0.0391	1.20
675	4	0.0019	0.0112	0.0896	0.0014	0.2724	0.4807	0.0356	1.13
675	4.5	0.0017	0.0103	0.0820	0.0016	0.2498	0.5219	0.0326	1.08
675	5	0.0016	0.0096	0.0756	0.0017	0.2306	0.5568	0.0301	1.05
675	5.5	0.0015	0.0089	0.0700	0.0017	0.2141	0.5867	0.0280	1.02
675	6	0.0014	0.0083	0.0653	0.0018	0.1998	0.6126	0.0261	1.01
675	6.5	0.0013	0.0078	0.0611	0.0018	0.1873	0.6353	0.0245	1.01
675	7	0.0012	0.0074	0.0574	0.0018	0.1763	0.6553	0.0230	1.03
675	7.5	0.0012	0.0070	0.0542	0.0019	0.1665	0.6731	0.0218	1.05
675	8	0.0011	0.0066	0.0513	0.0019	0.1578	0.6891	0.0206	1.09
675	8.5	0.0011	0.0063	0.0486	0.0019	0.1499	0.7034	0.0196	1.14
675	9	0.0010	0.0060	0.0463	0.0019	0.1427	0.7164	0.0186	1.21
675	9.5	0.0010	0.0058	0.0441	0.0019	0.1363	0.7282	0.0178	1.27
675	10	0.0009	0.0055	0.0422	0.0019	0.1303	0.7390	0.0170	1.34
700	3	0.0029	0.0145	0.1105	0.0009	0.3331	0.3693	0.0425	1.35
700	3.5	0.0026	0.0132	0.0992	0.0012	0.2999	0.4297	0.0383	1.26
700	4	0.0024	0.0120	0.0900	0.0013	0.2727	0.4792	0.0348	1.20
700	4.5	0.0022	0.0111	0.0824	0.0014	0.2500	0.5205	0.0319	1.14
700	5	0.0020	0.0103	0.0759	0.0015	0.2309	0.5554	0.0295	1.09
700	5.5	0.0019	0.0096	0.0704	0.0016	0.2144	0.5854	0.0274	1.05
700	6	0.0018	0.0089	0.0656	0.0016	0.2001	0.6114	0.0255	1.02
700	6.5	0.0017	0.0084	0.0615	0.0017	0.1876	0.6341	0.0240	1.00
700	7	0.0016	0.0079	0.0578	0.0017	0.1766	0.6542	0.0225	0.99
700	7.5	0.0015	0.0075	0.0545	0.0017	0.1668	0.6721	0.0213	0.99
700	8	0.0014	0.0071	0.0516	0.0017	0.1580	0.6880	0.0202	1.00
700	8.5	0.0013	0.0068	0.0490	0.0017	0.1501	0.7024	0.0192	1.02
700	9	0.0013	0.0064	0.0466	0.0017	0.1430	0.7154	0.0183	1.04
700	9.5	0.0012	0.0062	0.0444	0.0017	0.1365	0.7273	0.0174	1.07
700	10	0.0012	0.0059	0.0425	0.0017	0.1306	0.7381	0.0167	1.12
725	3	0.0036	0.0155	0.1109	0.0008	0.3334	0.3675	0.0416	1.54
725	3.5	0.0032	0.0140	0.0997	0.0011	0.3002	0.4280	0.0375	1.45

Table B.1 Trio-equilibrium reaction model calculation result for Mo_2C/Al_2O_3 catalyst

Temp (^{o}C)	H_2/ n-alkanes	Effluent Composition							RSS
		H_2	heptene	hexene	octene	benzene	toluene	xylene	
725	4.5	0.0027	0.0118	0.0828	0.0013	0.2503	0.5190	0.0118	1.30
725	5	0.0025	0.0109	0.0764	0.0014	0.2311	0.5540	0.0109	1.22
725	5.5	0.0023	0.0101	0.0708	0.0015	0.2147	0.5840	0.0101	1.17
725	6	0.0022	0.0095	0.0660	0.0015	0.2004	0.6101	0.0095	1.13
725	6.5	0.0021	0.0089	0.0619	0.0015	0.1879	0.6329	0.0089	1.08
725	7	0.0019	0.0084	0.0582	0.0016	0.1769	0.6530	0.0084	1.05
725	7.5	0.0018	0.0079	0.0549	0.0016	0.1671	0.6709	0.0079	1.03
725	8	0.0017	0.0075	0.0519	0.0016	0.1583	0.6869	0.0075	1.01
725	8.5	0.0017	0.0072	0.0493	0.0016	0.1504	0.7013	0.0072	1.00
725	9	0.0016	0.0068	0.0469	0.0016	0.1432	0.7144	0.0068	1.00
725	9.5	0.0015	0.0065	0.0448	0.0016	0.1367	0.7263	0.0065	1.00
725	10	0.0014	0.0062	0.0428	0.0016	0.1308	0.7371	0.0062	1.01

Table B.2 Duo-equilibrium reaction model calculation result for Mo_2C/SiO_2 catalyst

Temp ($^{\circ}$C)	H_2/ n-alkanes	Effluent Composition							
		H_2	heptene	hexene	octene	benzene	toluene	xylene	RSS
450	3	0.0785	0.0145	0.0490	0.0006	0.2416	0.4628	0.0962	1.94
450	3.5	0.0721	0.0134	0.0439	0.0008	0.2162	0.5152	0.0864	1.65
450	4	0.0666	0.0125	0.0397	0.0009	0.1956	0.5579	0.0785	1.55
450	4.5	0.0619	0.0117	0.0363	0.0010	0.1786	0.5936	0.0719	1.52
450	5	0.0578	0.0109	0.0334	0.0010	0.1644	0.6237	0.0663	1.45
450	5.5	0.0542	0.0103	0.0309	0.0011	0.1522	0.6495	0.0615	1.49
450	6	0.0510	0.0097	0.0287	0.0011	0.1417	0.6719	0.0574	1.50
450	6.5	0.0481	0.0092	0.0269	0.0011	0.1326	0.6915	0.0538	1.56
450	7	0.0456	0.0087	0.0252	0.0011	0.1246	0.7087	0.0506	1.71
450	7.5	0.0433	0.0083	0.0238	0.0011	0.1175	0.7241	0.0478	1.57
450	8	0.0412	0.0079	0.0225	0.0011	0.1112	0.7378	0.0452	1.82
450	8.5	0.0393	0.0075	0.0213	0.0011	0.1055	0.7502	0.0430	1.70
450	9	0.0376	0.0072	0.0203	0.0011	0.1003	0.7613	0.0409	1.83
450	9.5	0.0360	0.0069	0.0193	0.0011	0.0957	0.7715	0.0391	2.05
450	10	0.0346	0.0067	0.0184	0.0011	0.0914	0.7808	0.0373	1.93
500	3	0.0809	0.0173	0.0489	0.0005	0.2410	0.4603	0.0945	1.41
500	3.5	0.0740	0.0159	0.0438	0.0007	0.2159	0.5129	0.0849	1.30
500	4	0.0681	0.0147	0.0397	0.0008	0.1955	0.5559	0.0771	1.26
500	4.5	0.0630	0.0136	0.0362	0.0009	0.1787	0.5917	0.0706	1.22
500	5	0.0587	0.0127	0.0333	0.0009	0.1645	0.6220	0.0651	1.24
500	5.5	0.0549	0.0119	0.0309	0.0010	0.1524	0.6480	0.0604	1.24
500	6	0.0515	0.0112	0.0288	0.0010	0.1420	0.6705	0.0563	1.17
500	6.5	0.0486	0.0106	0.0269	0.0010	0.1329	0.6901	0.0528	1.25
500	7	0.0459	0.0100	0.0253	0.0010	0.1249	0.7075	0.0496	1.20
500	7.5	0.0435	0.0095	0.0238	0.0010	0.1178	0.7229	0.0469	1.34
500	8	0.0414	0.0090	0.0225	0.0010	0.1115	0.7367	0.0444	1.30
500	8.5	0.0395	0.0086	0.0214	0.0010	0.1058	0.7491	0.0421	1.27
500	9	0.0377	0.0082	0.0203	0.0010	0.1007	0.7603	0.0401	1.25
500	9.5	0.0361	0.0079	0.0194	0.0010	0.0960	0.7705	0.0383	1.49
500	10	0.0346	0.0076	0.0185	0.0010	0.0918	0.7798	0.0366	1.45
550	3	0.0822	0.0199	0.0489	0.0005	0.2411	0.4582	0.0927	1.10
550	3.5	0.0749	0.0182	0.0438	0.0006	0.2161	0.5111	0.0832	1.08
550	4	0.0687	0.0167	0.0396	0.0007	0.1958	0.5543	0.0755	1.06
550	4.5	0.0635	0.0155	0.0362	0.0008	0.1791	0.5903	0.0692	1.06
550	5	0.0590	0.0144	0.0333	0.0008	0.1649	0.4628	0.0638	1.06
550	5.5	0.0550	0.0135	0.0309	0.0009	0.1529	0.5152	0.0592	1.06

Table B.2 Duo-equilibrium reaction model calculation result for Mo_2C/SiO_2 catalyst

Temp ($^{\circ}$C)	H_2/ n-alkanes	Effluent Composition							RSS
		H_2	heptene	hexene	octene	benzene	toluene	xylene	
550	6.5	0.0486	0.0116e	0.0269	0.0009	0.1334	0.6891	0.0517	1.10
550	7	0.0458	0.0119	0.0253	0.0009	0.1254	0.7065	0.0486	1.11
550	7.5	0.0434	0.0113	0.0238	0.0009	0.1183	0.7219	0.0459	1.13
550	8	0.0413	0.0107	0.0225	0.0009	0.1120	0.7357	0.0435	1.15
550	8.5	0.0393	0.0101	0.0214	0.0009	0.1063	0.7481	0.0413	1.15
550	9	0.0375	0.0097	0.0203	0.0009	0.1011	0.7594	0.0393	1.18
550	9.5	0.0359	0.0092	0.0194	0.0009	0.0965	0.7696	0.0375	1.18
550	10	0.0343	0.0088	0.0185	0.0009	0.0922	0.7789	0.0359	1.22
600	3	0.0827	0.0085	0.0488	0.0004	0.2416	0.4567	0.0908	1.00
600	3.5	0.0751	0.0224	0.0437	0.0006	0.2167	0.5097	0.0815	0.98
600	4	0.0688	0.0204	0.0396	0.0006	0.1965	0.5531	0.0740	0.98
600	4.5	0.0634	0.0187	0.0362	0.0007	0.1797	0.5892	0.0677	0.97
600	5	0.0588	0.0173	0.0333	0.0007	0.1656	0.6197	0.0625	0.99
600	5.5	0.0548	0.0160	0.0309	0.0008	0.1535	0.6458	0.0579	1.00
600	6	0.0513	0.0150	0.0288	0.0008	0.1431	0.6684	0.0540	1.01
600	6.5	0.0482	0.0140	0.0269	0.0008	0.1340	0.6881	0.0506	1.02
600	7	0.0455	0.0132	0.0253	0.0008	0.1260	0.7055	0.0476	1.04
600	7.5	0.0431	0.0124	0.0238	0.0008	0.1189	0.7210	0.0449	1.06
600	8	0.0409	0.0118	0.0226	0.0008	0.1125	0.7348	0.0425	1.08
600	8.5	0.0389	0.0112	0.0214	0.0008	0.1068	0.7472	0.0404	1.10
600	9	0.0371	0.0107	0.0203	0.0008	0.1017	0.7585	0.0385	1.12
600	9.5	0.0355	0.0102	0.0194	0.0008	0.0970	0.7687	0.0367	1.13
600	10	0.0340	0.0097	0.0185	0.0008	0.0927	0.7780	0.0351	1.16
650	3	0.0827	0.0093	0.0487	0.0004	0.2425	0.4555	0.0888	0.97
650	3.5	0.0749	0.0248	0.0437	0.0005	0.2176	0.5087	0.0798	0.97
650	4	0.0684	0.0225	0.0396	0.0006	0.1973	0.5521	0.0724	0.97
650	4.5	0.0630	0.0206	0.0362	0.0006	0.1805	0.5882	0.0663	0.98
650	5	0.0583	0.0189	0.0333	0.0007	0.1664	0.6187	0.0611	0.98
650	5.5	0.0543	0.0176	0.0309	0.0007	0.1543	0.6449	0.0567	0.99
650	6	0.0508	0.0164	0.0288	0.0007	0.1438	0.6675	0.0529	1.00
650	6.5	0.0477	0.0153	0.0269	0.0007	0.1347	0.6872	0.0495	1.02
650	7	0.0450	0.0144	0.0253	0.0007	0.1267	0.7046	0.0466	1.04
650	7.5	0.0426	0.0136	0.0239	0.0008	0.1195	0.7201	0.0440	1.06
650	8	0.0404	0.0128	0.0226	0.0008	0.1131	0.7339	0.0416	1.09
650	8.5	0.0384	0.0122	0.0214	0.0008	0.1074	0.7463	0.0395	1.11
650	9	0.0366	0.0116	0.0204	0.0008	0.1022	0.7575	0.0376	1.13

Table B.2 Duo-equilibrium reaction model calculation result for Mo_2C/SiO_2 catalyst

Temp ($^\circ$C)	H_2/ n-alkanes	Effluent Composition							RSS
		H_2	heptene	hexene	octene	benzene	toluene	xylene	
650	9.5	0.0350	0.0101	0.0194	0.0008	0.0932	0.7770	0.0343	1.16
650	10	0.0335	0.0270	0.0185	0.0008	0.2435	0.4545	0.0869	1.18
675	3	0.0822	0.0244	0.0487	0.0004	0.2186	0.5078	0.0781	0.99
675	3.5	0.0743	0.0223	0.0437	0.0005	0.1983	0.5512	0.0709	0.97
675	4	0.0678	0.0205	0.0396	0.0005	0.1815	0.5874	0.0649	0.97
675	4.5	0.0623	0.0190	0.0362	0.0006	0.1672	0.6179	0.0598	0.96
675	5	0.0577	0.0177	0.0333	0.0006	0.1551	0.6440	0.0555	0.97
675	5.5	0.0536	0.0165	0.0309	0.0006	0.1446	0.6666	0.0517	0.99
675	6	0.0501	0.0155	0.0288	0.0007	0.1354	0.6864	0.0485	1.01
675	6.5	0.0471	0.0146	0.0269	0.0007	0.1273	0.7038	0.0456	1.03
675	7	0.0444	0.0138	0.0253	0.0007	0.1202	0.7192	0.0430	1.06
675	7.5	0.0419	0.0131	0.0239	0.0007	0.1138	0.7330	0.0407	1.08
675	8	0.0398	0.0125	0.0226	0.0007	0.1080	0.7454	0.0387	1.12
675	8.5	0.0378	0.0119	0.0214	0.0007	0.1028	0.7565	0.0368	1.15
675	9	0.0360	0.0114	0.0204	0.0007	0.0981	0.7667	0.0351	1.18
675	9.5	0.0344	0.0109	0.0194	0.0007	0.0938	0.7760	0.0336	1.22
675	10	0.0329	0.0291	0.0186	0.0007	0.2447	0.4538	0.0851	1.25
700	3	0.0814	0.0263	0.0487	0.0003	0.2197	0.5070	0.0764	1.02
700	3.5	0.0735	0.0240	0.0437	0.0004	0.1993	0.5505	0.0693	0.98
700	4	0.0670	0.0220	0.0396	0.0005	0.1824	0.5866	0.0635	0.99
700	4.5	0.0615	0.0204	0.0362	0.0005	0.1681	0.6172	0.0585	0.99
700	5	0.0569	0.0189	0.0333	0.0006	0.1559	0.6432	0.0543	1.00
700	5.5	0.0529	0.0177	0.0309	0.0006	0.1454	0.6658	0.0506	1.03
700	6	0.0494	0.0166	0.0288	0.0006	0.1362	0.6855	0.0474	1.06
700	6.5	0.0463	0.0156	0.0269	0.0006	0.1280	0.7028	0.0446	1.10
700	7	0.0436	0.0148	0.0253	0.0006	0.1208	0.7182	0.0421	1.12
700	7.5	0.0412	0.0140	0.0239	0.0006	0.1144	0.7320	0.0398	1.17
700	8	0.0391	0.0133	0.0226	0.0006	0.1086	0.7443	0.0378	1.20
700	8.5	0.0371	0.0127	0.0214	0.0006	0.1034	0.7555	0.0360	1.27
700	9	0.0354	0.0121	0.0204	0.0006	0.0986	0.7656	0.0343	1.29
700	9.5	0.0338	0.0116	0.0194	0.0006	0.0943	0.7749	0.0328	1.32
700	10	0.0323	0.0311	0.0186	0.0006	0.2459	0.4531	0.0833	1.41
725	3	0.0804	0.0280	0.0486	0.0003	0.2208	0.5064	0.0748	1.25
725	3.5	0.0725	0.0255	0.0436	0.0004	0.2004	0.5498	0.0679	1.22
725	4	0.0660	0.0234	0.0396	0.0005	0.1834	0.5859	0.0621	1.22
725	4.5	0.0606	0.0217	0.0362	0.0005	0.1690	0.6164	0.0573	1.23
725	5	0.0560	0.0201	0.0333	0.0005	0.1567	0.6424	0.0531	1.25

Table B.2 Duo-equilibrium reaction model calculation result for Mo_2C/SiO_2 catalyst

Temp (^{o}C)	$H_2/$ n-alkanes	Effluent Composition							RSS
		H_2	heptene	hexene	octene	benzene	toluene	xylene	
725	5.5	0.0520	0.0101	0.0309	0.0005	0.0932	0.7770	0.0343	1.28
725	6	0.0486	0.0188	0.0288	0.0006	0.1461	0.6649	0.0495	1.34
725	6.5	0.0455	0.0176	0.0269	0.0006	0.1369	0.6846	0.0464	1.36
725	7	0.0429	0.0166	0.0253	0.0006	0.1287	0.7019	0.0436	1.40
725	7.5	0.0405	0.0157	0.0238	0.0006	0.1215	0.7172	0.0412	1.44
725	8	0.0384	0.0149	0.0226	0.0006	0.1150	0.7309	0.0390	1.50
725	8.5	0.0365	0.0141	0.0214	0.0006	0.1092	0.7432	0.0370	1.58
725	9	0.0347	0.0135	0.0204	0.0006	0.1039	0.7544	0.0352	1.62
725	9.5	0.0332	0.0128	0.0194	0.0006	0.0991	0.7644	0.0336	1.66
725	10	0.0317	0.0123	0.0185	0.0006	0.0948	0.7736	0.0321	1.72

Table B.3 Trio-equilibrium reaction model calculation result for Mo_2C/ZSM-5(80) catalyst

Temp (^{o}C)	H_2/ n-alkanes	Effluent Composition							RSS
		H_2	heptene	hexene	octene	benzene	toluene	xylene	
650	5	0.0010	0.0078	0.0077	0.0014	0.1778	0.7311	0.0732	1.86
650	5.5	0.0010	0.0074	0.0065	0.0014	0.1638	0.7521	0.0677	1.26
650	6	0.0010	0.0070	0.0056	0.0015	0.1518	0.7701	0.0630	1.29
650	6.5	0.0009	0.0066	0.0049	0.0015	0.1414	0.7857	0.0589	1.41
650	7	0.0009	0.0063	0.0043	0.0015	0.1324	0.7993	0.0553	1.50
650	7.5	0.0009	0.0061	0.0038	0.0015	0.1244	0.8113	0.0521	1.61
650	8	0.0009	0.0058	0.0033	0.0015	0.1174	0.8219	0.0493	1.69
650	8.5	0.0009	0.0056	0.0030	0.0015	0.1110	0.8313	0.0467	1.76
650	9	0.0009	0.0053	0.0026	0.0015	0.1054	0.8399	0.0444	1.84
650	9.5	0.0009	0.0051	0.0024	0.0015	0.1003	0.8475	0.0423	1.85
650	10	0.0009	0.0049	0.0021	0.0015	0.0956	0.8545	0.0404	1.92
675	5	0.0017	0.0098	0.0065	0.0012	0.1770	0.7314	0.0724	2.20
675	5.5	0.0016	0.0092	0.0056	0.0013	0.1632	0.7522	0.0669	2.15
675	6	0.0016	0.0087	0.0049	0.0013	0.1513	0.7701	0.0622	2.12
675	6.5	0.0015	0.0082	0.0043	0.0013	0.1410	0.7855	0.0582	2.10
675	7	0.0015	0.0078	0.0038	0.0013	0.1321	0.7990	0.0546	2.21
675	7.5	0.0014	0.0074	0.0033	0.0013	0.1242	0.8109	0.0514	2.22
675	8	0.0014	0.0071	0.0030	0.0013	0.1172	0.8214	0.0486	2.24
675	8.5	0.0014	0.0068	0.0027	0.0013	0.1109	0.8308	0.0461	2.24
675	9	0.0014	0.0065	0.0024	0.0013	0.1053	0.8393	0.0438	2.25
675	9.5	0.0013	0.0062	0.0022	0.0013	0.1002	0.8470	0.0417	2.26
675	10	0.0013	0.0060	0.0020	0.0013	0.0956	0.8539	0.0398	2.23
700	5	0.0025	0.0117	0.0060	0.0011	0.1768	0.7305	0.0713	1.62
700	5.5	0.0024	0.0110	0.0053	0.0011	0.1630	0.7513	0.0659	1.65
700	6	0.0023	0.0103	0.0046	0.0012	0.1513	0.7691	0.0612	1.70
700	6.5	0.0022	0.0097	0.0041	0.0012	0.1411	0.7845	0.0572	1.73
700	7	0.0022	0.0092	0.0037	0.0012	0.1322	0.7979	0.0537	1.77
700	7.5	0.0021	0.0088	0.0033	0.0012	0.1243	0.8098	0.0505	1.80
700	8	0.0020	0.0083	0.0030	0.0012	0.1173	0.8204	0.0478	1.85
700	8.5	0.0020	0.0079	0.0027	0.0012	0.1111	0.8298	0.0453	1.88
700	9	0.0019	0.0076	0.0025	0.0012	0.1055	0.8383	0.0430	3.06
700	9.5	0.0019	0.0073	0.0023	0.0012	0.1005	0.8459	0.0410	2.93
700	10	0.0018	0.0070	0.0021	0.0012	0.0959	0.8529	0.0391	2.83
725	5	0.0035	0.0137	0.0061	0.0010	0.1770	0.7288	0.0700	1.59
725	5.5	0.0033	0.0127	0.0054	0.0010	0.1633	0.7496	0.0647	1.63
725	6	0.0032	0.0119	0.0048	0.0010	0.1515	0.7674	0.0601	1.66

Table B.3 Trio-equilibrium reaction model calculation result for $Mo_2C/ZSM-5(80)$ catalyst

Temp (°C)	H_2/ n-alkanes	Effluent Composition							RSS
		H_2	heptene	hexene	octene	benzene	toluene	xylene	
725	6.5	0.0030	0.0112	0.0043	0.0011	0.1414	0.7828	0.0561	1.70
725	7	0.0029	0.0106	0.0039	0.0011	0.1325	0.7963	0.0527	1.73
725	7.5	0.0028	0.0101	0.0036	0.0011	0.1247	0.8083	0.0496	1.76
725	8	0.0027	0.0095	0.0033	0.0011	0.1177	0.8189	0.0469	1.79
725	8.5	0.0026	0.0091	0.0030	0.0011	0.1115	0.8283	0.0444	1.82
725	9	0.0025	0.0087	0.0028	0.0011	0.1059	0.8369	0.0422	1.85
725	9.5	0.0024	0.0083	0.0026	0.0011	0.1008	0.8446	0.0402	1.88
725	10	0.0023	0.0079	0.0024	0.0011	0.0962	0.8516	0.0384	1.90
750	5	0.0046	0.0155	0.0065	0.0009	0.1774	0.7265	0.0686	3.31
750	5.5	0.0043	0.0144	0.0058	0.0009	0.1638	0.7474	0.0634	2.25
750	6	0.0041	0.0135	0.0052	0.0009	0.1521	0.7653	0.0589	2.14
750	6.5	0.0039	0.0127	0.0048	0.0010	0.1419	0.7808	0.0550	2.08
750	7	0.0037	0.0119	0.0044	0.0010	0.1330	0.7944	0.0516	2.04
750	7.5	0.0036	0.0113	0.0040	0.0010	0.1252	0.8064	0.0486	2.02
750	8	0.0034	0.0107	0.0037	0.0010	0.1182	0.8171	0.0459	2.01
750	8.5	0.0033	0.0102	0.0035	0.0010	0.1120	0.8266	0.0435	2.00
750	9	0.0031	0.0097	0.0032	0.0010	0.1064	0.8352	0.0413	2.00
750	9.5	0.0030	0.0093	0.0030	0.0010	0.1013	0.8430	0.0394	2.00
750	10	0.0029	0.0089	0.0029	0.0010	0.0967	0.8501	0.0376	2.00

Appendix C: Manipulated Equilibrium Model Results and Validation

Table C.1 Manipulated Trio-equilibrium reaction model calculation result for Mo_2C/Al_2O_3 catalyst

Temp ($^\circ$C)	H_2/ n-alkanes	Effluent Composition							RSS
		H_2	heptene	hexene	octene	benzene	toluene	xylene	
450	3	0.0005	0.0073	0.0974	0.0311	0.3371	0.3495	0.0486	4.37
450	3.5	0.0005	0.0068	0.0850	0.0327	0.3034	0.4102	0.0438	3.81
450	4	0.0005	0.0063	0.0749	0.0340	0.2757	0.4598	0.0399	3.52
450	4.5	0.0004	0.0059	0.0665	0.0351	0.2527	0.5011	0.0366	3.36
450	5	0.0004	0.0056	0.0594	0.0360	0.2333	0.5360	0.0338	3.32
450	5.5	0.0004	0.0052	0.0534	0.0368	0.2166	0.5660	0.0315	3.38
450	6	0.0004	0.0050	0.0482	0.0375	0.2021	0.5919	0.0294	3.53
450	6.5	0.0004	0.0047	0.0436	0.0381	0.1894	0.6146	0.0276	3.77
450	7	0.0004	0.0045	0.0396	0.0386	0.1783	0.6345	0.0260	4.09
450	7.5	0.0004	0.0043	0.0360	0.0391	0.1683	0.6523	0.0245	4.45
450	8	0.0003	0.0041	0.0328	0.0395	0.1595	0.6682	0.0233	4.74
450	8.5	0.0003	0.0039	0.0300	0.0399	0.1515	0.6825	0.0221	5.19
450	9	0.0003	0.0037	0.0274	0.0402	0.1443	0.6954	0.0211	5.70
450	9.5	0.0003	0.0036	0.0251	0.0405	0.1377	0.7072	0.0201	6.42
450	10	0.0003	0.0034	0.0229	0.0408	0.1317	0.7179	0.0192	6.88
500	3	0.0008	0.0087	0.0968	0.0311	0.3371	0.3498	0.0478	1.73
500	3.5	0.0007	0.0081	0.0845	0.0327	0.3034	0.4103	0.0431	1.48
500	4	0.0007	0.0075	0.0745	0.0340	0.2758	0.4597	0.0392	1.35
500	4.5	0.0006	0.0069	0.0662	0.0351	0.2528	0.5009	0.0360	1.30
500	5	0.0006	0.0065	0.0592	0.0360	0.2334	0.5358	0.0333	1.31
500	5.5	0.0006	0.0061	0.0532	0.0368	0.2167	0.5657	0.0309	1.38
500	6	0.0006	0.0057	0.0481	0.0375	0.2022	0.5915	0.0289	1.50
500	6.5	0.0005	0.0054	0.0435	0.0381	0.1896	0.6142	0.0271	1.66
500	7	0.0005	0.0051	0.0395	0.0386	0.1784	0.6341	0.0255	1.84
500	7.5	0.0005	0.0049	0.0360	0.0391	0.1685	0.6519	0.0241	2.08
500	8	0.0005	0.0047	0.0328	0.0395	0.1597	0.6677	0.0228	2.36
500	8.5	0.0005	0.0044	0.0300	0.0398	0.1517	0.6820	0.0217	2.69
500	9	0.0005	0.0042	0.0274	0.0402	0.1444	0.6949	0.0207	3.01
500	9.5	0.0005	0.0041	0.0251	0.0405	0.1379	0.7067	0.0197	3.40
500	10	0.0004	0.0039	0.0230	0.0408	0.1319	0.7174	0.0189	3.83
550	3	0.0011	0.0101	0.0965	0.0311	0.3372	0.3495	0.0470	0.74
550	3.5	0.0010	0.0092	0.0843	0.0327	0.3035	0.4099	0.0423	0.59

Table C.1 Manipulated Trio-equilibrium reaction model calculation result for Mo_2C/Al_2O_3 catalyst

Temp (°C)	H_2/ n-alkanes	Effluent Composition							RSS
		H_2	heptene	hexene	octene	benzene	toluene	xylene	
550	4	0.0009	0.0085	0.0744	0.0340	0.2760	0.4592	0.0385	0.52
550	4.5	0.0009	0.0079	0.0662	0.0351	0.2530	0.5004	0.0353	0.50
550	5	0.0008	0.0074	0.0592	0.0360	0.2336	0.5352	0.0326	0.51
550	5.5	0.0008	0.0069	0.0533	0.0368	0.2169	0.5650	0.0303	0.56
550	6	0.0008	0.0065	0.0481	0.0374	0.2025	0.5909	0.0283	0.64
550	6.5	0.0007	0.0061	0.0436	0.0380	0.1898	0.6135	0.0266	0.74
550	7	0.0007	0.0058	0.0396	0.0386	0.1787	0.6335	0.0250	0.88
550	7.5	0.0007	0.0055	0.0361	0.0390	0.1688	0.6512	0.0236	1.04
550	8	0.0007	0.0052	0.0329	0.0395	0.1599	0.6671	0.0224	1.22
550	8.5	0.0006	0.0050	0.0301	0.0398	0.1519	0.6813	0.0213	1.43
550	9	0.0006	0.0048	0.0275	0.0402	0.1447	0.6943	0.0203	1.66
550	9.5	0.0006	0.0046	0.0252	0.0405	0.1381	0.7060	0.0193	1.96
550	10	0.0006	0.0044	0.0231	0.0408	0.1321	0.7167	0.0185	2.26
600	3	0.0015	0.0114	0.0964	0.0311	0.3373	0.3488	0.0460	0.36
600	3.5	0.0013	0.0104	0.0844	0.0327	0.3037	0.4090	0.0415	0.25
600	4	0.0013	0.0095	0.0745	0.0340	0.2762	0.4584	0.0377	0.20
600	4.5	0.0012	0.0088	0.0663	0.0350	0.2533	0.4995	0.0346	0.17
600	5	0.0011	0.0082	0.0593	0.0360	0.2339	0.5343	0.0320	0.18
600	5.5	0.0011	0.0077	0.0534	0.0367	0.2172	0.5641	0.0297	0.20
600	6	0.0010	0.0072	0.0482	0.0374	0.2028	0.5900	0.0277	0.24
600	6.5	0.0010	0.0068	0.0438	0.0380	0.1901	0.6126	0.0260	0.31
600	7	0.0009	0.0064	0.0398	0.0385	0.1790	0.6326	0.0245	0.40
600	7.5	0.0009	0.0061	0.0363	0.0390	0.1690	0.6503	0.0231	0.49
600	8	0.0009	0.0058	0.0331	0.0394	0.1601	0.6662	0.0219	0.63
600	8.5	0.0008	0.0055	0.0303	0.0398	0.1522	0.6805	0.0208	0.77
600	9	0.0008	0.0052	0.0277	0.0401	0.1449	0.6934	0.0198	0.94
600	9.5	0.0008	0.0050	0.0254	0.0405	0.1383	0.7052	0.0189	1.11
600	10	0.0008	0.0048	0.0233	0.0407	0.1323	0.7159	0.0181	1.33
625	3	0.0019	0.0126	0.0966	0.0310	0.3376	0.3476	0.0451	0.23
625	3.5	0.0018	0.0114	0.0845	0.0326	0.3040	0.4079	0.0406	0.14
625	4	0.0016	0.0105	0.0747	0.0339	0.2765	0.4572	0.0370	0.09
625	4.5	0.0015	0.0097	0.0665	0.0350	0.2536	0.4983	0.0339	0.05
625	5	0.0015	0.0090	0.0596	0.0359	0.2342	0.5331	0.0313	0.04
625	5.5	0.0014	0.0084	0.0536	0.0367	0.2175	0.5630	0.0291	0.04

Table C.1 Manipulated Trio-equilibrium reaction model calculation result for Mo_2C/Al_2O_3 catalyst

Temp (^{o}C)	H_2/ n-alkanes	Effluent Composition							RSS
		H_2	heptene	hexene	octene	benzene	toluene	xylene	
625	6	0.0013	0.0079	0.0485	0.0374	0.2031	0.5889	0.0271	0.07
625	6.5	0.0013	0.0074	0.0440	0.0380	0.1904	0.6115	0.0255	0.10
625	7	0.0012	0.0070	0.0400	0.0385	0.1792	0.6315	0.0240	0.15
625	7.5	0.0012	0.0066	0.0365	0.0390	0.1693	0.6493	0.0226	0.21
625	8	0.0011	0.0063	0.0333	0.0394	0.1604	0.6652	0.0215	0.30
625	8.5	0.0011	0.0060	0.0305	0.0398	0.1524	0.6795	0.0204	0.40
625	9	0.0011	0.0057	0.0279	0.0401	0.1452	0.6925	0.0194	0.50
625	9.5	0.0010	0.0055	0.0256	0.0404	0.1386	0.7043	0.0185	0.63
625	10	0.0010	0.0052	0.0235	0.0407	0.1326	0.7150	0.0177	0.77
650	3	0.0025	0.0137	0.0968	0.0310	0.3378	0.3462	0.0441	0.24
650	3.5	0.0023	0.0124	0.0848	0.0326	0.3043	0.4064	0.0397	0.15
650	4	0.0021	0.0114	0.0750	0.0339	0.2768	0.4558	0.0362	0.09
650	4.5	0.0020	0.0105	0.0668	0.0350	0.2539	0.4969	0.0332	0.05
650	5	0.0019	0.0097	0.0599	0.0359	0.2345	0.5318	0.0306	0.02
650	5.5	0.0018	0.0091	0.0539	0.0367	0.2178	0.5617	0.0285	0.01
650	6	0.0017	0.0085	0.0488	0.0374	0.2034	0.5876	0.0266	0.00
650	6.5	0.0016	0.0080	0.0443	0.0380	0.1907	0.6103	0.0249	0.01
650	7	0.0015	0.0075	0.0403	0.0385	0.1795	0.6303	0.0235	0.03
650	7.5	0.0015	0.0071	0.0368	0.0390	0.1696	0.6481	0.0222	0.06
650	8	0.0014	0.0068	0.0336	0.0394	0.1607	0.6641	0.0210	0.11
650	8.5	0.0014	0.0064	0.0308	0.0398	0.1527	0.6784	0.0199	0.16
650	9	0.0014	0.0061	0.0282	0.0401	0.1455	0.6914	0.0190	0.24
650	9.5	0.0013	0.0059	0.0259	0.0404	0.1389	0.7032	0.0181	0.31
650	10	0.0013	0.0056	0.0237	0.0407	0.1328	0.7140	0.0174	0.39
675	3	0.0031	0.0148	0.0972	0.0310	0.3381	0.3445	0.0432	0.35
675	3.5	0.0029	0.0134	0.0852	0.0325	0.3046	0.4048	0.0389	0.25
675	4	0.0027	0.0122	0.0754	0.0338	0.2771	0.4542	0.0354	0.19
675	4.5	0.0025	0.0113	0.0672	0.0349	0.2542	0.4954	0.0325	0.13
675	5	0.0024	0.0104	0.0602	0.0359	0.2348	0.5303	0.0300	0.09
675	5.5	0.0022	0.0097	0.0543	0.0366	0.2181	0.5602	0.0278	0.06
675	6	0.0021	0.0091	0.0491	0.0373	0.2037	0.5862	0.0260	0.03
675	6.5	0.0020	0.0085	0.0446	0.0379	0.1910	0.6090	0.0244	0.02
675	7	0.0019	0.0081	0.0406	0.0385	0.1798	0.6290	0.0230	0.01
675	7.5	0.0019	0.0076	0.0371	0.0389	0.1699	0.6469	0.0217	0.02
675	8	0.0018	0.0072	0.0339	0.0393	0.1610	0.6629	0.0205	0.03

Table C.1 Manipulated Trio-equilibrium reaction model calculation result for Mo_2C/Al_2O_3 catalyst

Temp (°C)	H_2/ n-alkanes	Effluent Composition							RSS
		H_2	heptene	hexene	octene	benzene	toluene	xylene	
675	8.5	0.0017	0.0069	0.0311	0.0397	0.1530	0.6773	0.0195	0.06
675	9	0.0017	0.0066	0.0285	0.0401	0.1457	0.6903	0.0186	0.09
675	9.5	0.0017	0.0063	0.0262	0.0404	0.1391	0.7021	0.0178	0.14
675	10	0.0016	0.0060	0.0240	0.0407	0.1331	0.7129	0.0170	0.19
675	3	0.0039	0.0157	0.0977	0.0309	0.3383	0.3426	0.0422	0.67
675	3.5	0.0036	0.0143	0.0857	0.0325	0.3048	0.4030	0.0380	0.55
675	4	0.0033	0.0130	0.0758	0.0338	0.2774	0.4524	0.0346	0.45
675	4.5	0.0031	0.0120	0.0676	0.0349	0.2545	0.4937	0.0318	0.36
675	5	0.0029	0.0111	0.0607	0.0358	0.2351	0.5287	0.0293	0.28
675	5.5	0.0027	0.0103	0.0547	0.0366	0.2184	0.5587	0.0272	0.22
675	6	0.0026	0.0097	0.0495	0.0373	0.2039	0.5847	0.0254	0.18
675	6.5	0.0025	0.0091	0.0450	0.0379	0.1913	0.6075	0.0239	0.13
675	7	0.0024	0.0086	0.0410	0.0384	0.1801	0.6276	0.0225	0.10
675	7.5	0.0023	0.0081	0.0375	0.0389	0.1701	0.6455	0.0212	0.08
675	8	0.0022	0.0077	0.0343	0.0393	0.1612	0.6616	0.0201	0.07
675	8.5	0.0021	0.0073	0.0314	0.0397	0.1532	0.6760	0.0191	0.07
675	9	0.0021	0.0070	0.0288	0.0400	0.1460	0.6890	0.0182	0.07
675	9.5	0.0020	0.0066	0.0265	0.0404	0.1394	0.7009	0.0174	0.09
675	10	0.0020	0.0064	0.0243	0.0406	0.1333	0.7117	0.0166	0.11

CHULALONGKORN UNIVERSITY

Table C.2 Manipulated Duo-equilibrium reaction model calculation result for

Mo$_2$C/SiO$_2$ catalyst

Temp (°C)	H$_2$/ n-alkanes	Effluent Composition							
		H$_2$	heptene	hexene	octene	benzene	toluene	xylene	RSS
450	3	0.0762	0.0179	0.0428	0.0142	0.2465	0.4518	0.0936	299.26
450	3.5	0.0703	0.0165	0.0375	0.0149	0.2206	0.5038	0.0840	113.80
450	4	0.0652	0.0154	0.0332	0.0154	0.1997	0.5463	0.0762	50.27
450	4.5	0.0608	0.0144	0.0296	0.0159	0.1825	0.5816	0.0697	25.51
450	5	0.0570	0.0135	0.0266	0.0163	0.1680	0.6115	0.0643	16.96
450	5.5	0.0537	0.0127	0.0241	0.0166	0.1556	0.6370	0.0596	9.90
450	6	0.0508	0.0120	0.0219	0.0169	0.1450	0.6591	0.0555	6.88
450	6.5	0.0482	0.0114	0.0200	0.0171	0.1357	0.6784	0.0520	4.50
450	7	0.0459	0.0109	0.0183	0.0174	0.1276	0.6954	0.0489	2.82
450	7.5	0.0438	0.0104	0.0169	0.0176	0.1204	0.7105	0.0461	3.06
450	8	0.0420	0.0099	0.0156	0.0177	0.1139	0.7240	0.0436	1.80
450	8.5	0.0403	0.0095	0.0144	0.0179	0.1081	0.7361	0.0414	1.90
450	9	0.0388	0.0092	0.0134	0.0180	0.1029	0.7470	0.0393	1.46
450	9.5	0.0374	0.0088	0.0124	0.0182	0.0982	0.7570	0.0375	1.15
450	10	0.0361	0.0085	0.0116	0.0183	0.0939	0.7660	0.0358	1.16
500	3	0.0790	0.0204	0.0427	0.0142	0.2456	0.4490	0.0921	31.43
500	3.5	0.0726	0.0188	0.0375	0.0149	0.2201	0.5012	0.0827	13.35
500	4	0.0671	0.0174	0.0333	0.0154	0.1994	0.5438	0.0750	6.43
500	4.5	0.0625	0.0162	0.0298	0.0159	0.1823	0.5792	0.0686	4.06
500	5	0.0585	0.0151	0.0268	0.0162	0.1680	0.6091	0.0631	2.28
500	5.5	0.0550	0.0142	0.0243	0.0166	0.1557	0.6347	0.0585	1.58
500	6	0.0520	0.0135	0.0222	0.0169	0.1451	0.6568	0.0545	1.80
500	6.5	0.0494	0.0128	0.0203	0.0171	0.1359	0.6761	0.0510	0.95
500	7	0.0470	0.0121	0.0187	0.0173	0.1278	0.6931	0.0479	1.04
500	7.5	0.0449	0.0116	0.0173	0.0175	0.1206	0.7082	0.0452	0.52
500	8	0.0430	0.0111	0.0160	0.0177	0.1142	0.7216	0.0427	0.55
500	8.5	0.0413	0.0106	0.0149	0.0179	0.1085	0.7337	0.0405	0.60
500	9	0.0398	0.0102	0.0138	0.0180	0.1033	0.7446	0.0385	0.64
500	9.5	0.0384	0.0098	0.0129	0.0181	0.0985	0.7544	0.0367	0.32
500	10	0.0372	0.0095	0.0121	0.0182	0.0943	0.7634	0.0350	0.33
550	3	0.0808	0.0228	0.0427	0.0141	0.2454	0.4467	0.0905	6.44
550	3.5	0.0741	0.0209	0.0376	0.0148	0.2201	0.4990	0.0812	2.32
550	4	0.0684	0.0193	0.0334	0.0154	0.1995	0.5416	0.0736	1.12
550	4.5	0.0636	0.0179	0.0300	0.0158	0.1825	0.5770	0.0673	0.64
550	5	0.0596	0.0167	0.0271	0.0162	0.1682	0.6069	0.0620	0.40

Table C.2 Manipulated Duo-equilibrium reaction model calculation result for
Mo_2C/SiO_2 catalyst

Temp (°C)	H_2/ n-alkanes	Effluent Composition							RSS
		H_2	heptene	hexene	octene	benzene	toluene	xylene	
550	5.5	0.0560	0.0157	0.0247	0.0165	0.1560	0.6324	0.0574	0.30
550	6	0.0530	0.0148	0.0226	0.0168	0.1455	0.6545	0.0534	0.21
550	6.5	0.0503	0.0141	0.0207	0.0171	0.1363	0.6737	0.0500	0.15
550	7	0.0479	0.0134	0.0192	0.0173	0.1282	0.6907	0.0469	0.14
550	7.5	0.0458	0.0128	0.0178	0.0175	0.1211	0.7057	0.0442	0.13
550	8	0.0440	0.0122	0.0165	0.0177	0.1147	0.7190	0.0417	0.12
550	8.5	0.0423	0.0117	0.0154	0.0178	0.1089	0.7310	0.0395	0.14
550	9	0.0408	0.0113	0.0145	0.0180	0.1037	0.7418	0.0376	0.14
550	9.5	0.0394	0.0109	0.0136	0.0181	0.0990	0.7516	0.0357	0.16
550	10	0.0382	0.0105	0.0128	0.0182	0.0947	0.7605	0.0341	0.15
600	3	0.0819	0.0249	0.0428	0.0141	0.2455	0.4448	0.0889	1.21
600	3.5	0.0750	0.0228	0.0377	0.0148	0.2204	0.4970	0.0797	0.56
600	4	0.0692	0.0210	0.0336	0.0153	0.1999	0.5396	0.0722	0.31
600	4.5	0.0644	0.0195	0.0303	0.0158	0.1830	0.5749	0.0660	0.25
600	5	0.0603	0.0182	0.0275	0.0162	0.1687	0.6047	0.0607	0.11
600	5.5	0.0568	0.0171	0.0251	0.0165	0.1565	0.6302	0.0562	0.09
600	6	0.0537	0.0162	0.0230	0.0168	0.1460	0.6521	0.0523	0.07
600	6.5	0.0511	0.0153	0.0213	0.0171	0.1368	0.6712	0.0488	0.08
600	7	0.0488	0.0146	0.0197	0.0173	0.1288	0.6881	0.0458	0.08
600	7.5	0.0467	0.0139	0.0184	0.0175	0.1216	0.7029	0.0431	0.09
600	8	0.0449	0.0133	0.0172	0.0176	0.1152	0.7162	0.0407	0.10
600	8.5	0.0432	0.0128	0.0161	0.0178	0.1095	0.7281	0.0385	0.11
600	9	0.0418	0.0123	0.0152	0.0179	0.1043	0.7388	0.0366	0.12
600	9.5	0.0405	0.0119	0.0144	0.0181	0.0996	0.7484	0.0348	0.14
600	10	0.0393	0.0115	0.0136	0.0182	0.0953	0.7572	0.0331	0.15
625	3	0.0825	0.0270	0.0429	0.0141	0.2460	0.4432	0.0873	0.51
625	3.5	0.0755	0.0246	0.0379	0.0148	0.2209	0.4953	0.0783	0.25
625	4	0.0698	0.0227	0.0339	0.0153	0.2005	0.5377	0.0708	0.14
625	4.5	0.0650	0.0211	0.0307	0.0158	0.1836	0.5728	0.0647	0.10
625	5	0.0609	0.0197	0.0279	0.0162	0.1693	0.6025	0.0594	0.07
625	5.5	0.0574	0.0185	0.0256	0.0165	0.1572	0.6277	0.0550	0.07
625	6	0.0545	0.0175	0.0236	0.0168	0.1467	0.6495	0.0511	0.07
625	6.5	0.0519	0.0166	0.0219	0.0170	0.1375	0.6685	0.0477	0.08
625	7	0.0496	0.0158	0.0204	0.0172	0.1294	0.6851	0.0447	0.09
625	7.5	0.0476	0.0151	0.0192	0.0174	0.1223	0.6999	0.0420	0.10

Table C.2 Manipulated Duo-equilibrium reaction model calculation result for Mo$_2$C/SiO$_2$ catalyst

Temp (°C)	H$_2$/ n-alkanes	Effluent Composition							RSS
		H$_2$	heptene	hexene	octene	benzene	toluene	xylene	
625	8	0.0459	0.0144	0.0180	0.0176	0.1159	0.7130	0.0396	0.12
625	8.5	0.0443	0.0139	0.0170	0.0178	0.1101	0.7247	0.0375	0.13
625	9	0.0429	0.0134	0.0161	0.0179	0.1050	0.7353	0.0355	0.15
625	9.5	0.0417	0.0129	0.0153	0.0180	0.1002	0.7448	0.0337	0.17
625	10	0.0405	0.0125	0.0146	0.0181	0.0960	0.7535	0.0321	0.18
650	3	0.0828	0.0289	0.0430	0.0141	0.2467	0.4417	0.0857	0.25
650	3.5	0.0758	0.0264	0.0382	0.0148	0.2216	0.4935	0.0768	0.12
650	4	0.0701	0.0243	0.0343	0.0153	0.2012	0.5357	0.0694	0.06
650	4.5	0.0654	0.0226	0.0311	0.0158	0.1843	0.5706	0.0633	0.04
650	5	0.0615	0.0211	0.0285	0.0161	0.1701	0.6000	0.0581	0.03
650	5.5	0.0581	0.0198	0.0263	0.0165	0.1579	0.6250	0.0537	0.03
650	6	0.0552	0.0187	0.0244	0.0167	0.1474	0.6466	0.0498	0.04
650	6.5	0.0527	0.0178	0.0227	0.0170	0.1382	0.6654	0.0465	0.06
650	7	0.0506	0.0170	0.0213	0.0172	0.1301	0.6818	0.0435	0.07
650	7.5	0.0487	0.0162	0.0201	0.0174	0.1230	0.6964	0.0408	0.09
650	8	0.0470	0.0156	0.0190	0.0176	0.1166	0.7093	0.0385	0.11
650	8.5	0.0455	0.0150	0.0180	0.0177	0.1108	0.7209	0.0363	0.14
650	9	0.0442	0.0144	0.0171	0.0179	0.1057	0.7313	0.0344	0.16
650	9.5	0.0430	0.0140	0.0164	0.0180	0.1009	0.7407	0.0327	0.20
650	10	0.0419	0.0135	0.0157	0.0181	0.0967	0.7493	0.0311	0.22
675	3	0.0827	0.0307	0.0433	0.0141	0.2475	0.4403	0.0842	0.14
675	3.5	0.0759	0.0280	0.0386	0.0147	0.2224	0.4918	0.0753	0.06
675	4	0.0704	0.0258	0.0348	0.0153	0.2020	0.5336	0.0680	0.01
675	4.5	0.0658	0.0240	0.0317	0.0157	0.1851	0.5682	0.0619	0.00
675	5	0.0620	0.0225	0.0292	0.0161	0.1709	0.5973	0.0568	0.01
675	5.5	0.0588	0.0212	0.0270	0.0164	0.1587	0.6221	0.0524	0.02
675	6	0.0561	0.0200	0.0252	0.0167	0.1482	0.6434	0.0485	0.04
675	6.5	0.0537	0.0190	0.0236	0.0170	0.1390	0.6619	0.0452	0.08
675	7	0.0517	0.0182	0.0223	0.0172	0.1309	0.6781	0.0422	0.09
675	7.5	0.0499	0.0174	0.0211	0.0174	0.1237	0.6925	0.0396	0.14
675	8	0.0483	0.0167	0.0201	0.0175	0.1173	0.7052	0.0373	0.16
675	8.5	0.0469	0.0161	0.0192	0.0177	0.1116	0.7166	0.0352	0.24
675	9	0.0457	0.0155	0.0183	0.0178	0.1064	0.7269	0.0332	0.26
675	9.5	0.0446	0.0150	0.0176	0.0179	0.1017	0.7361	0.0315	0.28

Table C.2 Manipulated Duo-equilibrium reaction model calculation result for Mo_2C/SiO_2 catalyst

Temp (^{o}C)	H_2/n-alkanes	Effluent Composition							RSS
		H_2	heptene	hexene	octene	benzene	toluene	xylene	
675	10	0.0436	0.0146	0.0170	0.0180	0.0974	0.7446	0.0299	0.40
700	3	0.0826	0.0324	0.0435	0.0140	0.2484	0.4389	0.0826	0.28
700	3.5	0.0760	0.0296	0.0390	0.0147	0.2233	0.4900	0.0737	0.19
700	4	0.0707	0.0273	0.0354	0.0153	0.2029	0.5314	0.0665	0.17
700	4.5	0.0663	0.0254	0.0324	0.0157	0.1860	0.5656	0.0605	0.18
700	5	0.0627	0.0238	0.0300	0.0161	0.1717	0.5943	0.0554	0.19
700	5.5	0.0596	0.0225	0.0279	0.0164	0.1595	0.6188	0.0510	0.23
700	6	0.0571	0.0213	0.0262	0.0167	0.1490	0.6398	0.0472	0.30
700	6.5	0.0548	0.0203	0.0247	0.0169	0.1398	0.6580	0.0439	0.33
700	7	0.0529	0.0194	0.0234	0.0171	0.1317	0.6740	0.0409	0.38
700	7.5	0.0512	0.0186	0.0223	0.0173	0.1245	0.6881	0.0383	0.44
700	8	0.0498	0.0179	0.0213	0.0175	0.1181	0.7006	0.0360	0.51
700	8.5	0.0485	0.0172	0.0205	0.0176	0.1124	0.7118	0.0339	0.63
700	9	0.0473	0.0167	0.0197	0.0178	0.1072	0.7219	0.0320	0.69
700	9.5	0.0463	0.0161	0.0190	0.0179	0.1025	0.7310	0.0303	0.76
700	10	0.0454	0.0157	0.0184	0.0180	0.0981	0.7393	0.0287	0.84

Table C.3 Manipulated Trio-equilibrium reaction model calculation result for
Mo$_2$C/ZSM-5(80) catalyst

Temp (°C)	H$_2$/ n-alkanes	Effluent Composition							
		H$_2$	heptene	hexene	octene	benzene	toluene	xylene	RSS
650	5	0.0006	0.0070	0.0183	0.0125	0.1948	0.7006	0.0661	1.23
650	5.5	0.0006	0.0067	0.0159	0.0127	0.1795	0.7234	0.0612	1.12
650	6	0.0006	0.0063	0.0139	0.0129	0.1665	0.7430	0.0569	1.05
650	6.5	0.0006	0.0060	0.0122	0.0130	0.1552	0.7599	0.0532	1.01
650	7	0.0006	0.0057	0.0107	0.0132	0.1453	0.7747	0.0499	1.01
650	7.5	0.0005	0.0055	0.0094	0.0133	0.1366	0.7877	0.0470	1.02
650	8	0.0005	0.0052	0.0083	0.0134	0.1289	0.7992	0.0445	1.06
650	8.5	0.0005	0.0050	0.0073	0.0135	0.1220	0.8095	0.0422	1.12
650	9	0.0005	0.0048	0.0065	0.0136	0.1158	0.8187	0.0401	1.20
650	9.5	0.0005	0.0046	0.0057	0.0136	0.1102	0.8271	0.0382	1.28
650	10	0.0005	0.0045	0.0050	0.0137	0.1051	0.8347	0.0365	1.38
675	5	0.0010	0.0088	0.0171	0.0125	0.1941	0.7011	0.0654	0.47
675	5.5	0.0009	0.0083	0.0148	0.0127	0.1790	0.7238	0.0605	0.38
675	6	0.0009	0.0078	0.0130	0.0129	0.1660	0.7431	0.0562	0.32
675	6.5	0.0009	0.0074	0.0114	0.0130	0.1548	0.7599	0.0525	0.29
675	7	0.0009	0.0070	0.0100	0.0132	0.1450	0.7746	0.0493	0.27
675	7.5	0.0008	0.0067	0.0089	0.0133	0.1364	0.7875	0.0464	0.27
675	8	0.0008	0.0064	0.0078	0.0134	0.1287	0.7990	0.0439	0.29
675	8.5	0.0008	0.0061	0.0069	0.0135	0.1219	0.8092	0.0416	0.32
675	9	0.0008	0.0058	0.0061	0.0135	0.1157	0.8184	0.0396	0.36
675	9.5	0.0008	0.0056	0.0054	0.0136	0.1102	0.8267	0.0377	0.42
675	10	0.0008	0.0054	0.0047	0.0137	0.1051	0.8343	0.0360	0.48
700	5	0.0014	0.0106	0.0164	0.0125	0.1939	0.7007	0.0644	0.27
700	5.5	0.0014	0.0099	0.0143	0.0127	0.1789	0.7232	0.0595	0.19
700	6	0.0013	0.0093	0.0126	0.0129	0.1660	0.7425	0.0553	0.13
700	6.5	0.0013	0.0088	0.0111	0.0130	0.1549	0.7593	0.0517	0.08
700	7	0.0013	0.0083	0.0098	0.0131	0.1451	0.7739	0.0485	0.06
700	7.5	0.0012	0.0079	0.0087	0.0133	0.1365	0.7867	0.0457	0.05
700	8	0.0012	0.0075	0.0077	0.0134	0.1289	0.7982	0.0432	0.05
700	8.5	0.0012	0.0072	0.0068	0.0135	0.1221	0.8084	0.0409	0.06
700	9	0.0012	0.0069	0.0060	0.0135	0.1159	0.8176	0.0389	0.08
700	9.5	0.0012	0.0066	0.0053	0.0136	0.1104	0.8259	0.0370	0.11
700	10	0.0012	0.0063	0.0047	0.0137	0.1053	0.8334	0.0354	0.15
725	5	0.0020	0.0123	0.0162	0.0125	0.1941	0.6995	0.0633	0.28
725	5.5	0.0020	0.0115	0.0142	0.0127	0.1791	0.7220	0.0585	0.20

Table C.3 Manipulated Trio-equilibrium reaction model calculation result for

Mo$_2$C/ZSM-5(80) catalyst

Temp (°C)	H$_2$/ n-alkanes	Effluent Composition							RSS
		H$_2$	heptene	hexene	octene	benzene	toluene	xylene	
725	6	0.0019	0.0108	0.0125	0.0129	0.1663	0.7413	0.0543	0.14
725	6.5	0.0018	0.0102	0.0111	0.0130	0.1552	0.7580	0.0507	0.08
725	7	0.0018	0.0096	0.0098	0.0131	0.1454	0.7727	0.0476	0.05
725	7.5	0.0017	0.0091	0.0087	0.0133	0.1369	0.7855	0.0448	0.02
725	8	0.0017	0.0086	0.0078	0.0134	0.1292	0.7970	0.0424	0.01
725	8.5	0.0016	0.0082	0.0069	0.0134	0.1224	0.8072	0.0401	0.00
725	9	0.0016	0.0078	0.0062	0.0135	0.1163	0.8164	0.0381	0.01
725	9.5	0.0016	0.0075	0.0055	0.0136	0.1107	0.8247	0.0363	0.02
725	10	0.0016	0.0072	0.0049	0.0137	0.1057	0.8323	0.0347	0.04
750	5	0.0028	0.0140	0.0164	0.0125	0.1945	0.6978	0.0620	0.38
750	5.5	0.0026	0.0130	0.0144	0.0127	0.1796	0.7203	0.0573	0.30
750	6	0.0025	0.0122	0.0128	0.0128	0.1667	0.7397	0.0533	0.23
750	6.5	0.0024	0.0115	0.0114	0.0130	0.1556	0.7564	0.0497	0.17
750	7	0.0023	0.0108	0.0101	0.0131	0.1459	0.7710	0.0466	0.13
750	7.5	0.0023	0.0102	0.0091	0.0132	0.1373	0.7840	0.0439	0.09
750	8	0.0022	0.0097	0.0081	0.0133	0.1297	0.7955	0.0415	0.06
750	8.5	0.0022	0.0092	0.0073	0.0134	0.1229	0.8057	0.0393	0.04
750	9	0.0021	0.0088	0.0065	0.0135	0.1167	0.8150	0.0374	0.03
750	9.5	0.0021	0.0084	0.0058	0.0136	0.1112	0.8233	0.0356	0.03
750	10	0.0021	0.0080	0.0052	0.0137	0.1061	0.8309	0.0340	0.03

Appendix D: Experiment Extrapolation Results

Table D.1 Experiment Extrapolations results

| Catalyst | H_2/n-alkanes | Temp (°C) | Equilibrium Model | Model Result | | | | AARD (%) |
				$X_{alkanes}$	S_{C6H6}	S_{C7H8}	Y	
K/CaO	4	700	duo-equilibrium	25.7	22.6	27.6	12.9	190.03
K/CaOa	4	750	duo-equilibrium	26.0	22.3	27.6	13.0	4.62
K/CaO	8	750	duo-equilibrium	14.9	38.8	17.1	8.4	16.46
Rb/CaO	4	700	duo-equilibrium	24.8	20.2	27.0	11.7	150.02
Rb/CaOa	4	750	duo-equilibrium	25.1	19.9	27.0	11.8	5.33
Rb/CaO	8	750	duo-equilibrium	14.2	35.1	17.6	7.5	14.39
Cs/CaO	4	700	duo-equilibrium	22.0	21.8	13.4	7.7	257.77
Cs/CaOa	4	750	duo-equilibrium	22.3	21.5	13.4	7.8	51.00
Cs/CaO	8	750	duo-equilibrium	12.7	37.7	4.7	5.4	48.36
SrO/La$_2$O$_3$	4	750	duo-equilibrium	34.4	20.4	52.2	24.9	262.41
SrO/La$_2$O$_3$	4	800	duo-equilibrium	34.8	20.1	52.5	25.3	38.18
SrO/La$_2$O$_3$	4	850	duo-equilibrium	35.4	19.8	53.1	25.8	44.24
SrO/La$_2$O$_3$	8	850	duo-equilibrium	21.5	32.6	45.1	16.7	15.58
SrO/La$_2$O$_3$	16	850	duo-equilibrium	15.1	46.3	37.8	12.7	29.92
SrO/La$_2$O$_3$	20	850	duo-equilibrium	13.9	50.2	35.9	12.0	27.44
SrO/Nd$_2$O$_3$	4	750	duo-equilibrium	28.1	22.8	33.6	15.8	283.59
SrO/Nd$_2$O$_3$	4	800	duo-equilibrium	28.4	22.5	33.9	16.0	8.54
SrO/Nd$_2$O$_3$	4	850	duo-equilibrium	28.7	22.3	34.5	16.3	6.35
SrO/Nd$_2$O$_3$	8	850	duo-equilibrium	17.2	37.1	26.7	11.0	19.66

Table D.1 Experiment Extrapolations results

Catalyst	H₂/n-alkanes	Temp (°C)	Equilibrium Model	Model Result				AARD (%)
				$X_{alkanes}$	S_{C6H6}	S_{C7H8}	Y	
SrO/Nd$_2$O$_3$	16	850	duo-equilibrium	11.9	53.6	20.3	8.8	12.33
SrO/Nd$_2$O$_3$	20	850	duo-equilibrium	11.0	58.4	18.8	8.5	15.01
SrO/La$_2$O$_3$-Nd$_2$O$_3$	4	750	duo-equilibrium	36.2	23.7	51.6	27.3	528.15
SrO/La$_2$O$_3$-Nd$_2$O$_3$	4	800	duo-equilibrium	36.7	23.4	52.0	27.7	181.91
SrO/La$_2$O$_3$-Nd$_2$O$_3$	4	850	duo-equilibrium	37.3	23.1	52.6	28.2	38.65
SrO/La$_2$O$_3$-Nd$_2$O$_3$	8	850	duo-equilibrium	23.0	37.4	42.9	18.5	17.73
SrO/La$_2$O$_3$-Nd$_2$O$_3$	16	850	duo-equilibrium	16.5	52.0	34.2	14.3	21.81
SrO/La$_2$O$_3$-Nd$_2$O$_3$	20	850	duo-equilibrium	15.4	56.0	32.1	13.5	21.35
SnBaTiO$_3$	2	725	duo-equilibrium	53.3	9.0	50.5	31.7	48.97
SnBaTiO$_3$	3	725	duo-equilibrium	38.3	12.5	49.3	23.7	35.69
SnBaTiO$_3$	4	725	duo-equilibrium	29.5	16.3	46.4	18.5	50.87
SnBaTiO$_3$	4.5	725	duo-equilibrium	26.6	18.0	45.0	16.8	71.58
SnBaTiO$_3$	2	750	duo-equilibrium	53.6	9.0	50.2	31.7	23.32
SnBaTiO$_3$	3	750	duo-equilibrium	38.4	12.5	49.2	23.7	3.85
SnBaTiO$_3$	4	750	duo-equilibrium	29.7	16.2	46.4	18.6	13.95
SnBaTiO$_3$	4.5	750	duo-equilibrium	26.8	17.9	45.1	16.9	18.37
SnBaTiO$_3$	2	775	duo-equilibrium	53.8	8.9	50.0	31.7	33.21
SnBaTiO$_3$	3	775	duo-equilibrium	38.6	12.4	49.2	23.8	17.63
SnBaTiO$_3$	4	775	duo-equilibrium	29.9	16.1	46.5	18.7	23.54
SnBaTiO$_3$	4.5	775	duo-equilibrium	27.0	17.8	45.3	17.0	24.43

Table D.1 Experiment Extrapolations results

Catalyst	H_2/n-alkanes	Temp (°C)	Equilibrium Model	Model Result				AARD (%)
				$X_{alkanes}$	S_{C6H6}	S_{C7H8}	Y	
La/MgO	4	700	duo-equilibrium	29.1	26.8	32.8	17.3	15.82
La/MgO	4	750	duo-equilibrium	29.4	26.5	32.8	17.5	2.03
La/MgO[a]		800	duo-equilibrium	29.7	26.3	33.1	17.6	2.24
La/MgO	4	850	duo-equilibrium	30.1	25.9	33.7	17.9	3.33
Li/MgO	4	700	duo-equilibrium	24.2	19.0	24.7	10.6	45.69
Li/MgO		740	duo-equilibrium	24.4	18.8	24.9	10.7	23.31
Li/MgO[a]		780	duo-equilibrium	24.6	18.7	25.2	10.8	4.68
Li/MgO		820	duo-equilibrium	24.9	18.5	25.7	11.0	12.74
Li/MgO	4	860	duo-equilibrium	25.1	18.3	26.4	11.2	80.68
Sn/BaTiO3	1	775	duo-equilibrium	71.5	5.0	26.6	22.6	18.69
Sn/BaTiO3[a]	2	775	duo-equilibrium	47.6	7.6	39.9	22.6	5.69
Sn/BaTiO3	4	775	duo-equilibrium	26.1	13.8	37.7	13.4	5.99
K/BaCO3	4	780	duo-equilibrium	23.0	9.6	29.3	8.9	68.46
K/BaCO3[a]	4	820	duo-equilibrium	23.2	9.5	29.8	9.1	14.75
K/BaCO$_3$	4	860	duo-equilibrium	23.5	9.4	30.5	9.4	22.38
Li/CaO	4	700	duo-equilibrium	26.4	23.5	28.7	13.8	113.30
Li/CaO[a]	4	750	duo-equilibrium	26.7	23.2	28.7	13.9	13.96
Li/CaO	8	750	duo-equilibrium	15.4	40.3	17.6	8.9	16.14
Na/CaO	4	700	duo-equilibrium	24.6	23.6	22.1	11.2	126.43
Na/CaO[a]	4	750	duo-equilibrium	24.9	23.3	22.1	11.3	23.64
Na/CaO	8	750	duo-equilibrium	14.3	40.5	11.7	7.5	24.54

[a] Reference value for extrapolation

Appendix E: International Conference

PIM 10th Panyapiwat National and 3rd International 2020 (PIM 2020)

Topic: MODELING PRODUCTION OF AROMATIC FROM N-PARAFFINS WITH CHEMICAL EQUILIBRIA.

Location: Panyapiwat Institute of Management Chaengwatthana Rd., Nonthaburi, Thailand

Conference Date: 17 July 2020

PIM 10th National and 3rd International Conference 2020
July 17th, 2020

MODELING PRODUCTION OF AROMATIC FROM N-PARAFFINS WITH CHEMICAL EQUILIBRIA

Thidarat Detsut[1*], Deacha Chatsiriwech[1,2]

[1]Department of Chemical Engineering, Faculty of Engineering, Chulalongkorn University
[2]Department of Chemical Reaction Engineering, Faculty of Engineering, Imperial College University of London
[*]**Corresponding author, E-mail:** mallowstlck@hotmail.com

ABSTRACT

Aromatics production from n-hexane, n-heptane and n-octane hydrocarbons are an interesting way to increase economic values and usage alternatives. This study was to model aromatics production from hexane heptane and octane, enabling industrial work to be more developed and actualized by reducing laboratory cost and experimental time. The model was regarded as an equilibrium state in which the forward reaction rate and the reverse reaction rate are equivalent, and a catalyst would be Pt/KL and various Mo_2C-containing catalysts under 1 atm and 500 ºC. The reactions in the models were from Aspen Plus V9 simulation. The reactions included main reactions and side reactions, which the catalyst performed to select and unselect certain reactions. Moreover, the reactions were grouped by splitting reactors, so the reactors connected in series to classify a procedure. It has been found that n-hexane, n-heptane and n-octane would be converted to ethylcyclohexane before ethylbenzene. Then, the aromatics were formed by hydrogenation, isomerization and thermal cracking.

Keywords: aromatization, reaction rate, hydrogenation, thermal cracking, aromatics production

Introduction

Natural gas is an energy source often used for heating, transportation, and electricity generation. The reservoir of natural gas increases rapidly higher than that of crude oil and expected to ahead of by the 21stcentury. The aromatization of n-alkanes is an important reaction with many industrial applications which could be carried out on both bifunctional (acid–metal) and monofunctional (only-metal) catalysts. Moreover, the direct conversion of alkanes into aromatics has been the subject of extensive research. The results obtained on various catalysts and the possible mechanisms of this complex process are well documented in several excellent reviews.

n-Hexane, n-Heptane and n-Octane are one of the components of natural gas liquids (NGL), and its reforming to olefins and aromatics is of practical importance which is use for a raw material in the petrochemical industry such as an ingredient and refined into gasoline, solvent industry is distilled and separated at various temperatures. Resulting in various types of solutions as follows white Spirit in the coating industry, dry cleaning, polishing process and the pesticide industry while mixtures of benzene, toluene and xylene are aromatic hydrocarbons and are also upstream petrochemicals which are used for further production processes.

At the present time, there are many researches demonstrating the experiments converting C_6, C_7, C_8 to aromatics including benzene, toluene and xylene with different conditions, e.g., catalyst, temperature, pressure and reactant components. It is obvious that aromatics production from n-hexane, n-heptane and n-octane are value enhancement because not only economic values of the aromatics but also C_6, C_7, and C_8 which can be more usage alternatives.

Therefore, the objective of this research is to develop the model of benzene, toluene and xylene productions from n-hexane, n-heptane and n-octane with chemical equilibria over the catalyst. All of these studies were exclusively restricted to the reactions of C_6, C_7, C_8 compounds, because no catalyst combination could convert methane into aromatics.

This research is sincerely expected finding optimized models would explain and more clarify the several reactions. Furthermore, it would be beneficial to develop and actualize in commercial part and predict reaction results with other conditions to save laboratory cost and simplify the method predicting the process of aromatics production. Then In this study, it is curious to use chemical equilibrium concept for describing the fraction of components and the models would originate with the assistance of computer simulation, Aspen Plus simulation to fit with research results.

Objective

To develop the model of benzene, toluene and xylene productions or aromatics production from Normal Paraffin with chemical equilibria over different catalysts.

Literature Review

In this research, the researcher studied related documents and research as a knowledge base for use in the study, with the following research points:

1. Oil quality improvement process

Various parts obtained from distillation can be used differently. Some have high demand and high value. Therefore, requires quality improvement processes to obtain the desired substance Which can be done in many ways as follows:

1.1 Cracking process

Cracking process is the conversion of large molecules of hydrocarbon compounds which are less useful into smaller molecules of hydrocarbon compounds that are more useful or the conversion of circular hydrocarbons into aromatic substances by using high heat and a catalyst.

1.1.1 Thermal Cracking

The process of breaking down diesel fuel or fuel oil by using high heat 400-500˚C under high pressure. The product is gas, gasoline that is high in aromatic with an octane value of 65-70.

1.1.2 Catalytic Cracking

The process of breaking down diesel fuel. By using catalysts such as Bentonite and Kaolin or synthetic clay that has high aluminum content or synthetic zeolite. The product obtained from this process is gasoline with a high-octane value greater than 90.

1.2 Reforming process

Reforming process is to convert a straight chain hydrocarbon compound into a branched chain such as iso-octane, which has good fuel efficiency in engines, gasoline. By using high heat and catalysts such as

$$CH_3CH_2CH_2CH_2CH_2CH_2CH_2CH_3 \xrightarrow[\text{ตัวเร่งปฏิกิริยา}]{\text{ความร้อนสูง}} CH_3-CHCH_2-C-CH_3$$
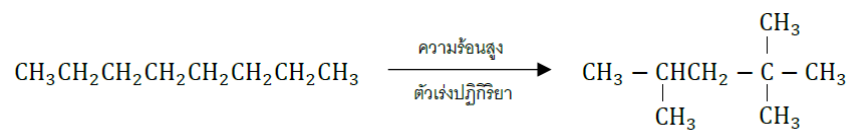
1.2.1 Thermal Reforming

Heat treatment process that changes the structure of low-octane hydrocarbons to high levels at 560˚C.

1.2.2 Catalytic Reforming

The main process for the production of high-octane gasoline. The molecular weight of the catalytic reforming process does not change much, but there will be a rearrangement of the structure. Including the reaction Isomerization, Cyclization, Aromatization, Combination.

2. Equilibrium modeling

The model demonstrates the oxidative coupling of methane reaction (OCM) over three different catalysts which were Pt ion-exchanged Ga- and Zn-silicate catalyst, ns Al_2O_3/H-GaAlMFI and TiO_2Zr_2. There were three proposed models including uni-equilibrium reaction model, Duo-equilibrium reaction model and trio-equilibrium reaction model, operating isothermally between 400˚C and 600 ˚C and feeding methane to oxygen ratio was around 3-10. From the research, all possible chemical reactions were proposed and based, containing catalytic reaction, non-catalytic reaction and both catalytic reactions. Then, all variables were calculated with Aspen Plus program, which was run with RK-Soave and Peng-Rob methods based on Aspen Plus component guideline and industrial guideline. As a result, the models were verified by using statistics of components in effluence and reactor performance. For the verification u̶ ̶ Residue Sum Square (RSS) was utilized as a model validation:

$$RSS = \sum_{i=1}^{N}\left[\frac{M_{exp}-M_{model}}{M_{exp}}\right]^2$$

Where M_{exp} and M_{model} are effluent mole flow of the experiment and the chemical equilibrium model, respectively. For the verification using reactor performance, conversion, yield and selectivity as a variable for performance evaluation were represented in terms of average absolute relative deviation (AARD) which is statistical information:

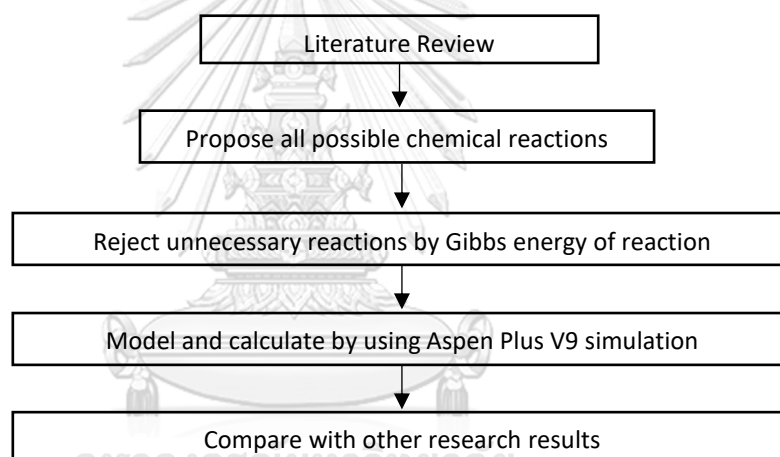$$AARD = \frac{1}{N}\sum_{i=1}^{N}\left|\frac{(P_{exp}-P_{model})}{P_{exp}}\right|$$

Where P_{exp} and P_{model} are the variable from the experiment and the equilibrium model, respectively.

Methods

Scopes of the research

1. To propose chemical reactions of Normal Paraffin to be aromatics (BTX) by using Aspen Plus V9 programs for calculation and other researches for comparison.

2. Interested variables which effected to the model were temperatures, pressures, and catalysts.

3. The reaction temperatures were vary between 4 0 0 ˚C and 6 0 0 ˚C to find the lowest temperature which the reaction can occur.

4. The reaction pressure was used to investigate the model were equal to the other researches and then vary between 1 atm and 10 atm to predict other conditions.

5. All existing compound in the main reactions (aromatization) and the sides reactions (thermal cracking) would be well-defined hydrocarbons, for example C_6, C_7, C_8.

6. The model would be an equilibrium model and kinetic energy is not considered.

Research methodology

```
┌─────────────────────────────────────────┐
│            Literature Review             │
└─────────────────────────────────────────┘
                    │
┌─────────────────────────────────────────┐
│      Propose all possible chemical reactions      │
└─────────────────────────────────────────┘
                    │
┌─────────────────────────────────────────┐
│  Reject unnecessary reactions by Gibbs energy of reaction  │
└─────────────────────────────────────────┘
                    │
┌─────────────────────────────────────────┐
│  Model and calculate by using Aspen Plus V9 simulation  │
└─────────────────────────────────────────┘
                    │
┌─────────────────────────────────────────┐
│      Compare with other research results      │
└─────────────────────────────────────────┘
```

1. Overview

Since C_5 -C_8 Normal Paraffin include plenty of components, there are several reactions occurring for aromatization, for example thermal cracking. Moreover, the different catalysts affected selectivity, enabling not only few unselective reactions to occur but also some selective reactions to disappear. Therefore, all possible reactions that would appear will be calculated in the model, and remarkable reactions will be selected for each catalyst by comparing with the researches.

The reactions were from Polymath calculation and Aspen Plus V9 simulation for more accuracy and approaching actual value as possible as. Solutions and necessary principles are demonstrated next.

2. Propose all possible chemical reactions

Interested reactants contain components, including propane, n-hexadecane (n-C16H34), n-hexane, 1-hexene, n-heptane, n-octane, and 1-octene.

The reactions would be divided into main reactions and side reactions. The main reactions were reaction producing benzene toluene and xylene directly while the side reactions were unexpected reactions, particularly thermal cracking, dehydrogenation and hydrocracking. Since most reactions are an endothermic reaction, it was unavoidable for thermal cracking.

Main reactions: Aromatization, Dehydrocyclization, Hybrid Cracking-Reforming Catalyst.
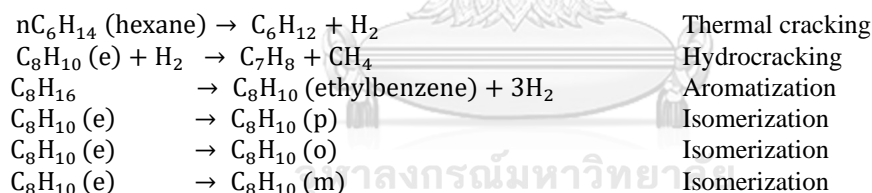
Side reactions: Thermal cracking, Dehydrogenation, Hydrocracking.

Therefore, all possible reactions that would appear will be calculated in the model, and remarkable reactions will be selected for Pt/KL and various Mo2 C-containing catalysts by comparing with the experiment in researches as shown in the table 1. Then, all possible chemical reactions were proposed.

Table 1: Effluent compositions of the experiment

Component	Experiment
C1–C5	0.264
Hexenes	0.07
Benzene	0.277
Toluene	0.283
Heptenes	0.30
Octenes	0.19
Ethylbenzene	0.65
m-Xylene	0.12
p-Xylene	0.02
o-Xylene	0.30

A summation of all fractions is less than 1 since certain components could not be defined, then the experimental result was neutralized before calculation.

nC_6H_{14} (hexane) $\rightarrow$ $C_6H_{12} + H_2$		Thermal cracking
C_8H_{10} (e) $+ H_2$ $\rightarrow$ $C_7H_8 + CH_4$		Hydrocracking
C_8H_{16} $\rightarrow$ C_8H_{10} (ethylbenzene) $+ 3H_2$		Aromatization
C_8H_{10} (e) $\rightarrow$ C_8H_{10} (p)		Isomerization
C_8H_{10} (e) $\rightarrow$ C_8H_{10} (o)		Isomerization
C_8H_{10} (e) $\rightarrow$ C_8H_{10} (m)		Isomerization

The proposed reactions were simulated in the Aspen plus V9, which Peng-Robinson method was preferred and equilibrium reactor was operated under 1 atm and 500 °C since the model was regarded as equilibrium state which the forward reaction rate and the reverse reaction rate are equivalent.

3. Calculation Gibbs energy

3.1 Gibbs energy of reaction

Gibbs energy of formation of individual components in a reaction is desired in order to calculation Gibbs energy of reaction as follows:

$$\Delta G_{reaction} = \sum (n\Delta G_f)_{products} - \sum (n\Delta G_f)_{reactants}$$

Gibbs energy of formation at any temperature obtained from the chemical properties' handbook. When Gibbs energy of reaction is negative value, the reaction is favorable outcome to reject unnecessary reactions.

3.2 Equilibrium constant

For a gas-phase reaction, $aA(g) + bB(g) \leftrightarrows cC(g) + dD(g)$, the expression for Kp is

$$K_P = \frac{(P_c)^c (P_D)^d}{(P_A)^a (P_B)^b}$$

In fact, there are many reactions occurring in the reactor, hence K_P would be represented as $K_{P(n)}$ where n is a number of any reaction. To illustrate, there are reactions as follows:

$$rR(g) \leftrightarrows sS(g) + tT(g) \qquad \text{-------- reaction (1)}$$
$$xX(g) \leftrightarrows yY(g) + zZ(g) \qquad \text{-------- reaction (2)}$$
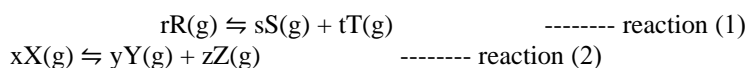
Then, Kp of both reactions would be

$$K_{p1} = \frac{(P_S)^s (P_T)^t}{(P_R)^r} \qquad \text{and} \qquad K_{p2} = \frac{(P_Y)^y (P_Z)^z}{(P_X)^x}$$

3.3 Relation of Gibbs energy of reactions and equilibrium constant

$$\Delta G^0 = -RT \ln K$$

Likewise, $Kp_{(n)}$ is the expression for equilibrium constant of any reaction when there is more than one reaction, ΔG_n^0 is also represented as Gibbs energy of any reactions as shown below:

$$\Delta G_1^0 = -RT \ln K_1$$

$$\Delta G_2^0 = -RT \ln K_2$$

3.4 Conversion

Conversion of each reaction that possibly occur in the reactor is important in the analysis of product quantity which was represented in terms of partial pressure and it is a key variable for the model test and result prediction.

4. Aspen Plus V9 simulation
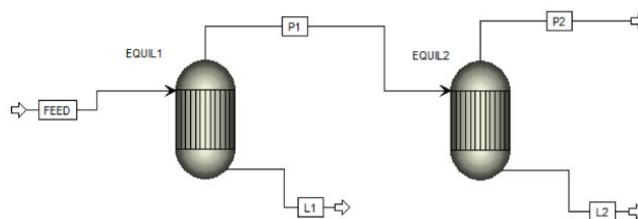
Figure 1 Example of connected reactors in series

The reactions were from Aspen Plus V9 simulation for more accuracy and approaching actual value as possible as. The reactions would be divided into main reactions and side reactions. The main reactions were reaction producing benzene toluene and xylene directly while the side reactions were unexpected reactions, particularly thermal cracking, dehydrogenation and hydrocracking. Then, all possible chemical reactions were proposed. However, the reactions in the model were grouped by splitting reactors, so there was more than one reactor connected in series to classify which reactions occurred before and after.

4.1 Base method

The components in the process are hydrocarbons, then Peng-Robinson method was preferred. However, the method would consider interaction between each component in the mixture, which it can be estimated from the Polymath with difficulty. Hence, ideal model was also performed for contrasting.

4.2 Equilibrium reactor

The model was regarded as equilibrium state which the forward reaction rate and the reverse reaction rate are equivalent, so equilibrium reactor was operated instead.

4.3 Effect of temperature on the reaction performance

From the formulas, temperature influents the reaction result, especially conversion. Although high temperature leads to higher conversion, coke formation probably occurs. Then, temperature varying was performed to estimate the lowest possible reaction temperature.

4.4 Effect of pressure on the reaction performance

Most experiments from the literature reviews are demonstrated at atmospheric pressure, then the model would be interested in higher operating pressure.

Results and Discussion

Model 1 and Model 2

The model 1 shows three groups of the reactions, including thermal cracking to aromatization, hydrogenation and isomerization. Since aromatics production from n-hexane n-heptane and n-octane is an interesting model, there are dehydrogenation of n-hexane n-heptane and n-octane in the reactor 1 in order to find equilibrium between them before converting to ethylcyclohexane and ethylbenzene, respectively. Then, aromatization of toluene and benzene were from hydrogenations and by-product of both reactions was methane because different by-product strongly influenced reaction equilibrium shifting and aromatics production, especially toluene and benzene fractions.

Model 1

Reactor 1	Reactor 2	Reactor 3
$n - C_6H_{14}$ (hexane) $\rightarrow C_6H_{12} + H_2$	C_8H_{10} (e) $+ H_2 \rightarrow C_7H_8 + CH_4$	C_8H_{10} (e) $\rightarrow C_8H_{10}$ (p)
$C_6H_{12} \rightarrow C_4H_8 + C_2H_4$	$C_7H_8 + H_2 \rightarrow C_6H_6 + CH_4$	C_8H_{10} (e) $\rightarrow C_8H_{10}$ (o)
$2C_4H_8 \rightarrow C_8H_{16}$ (ethylxyclohexane)	$C_6H_{14} + H_2 \rightarrow C_4H_8 + 2CH_4$	C_8H_{10} (e) $\rightarrow C_8H_{10}$ (m)
$C_8H_{16} \rightarrow C_8H_{10}$ (ethylbenzene) $+ 3H_2$	$C_6H_{14} + H_2 \rightarrow 2C_3H_8$	
$n - C_7H_{16}$ (heptane) $\rightarrow C_7H_{14} + H_2$	$C_7H_{16} + H_2 \rightarrow C_6H_{14} + CH_4$	
$C_7H_{14} \rightarrow C_4H_8 + C_3H_6$	$C_7H_{16} + H_2 \rightarrow C_5H_{10} + 2CH_4$	
$2C_4H_8 \rightarrow C_8H_{16}$ (ethylxyclohexane)	$C_7H_{16} + H_2 \rightarrow C_3H_6 + 2C_2H_6$	
$C_8H_{16} \rightarrow C_8H_{10}$ (ethylbenzene) $+ 3H_2$	$C_8H_{18} + H_2 \rightarrow C_7H_{16} + CH_4$	
$n - C_8H_{18}$ (octane) $\rightarrow C_8H_{16} + H_2$	$C_8H_{18} + H_2 \rightarrow C_6H_{12} + 2CH_4$	
$C_8H_{16} \rightarrow C_8H_{10}$ (ethylbenzene) $+ 3H_2$		

Model 2

Reactor 1		Reactor 2
$n - C_6H_{14}$ (hexane) $\rightarrow C_6H_{12} + H_2$	$C_6H_{14} + H_2 \rightarrow C_4H_8 + 2CH_4$	C_8H_{10} (e) $+ H_2 \rightarrow C_7H_8 + CH_4$
$C_6H_{12} \rightarrow C_4H_8 + C_2H_4$	$C_6H_{14} + H_2 \rightarrow 2C_3H_8$	$C_7H_8 + H_2 \rightarrow C_6H_6 + CH_4$
$2C_4H_8 \rightarrow C_8H_{16}$ (ethylxyclohexane)	$C_7H_{16} + H_2 \rightarrow C_6H_{14} + CH_4$	
$C_8H_{16} \rightarrow C_8H_{10}$ (ethylbenzene) $+ 3H_2$	$C_7H_{16} + H_2 \rightarrow C_5H_{10} + 2CH_4$	**Reactor 3**
$n - C_7H_{16}$ (heptane) $\rightarrow C_7H_{14} + H_2$	$C_7H_{16} + H_2 \rightarrow C_3H_6 + 2C_2H_6$	
$C_7H_{14} \rightarrow C_4H_8 + C_3H_6$	$C_8H_{18} + H_2 \rightarrow C_7H_{16} + CH_4$	C_8H_{10} (e) $\rightarrow C_8H_{10}$ (p)
$2C_4H_8 \rightarrow C_8H_{16}$ (ethylxyclohexane)	$C_8H_{18} + H_2 \rightarrow C_6H_{12} + 2CH_4$	C_8H_{10} (e) $\rightarrow C_8H_{10}$ (o)
$C_8H_{16} \rightarrow C_8H_{10}$ (ethylbenzene) $+ 3H_2$		C_8H_{10} (e) $\rightarrow C_8H_{10}$ (m)
$n - C_8H_{18}$ (octane) $\rightarrow C_8H_{16} + H_2$		
$C_8H_{16} \rightarrow C_8H_{10}$ (ethylbenzene) $+ 3H_2$		

Table 2: Compositions of Model 1 and Model 2 by Aspen plus simulation

Model	Model1			Model2		
Component	Reactor 1	Reactor 2	Reactor 3	Reactor 1	Reactor 2	Reactor 3
n-hexane	0.000276	0.000276	0.000276	0.000276	0.000276	0.000276
n-heptane	0.000276	0.000276	0.000276	0.000276	0.000276	0.000276
n-octane	0.000276	0.000276	0.000276	0.000276	0.000276	0.000276
hydrogen	0.05107	0.016502	0.016502	0.002466	9.06E-07	9.06E-07
methan	0	0.245539	0.245539	0.158708	0.178324	0.178324
ethan	0	0.010829	0.010829	0.012288	0.0122879	0.012288
propane	0	0.022938	0.022938	0.004362	0.0043624	0.004362
ethylene	0	0	0	0	0	0
propylene	0	0	0	0	0	0
butane	2.50E-05	3.36E-05	3.36E-05	0.000276	0.000276	0.000276
1-Pentene	0.002413	0.002413	0.002413	2.50E-05	2.50E-05	2.50E-05
benzene	0	0.491109	0.491109	0	0.2681	0.2681
toluene	0	0.158118	0.158118	0	0.306337	0.306337
o-xylene	0	0	3.18E-08	0	0	0.003111
m-xylene	0	0	6.46E-08	0	0	0.007326
p-xylene	0	0	2.62E-08	0	0	0.00897
ethylbenzene	0.537011	1.29E-07	1.25E-08	0.279407	0.153237	0.072417
ethylcyclohexane	1.09E-05	1.09E-05	1.09E-05	1.58E-09	1.58E-09	1.58E-09

Hydrogenations of n-hexane n-heptane and n-octane or hydrocracking in the reactor 2 were moved to the reactor 1 in the model 2, and it has seen that aromatics fractions are more similar to the experimental result as shown in figure 2 since ethylbenzene production which would be converted to other aromatics halved approximately. The hydrogenations are competitive reaction, which Pt/KL and various Mo2C-containing catalyst could not wholly eliminate, the experimental products were lower. Therefore, the desired product will be higher if another catalyst has functional elimination of the reactions from the reactor 1; however, the reactions are proper in the reactor 1 for the catalyst. Moreover, ethylcyclohexane from the both models were close to zero, it could be as an intermediate of the mechanism.
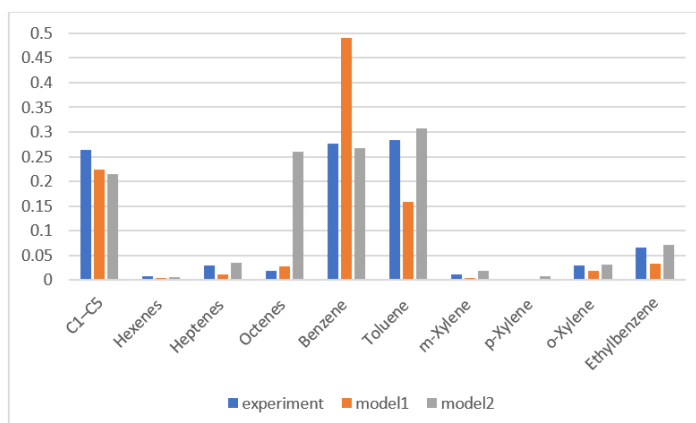
Figure 2 Effluent compositions of experiment, Model 1 and Model 2

Model 3 and Model 4

The reactor 4 represented thermal cracking, was added in the model 3 in order to adjust aromatic proportions to the experiment result. Besides, there was no hydrogen in the reactor 4 because it had been extremely depleted since reactor 2, then hydrogenation and dehydrogenation disappeared. The model 4 was designed to visualize how thermal cracking had occurred before isomerization happened. Benzene was risen dramatically by ethylbenzene, enabling toluene to be increased noticeably for reaching equilibrium state.

Model 3

Reactor 1		Reactor 3
$n - C_6H_{14}$ (hexane) $\rightarrow$ $C_6H_{12} + H_2$	$C_6H_{14} + H_2 \rightarrow C_4H_8 + 2CH_4$	C_8H_{10} (e) $\rightarrow$ C_8H_{10} (p)
$C_6H_{12} \rightarrow C_4H_8 + C_2H_4$	$C_6H_{14} + H_2 \rightarrow 2C_3H_8$	C_8H_{10} (e) $\rightarrow$ C_8H_{10} (o)
$2C_4H_8 \rightarrow C_8H_{16}$ (ethylxyclohexane)	$C_7H_{16} + H_2 \rightarrow C_6H_{14} + CH_4$	C_8H_{10} (e) $\rightarrow$ C_8H_{10} (m)
$C_8H_{16} \rightarrow C_8H_{10}$ (ethylbenzene) $+ 3H_2$	$C_7H_{16} + H_2 \rightarrow C_5H_{10} + 2CH_4$	
$n - C_7H_{16}$ (heptane) $\rightarrow$ $C_7H_{14} + H_2$	$C_7H_{16} + H_2 \rightarrow C_3H_6 + 2C_2H_6$	**Reactor 4**
$C_7H_{14} \rightarrow C_4H_8 + C_3H_6$	$C_8H_{18} + H_2 \rightarrow C_7H_{16} + CH_4$	
$2C_4H_8 \rightarrow C_8H_{16}$ (ethylxyclohexane)	$C_8H_{18} + H_2 \rightarrow C_6H_{12} + 2CH_4$	C_8H_{10} (p) $\rightarrow$ $C_6H_6 + C_2H_4$
$C_8H_{16} \rightarrow C_8H_{10}$ (ethylbenzene) $+ 3H_2$		C_8H_{10} (o) $\rightarrow$ $C_6H_6 + C_2H_4$
$n - C_8H_{18}$ (octane) $\rightarrow$ $C_8H_{16} + H_2$		C_8H_{10} (m) $\rightarrow$ $C_6H_6 + C_2H_4$
$C_8H_{16} \rightarrow C_8H_{10}$ (ethylbenzene) $+ 3H_2$	**Reactor 2**	
		$2C_7H_8 \rightarrow 2C_6H_6 + C_2H_4$
	C_8H_{10} (e) $+ H_2 \rightarrow C_7H_8 + CH_4$	
	$C_7H_8 + H_2 \rightarrow C_6H_6 + CH_4$	

Model 4

Reactor 1		Reactor 3
$n - C_6H_{14}$ (hexane) $\rightarrow$ $C_6H_{12} + H_2$	$C_6H_{14} + H_2 \rightarrow C_4H_8 + 2CH_4$	C_8H_{10} (e) $\rightarrow$ $C_6H_6 + C_2H_4$
$C_6H_{12} \rightarrow C_4H_8 + C_2H_4$	$C_6H_{14} + H_2 \rightarrow 2C_3H_8$	$2C_7H_8 \rightarrow 2C_6H_6 + C_2H_4$
$2C_4H_8 \rightarrow C_8H_{16}$ (ethylxyclohexane)	$C_7H_{16} + H_2 \rightarrow C_6H_{14} + CH_4$	
$C_8H_{16} \rightarrow C_8H_{10}$ (ethylbenzene) $+ 3H_2$	$C_7H_{16} + H_2 \rightarrow C_5H_{10} + 2CH_4$	
$n - C_7H_{16}$ (heptane) $\rightarrow$ $C_7H_{14} + H_2$	$C_7H_{16} + H_2 \rightarrow C_3H_6 + 2C_2H_6$	**Reactor 4**
$C_7H_{14} \rightarrow C_4H_8 + C_3H_6$	$C_8H_{18} + H_2 \rightarrow C_7H_{16} + CH_4$	
$2C_4H_8 \rightarrow C_8H_{16}$ (ethylxyclohexane)	$C_8H_{18} + H_2 \rightarrow C_6H_{12} + 2CH_4$	C_8H_{10} (e) $\rightarrow$ C_8H_{10} (p)
$C_8H_{16} \rightarrow C_8H_{10}$ (ethylbenzene) $+ 3H_2$	**Reactor 2**	C_8H_{10} (e) $\rightarrow$ C_8H_{10} (o)
$n - C_8H_{18}$ (octane) $\rightarrow$ $C_8H_{16} + H_2$		C_8H_{10} (e) $\rightarrow$ C_8H_{10} (m)
$C_8H_{16} \rightarrow C_8H_{10}$ (ethylbenzene) $+ 3H_2$	C_8H_{10} (e) $+ H_2 \rightarrow C_7H_8 + CH_4$	
	$C_7H_8 + H_2 \rightarrow C_6H_6 + CH_4$	

Table 3: Compositions of Model 3 and Model 4 by Aspen plus simulation

| Model	Model3				Model4	
Component	Reactor 1	Reactor 2	Reactor 3	Reactor 4	Reactor 3	Reactor 4
n-hexane	0.000276	0.000276	0.000276	0.000276	0.000276	0.000276
n-heptane	0.000276	0.000276	0.000276	0.000276	0.000276	0.000276
n-octane	0.000276	0.000276	0.000276	0.000276	0.000276	0.000276
hydrogen	0.002466	9.06E-07	9.06E-07	9.06E-07	9.06E-07	9.06E-07
methan	0.158708	0.178324	0.178324	0.178324	0.178324	0.178324
ethan	0.0012288	0.001229	0.002123	0.000123	0.0001229	0.000123
propane	0.0043624	0.004362	0.004362	0.004362	0.0043624	0.004362
ethylene	0	0	0	0.009685	0.022722	0.022722
propylene	0	0	0	0	0	0
butane	2.50E-05	2.50E-05	2.50E-05	2.50E-05	2.50E-05	2.50E-05
1-Pentene	0.0002141	0.000114	0.000114	0.000114	0.000025	0.000025
benzene	0	0.2781	0.2781	0.2781	0.2932765	0.293277
toluene	0	0.286337	0.286337	0.286337	0.308985	0.308985
o-xylene	0	0	0.02769	0.036106	0	0.03168
m-xylene	0	0	0.056185	0.025733	0	0.019792
p-xylene	0	0	0.022779	0.008297	0	0.005592
ethylbenzene	0.279407	0.153237	0.078417	0.078417	0.0592885	0.059288
ethylcyclohexane	1.58E-09	1.58E-09	1.58E-09	1.58E-09	1.58E-09	1.58E-09
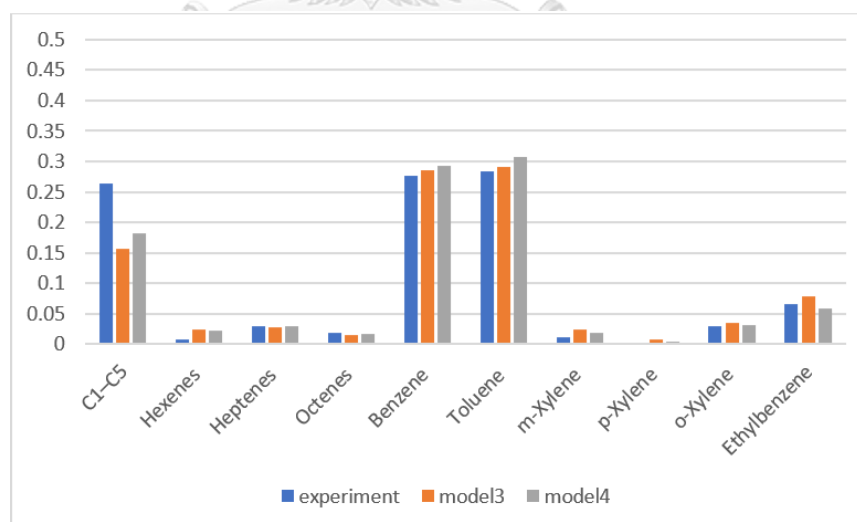
Figure 3 Effluent compositions of experiment, Model 3 and Model 4

Model 5 and Model 6

The model 5 explains how possible thermal cracking ways of the aromatics could be performed thoroughly in the reactor 4 since all effluent compositions of the model 5 are exactly equal to the model

3. Then, it illustrates that xylenes would be cracked by high heat to be toluene before it would be also cracked to be benzene. On the other hand, the reactors 3 and 4 or isomerization and thermal cracking grouped together in the model 6. Although the effluents are not quite different, and the almost models are closer to the experimental result than the model 1 as shown in the figures, so an exact model should be defined. Hence, Residua Sum Square (RSS) was applied to indicate the most suitable model as shown in the table 5. The number of reactions in model 5+6 are greater than that in the methodology section above

Model 5

Reactor 1		Reactor 3

Reactor 1

$n-C_6H_{14}$ (hexane) $\rightarrow$ $C_6H_{12} + H_2$
$C_6H_{12} \rightarrow C_4H_8 + C_2H_4$
$2C_4H_8 \rightarrow C_8H_{16}$ (ethylxyclohexane)
$C_8H_{16} \rightarrow C_8H_{10}$ (ethylbenzene) $+ 3H_2$
$n-C_7H_{16}$ (heptane) $\rightarrow$ $C_7H_{14} + H_2$
$C_7H_{14} \rightarrow C_4H_8 + C_3H_6$
$2C_4H_8 \rightarrow C_8H_{16}$ (ethylxyclohexane)
$C_8H_{16} \rightarrow C_8H_{10}$ (ethylbenzene) $+ 3H_2$
$n-C_8H_{18}$ (octane) $\rightarrow$ $C_8H_{16} + H_2$
$C_8H_{16} \rightarrow C_8H_{10}$ (ethylbenzene) $+ 3H_2$

$C_6H_{14} + H_2 \rightarrow C_4H_8 + 2CH_4$
$C_6H_{14} + H_2 \rightarrow 2C_3H_8$
$C_7H_{16} + H_2 \rightarrow C_6H_{14} + CH_4$
$C_7H_{16} + H_2 \rightarrow C_5H_{10} + 2CH_4$
$C_7H_{16} + H_2 \rightarrow C_3H_6 + 2C_2H_6$
$C_8H_{18} + H_2 \rightarrow C_7H_{16} + CH_4$
$C_8H_{18} + H_2 \rightarrow C_6H_{12} + 2CH_4$

Reactor 2

C_8H_{10} (e) $+ H_2 \rightarrow C_7H_8 + CH_4$
$C_7H_8 + H_2 \rightarrow C_6H_6 + CH_4$

Reactor 3

C_8H_{10} (e) $\rightarrow C_8H_{10}$ (p)
C_8H_{10} (e) $\rightarrow C_8H_{10}$ (o)
C_8H_{10} (e) $\rightarrow C_8H_{10}$ (m)

Reactor 4

$2C_8H_{10}$ (m) $\rightarrow 2C_7H_8 + C_2H_4$
$2C_8H_{10}$ (o) $\rightarrow 2C_7H_8 + C_2H_4$
$2C_8H_{10}$ (p) $\rightarrow 2C_7H_8 + C_2H_4$
C_8H_{10} (p) $+ C_8H_{10}$ (o) $\rightarrow 2C_7H_8 + C_2H_4$
C_8H_{10} (p) $+ C_8H_{10}$ (m) $\rightarrow 2C_7H_8 + C_2H_4$
C_8H_{10} (o) $+ C_8H_{10}$ (m) $\rightarrow 2C_7H_8 + C_2H_4$
$2C_7H_8 \rightarrow 2C_6H_6 + C_2H_4$

Model 6

Reactor 1

$n-C_6H_{14}$ (hexane) $\rightarrow$ $C_6H_{12} + H_2$
$C_6H_{12} \rightarrow C_4H_8 + C_2H_4$
$2C_4H_8 \rightarrow C_8H_{16}$ (ethylxyclohexane)
$C_8H_{16} \rightarrow C_8H_{10}$ (ethylbenzene) $+ 3H_2$
$n-C_7H_{16}$ (heptane) $\rightarrow$ $C_7H_{14} + H_2$
$C_7H_{14} \rightarrow C_4H_8 + C_3H_6$
$2C_4H_8 \rightarrow C_8H_{16}$ (ethylxyclohexane)
$C_8H_{16} \rightarrow C_8H_{10}$ (ethylbenzene) $+ 3H_2$
$n-C_8H_{18}$ (octane) $\rightarrow$ $C_8H_{16} + H_2$
$C_8H_{16} \rightarrow C_8H_{10}$ (ethylbenzene) $+ 3H_2$

$C_6H_{14} + H_2 \rightarrow C_4H_8 + 2CH_4$
$C_6H_{14} + H_2 \rightarrow 2C_3H_8$
$C_7H_{16} + H_2 \rightarrow C_6H_{14} + CH_4$
$C_7H_{16} + H_2 \rightarrow C_5H_{10} + 2CH_4$
$C_7H_{16} + H_2 \rightarrow C_3H_6 + 2C_2H_6$
$C_8H_{18} + H_2 \rightarrow C_7H_{16} + CH_4$
$C_8H_{18} + H_2 \rightarrow C_6H_{12} + 2CH_4$

Reactor 2

C_8H_{10} (e) $+ H_2 \rightarrow C_7H_8 + CH_4$
$C_7H_8 + H_2 \rightarrow C_6H_6 + CH_4$

Reactor 3

C_8H_{10} (e) $\rightarrow C_8H_{10}$ (p)
C_8H_{10} (e) $\rightarrow C_8H_{10}$ (o)
C_8H_{10} (e) $\rightarrow C_8H_{10}$ (m)

$2C_8H_{10}$ (m) $\rightarrow 2C_7H_8 + C_2H_4$
$2C_8H_{10}$ (o) $\rightarrow 2C_7H_8 + C_2H_4$
$2C_8H_{10}$ (p) $\rightarrow 2C_7H_8 + C_2H_4$
C_8H_{10} (p) $+ C_8H_{10}$ (o) $\rightarrow 2C_7H_8 + C_2H_4$
C_8H_{10} (p) $+ C_8H_{10}$ (m) $\rightarrow 2C_7H_8 + C_2H_4$
C_8H_{10} (o) $+ C_8H_{10}$ (m) $\rightarrow 2C_7H_8 + C_2H_4$
$2C_7H_8 \rightarrow 2C_6H_6 + C_2H_4$

Table 4: Compositions of Model 5 and Model 6 by Aspen plus simulation

| Model	Model5				Model6
Component	Reactor 1	Reactor 2	Reactor 3	Reactor 4	Reactor 3
n-hexane	0.000276	0.000276	0.000276	0.000276	0.000276
n-heptane	0.000276	0.000276	0.000276	0.000276	0.000276
n-octane	0.000276	0.000276	0.000276	0.000276	0.000276
hydrogen	0.002466	9.06E-07	9.06E-07	9.06E-07	9.06E-07
methan	0.158708	0.158708	0.155708	0.155708	0.156708
ethan	0.00122879	0.00122879	0.002122879	0.000122879	0.000122879
propane	0.00436239	0.00436239	0.00436239	0.00436239	0.00436239
ethylene	0	0	0	0.009685	0.009685
propylene	0	0	0	0	0
butane	2.50E-05	2.50E-05	2.50E-05	2.50E-05	2.50E-05
1-Pentene	0.00021413	0.00011413	0.00011413	0.000025	0.000025
benzene	0	0.2681	0.2681	0.292765	0.302811
toluene	0	0.298985	0.298985	0.298985	0.29251
o-xylene	0	0	0.036106	0.0349527	0.0359
m-xylene	0	0	0.056185	0.0256185	0.02915
p-xylene	0	0	0.029702	0.00829702	0.008715
ethylbenzene	0.279407	0.153237	0.07914	0.07914	0.07528
ethylcyclohexane	1.58E-09	1.58E-09	1.58E-09	1.58E-09	1.58E-09
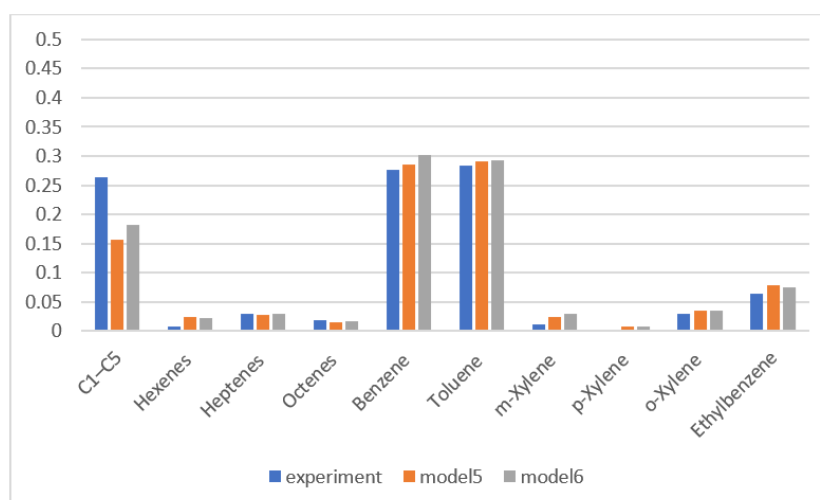
Figure 4 Effluent compositions of experiment, Model 5 and Model 6

Conclusions

The table 5 presents effluent differences where the negative sign represents greater model outlet than the experiment while the positive sign represents smaller model outlet. Furthermore, the smallest RSS value signified the appropriate model, which would be models 6. In addition, the majority product of a catalyst which has functional as in model 1 would be benzene, and hydrocracking will be prevented from appearing in the reactor 1, so aromatization remarkably increases. Moreover, advantage of equilibrium model compared to kinetic was its ease in utilization due to much lower number of parameters and equations in equilibrium model.

Table 5: Effluent differences and RSS

Component	Model 1	Model 2	Model 3	Model 4	Model 5	Model 6
n-hexane	0.95	0.99	0.99	0.99	0.99	0.99
n-heptane	0.95	0.99	0.99	0.99	0.99	0.99
n-octane	0.95	0.99	0.99	0.99	0.99	0.99
hydrogen	0.02	1.00	1.00	1.00	1.00	1.00
methan	-1.09	-0.52	-0.52	-0.52	-0.52	-0.52
ethan	0.37	0.30	0.30	0.30	0.30	0.30
propane	0.48	0.02	0.02	0.02	0.02	0.02
ethylene	1.00	1.00	-0.32	-2.1	-0.32	-0.34
propylene	1.00	1.00	1.00	1.00	1.00	1.00
benzene	-13.41	0.90	-0.20	-0.38	-0.20	-0.20
toluene	0.99	-0.15	-0.07	-0.86	-0.07	-0.08
xylene	1.00	-1.29	-0.76	0.57	-0.76	-0.79
ethylbenzene	1.00	-1.08	-1.08	0.61	-1.08	-0.62
RSS	187.18	8.01	5.23	9.32	5.23	4.52

References

Abildskov, J., Kontogeorgis, G.M., Gani, R., 2004. *Computer Aided Property Estimation for Process and Product Design*. Elsevier, The Netherlands, pp. 59–74.

Altgelt, K.H., Boduszynski, M.H., 1994. *Composition and Analysis of Heavy Petroleum Fractions*. Marcel Dekker, New York, pp. 107–128.

Belohlav Z, Zamostny P, Herink T. *The kinetic model of thermal cracking for olefinsproduction*. Chem Eng Process Process Intensif 2003; 42:461–73.

Bokade. (2007). Documentation of the TLVs and BEIs with Other World Wide Occupational Exposure Values. *American Conference of Governmental Industrial Hygienists* (p. 243-255*).* Cincinnati: Cincinnati state technical and community college, U.S.

Broughton DB. *Process for separating normal and isoparaffins*. United States patentUS4036745 A; 1977.

Bunyakiat, et al. (2011). *Production during Catalytic Dehydration of Ethanol over Ru- and Pt-modified H-beta Zeolite Catalysts*. Ph.D. dissertation, Chulalongkorn University.

Choudhary, V.R., D. Panjala, and S. Banerjee, *Aromatization of propene and n-butene over H‐galloaluminosilicate (ZSM-5 type) zeolite.* Applied Catalysis A: General, 2002. 231(1): p. 243-251.

Covavisaruch, S., et al., *What are petroleum chemicals?*, in *Petrochemical Encyclopedia*, K. Bunyakiat, Editor. 2011, WPS(Thailand)Co..Ltd.: Bangkok. p. 14-67.

Kumar, N., et al., *Synthesis and characterization of Pd-MCM-22 and Pt-SAPO-11 catalysts for transformation of n-butane to aromatic hydrocarbons.* Applied Catalysis A: General, 2002. 227(1): p. 97-103.

Morrow, N.L., *The industrial production and use of 1,3-butadiene.* Environmental health perspectives, 1990. 86: p. 7-8.

Ragil K, Bailly M, Jullian S, Clause O. *Process for chromatographic separation ofa C5–C8 feed or an intermediate feed into three effluents, respectively richin straight chain, mono-branched and multi- branched paraffins.* United Statespatent US6353144 B1; 2002.

Renon, H., Prausnitz, J.M., 1968. Local compositions in thermodynamic excess functions for liquid mixtures. *A.I.Ch.E. Journal* 14, 135–144.

Riazi, M.R., Nasimi, N., Roomi, Y.A., 1999. *Estimation of sulfur content of petroleum Products and crude oils.* Industrial and Engineering Chemistry Research 38, 4507–4512.

Riazi, M.R., Roomi, Y.A., 2001. *Use of the refractive index in the estimation of thermophysical properties of hydrocarbons and petroleum mixtures*. Industrial and Engineering Chemistry Research 40, 1975–1984.

Róbert, B. & Frigyes, S. (2005). Aromatization of n-heptane on Mo2C-containing catalysts. *Journal of Catalysis, 8*(1), 60-68.

S. Asaoka, K. Ito, S. Minohara, M.A. Ali, H.S. Bamufleh, Prepr. Pap.: Am. Chem. Soc. Div. Pet. Chem. 50 (2006) 372.

Siriporn, J., Paneeya, S., Thirasak, R., Somchai, O. & Daniel, R. (2003). n-Octane aromatization on a Pt/KL catalyst prepared by vapor-phase impregnation. *Journal of Catalysis, 11*(1), 218-229.

Smith, J.M., H.C. Van Ness, and M.M. Abbott, *Introduction to chemical engineering thermodynamics*. 2005, Boston: McGraw-Hill.

Song, C., et al., *Influence of reaction conditions on the aromatization of cofeeding n-butane with methanol over the Zn loaded ZSM-5/ZSM-11 zeolite catalyst.* Fuel Processing Technology, 2014. 126: p. 60-65.

Wongwailikhit, K., *Modeling of Oxidative Coupling of Methane to Ethylene with Chemical Equilibria*, in *Chemical Engineering*. 2013, Chulalongkorn University.

Yuan, S., et al., *Preparation of Mo2C/HZSM-5 and its catalytic performance for the conversion of n-butane into aromatics.* Journal of Molecular Catalysis A: Chemical, 2002. 184(1): p. 257-266.

REFERENCES

VITA

NAME	Thidarat Detsut
DATE OF BIRTH	5 June 1995
PLACE OF BIRTH	Nongkhai, Thailand
INSTITUTIONS ATTENDED	Finished high school from Pathumthep Witthayakarn school in 2014 Graduated in bachelor's degrees from Thammasat University in 2018.
HOME ADDRESS	60/2 Moo2 Vienghuk Nongkhai Thailand 43000

จุฬาลงกรณ์มหาวิทยาลัย

CHULALONGKORN UNIVERSITY